Theoretical Investigations on Cooperative Phenomena in a few Molecular and Macromolecular Systems

A Thesis

Submitted for the Degree of

Master of Science

By

Shrinwantu Pal

Chemistry and Physics of Materials Unit

Jawaharlal Nehru Centre for Advanced Scientific Research

Bangalore 560064

May 2008

Declaration

I hereby declare that the matter embodied in the thesis entitled "**Theoretical Investigations on Cooperative Phenomena in a few Molecular and Macromolecular Systems**" is the result of investigations carried out by me at the Chemistry and Physics of Materials Unit, Jawaharlal Nehru Centre for Advanced Scientific Research, Bangalore, India, under the supervision of Prof. Swapan K. Pati and that it has not been submitted elsewhere for the award of any degree or diploma.

In keeping with the general practice in reporting scientific observations, due acknowledgement has been made whenever the work described is based on the findings of other investigators.

_____

Shrinwantu Pal

Certificate

I hereby declare that the matter embodied in the thesis entitled "**Theoretical Investigations on Cooperative Phenomena in a few Molecular and Macromolecular Systems**" has been carried out by Mr. Shrinwantu Pal at the Chemistry and Physics of Materials Unit, Jawaharlal Nehru Centre for Advanced Scientific Research, Bangalore, India, under my supervision and that it has not been submitted elsewhere for the award of any degree or diploma.

_____

Prof. Swapan K. Pati

(Research Supervisor)

Acknowledgements

I take this opportunity to thank all the wonderful people who, in my becoming of what I am now, have all had equally important parts to play. Firstly, I would like to thank my parents. I thank my mother, who has always asked me to 'think' before I do anything, be it at home or in academics, and my father, who told me how many-a-time hard work far surpasses brilliance. Secondly, I remember my supervisor Prof. Pati, who endured (and still does) my endless number of mistakes and follies. I would also like to thank him for the freedom he gave me to pursue ideas I had, some of which, eventually however, didn't turn out to be anything claimable.

I would also like to thank Dibyendu, my friend, philosopher, and guide for giving me company and support (in matters pertaining to course work and life, in general) and my batch mates at IISc, especially, Arun, Mantu, Raju, Debasis and Geetanjali, not just for being friends, but for the warmth in which they kept me, in the days of strenuous course work at IISc. I would like to thank Ayan Da, for not just being a brother to me, but also for showing me the proper way to do things, be it the lab or in any other thing having the slightest flavor of science. I would also like to thank Dinesh, my room mate for being there, always smiling, be it rain, hail or storm, or me in the various colors of my mind. I would like to thank Neenu for being there, not just as a batch mate, but as a member of a team of two (me included), all the way from JNC to IISc.

I would like to thank all my professors at IISc, especially Prof. Jemmis (for making Computational Chemistry not only understandable, but enjoyable as well), and Prof. Uday Maitra (for making Organic Chemistry Physical). I take immense pleasure at thanking my professors at Ramakrishna Mission Vidyamandira, Belur Math for laying the path of Chemistry I took, and often recollect still, as I meander through the lecture notes I penned-down in my Baccalaureate years.

I also remember my lab-mates, Sudipta Da, Sairam, Sasmita, Mohan, Lakshmi, Debu Da, Arun and Prakash, some of whom are beside me even as I write this, and have always been there, no matter how busy they were, to support me, and to help me learn not just the techniques that one must, but to learn how things could be done fast, and

accurately. Academics apart, I also thank them for maintaining an amazing work environment, pleasurable to just the extent not interfering with science.

I must add to this list, Prof. C. N. R. Rao, not just for his re-invigorating lectures, but for showing me, in the summer of 2006, for the first time, how fundamentals of chemistry could be brought to life, and how fruits of proper reasoning coincide with outcome. In the same context, I would like to thank Vivek and Dr. Govindaraj, for being of great help during my summer project at Carbon Lab.

Further, I thank Prof. Kulkarni, for guidance during my lab course at JNC, and as the Int. Ph. D. convener, for giving us anything that we so desired, including the hike in the scholarship. I would like to express my gratitude to the complab and CCMS system admins, especially Vikas, Ershaad and Amit for their help and support in matters least known to me, installing packages on Linux platforms. Last but not the least; I would thank Sukanya Ma'am and Princy Ma'am for their utmost help, and the smiles, even when course cards came signed a month late.

I believe too many friends never spoil the evening, but the names of those too many can never be penned down here, for it is very un-overwhelming to find a thesis where the page count for the acknowledgement section overrides that for the subject matter. I would thus end this never-ending list here, and beg forgiveness from those people whose names I unavoidably could not write here, and from those about whom two lines should never be enough.

Table of Contents

Synopsis

In the present thesis, we have attempted to elucidate the nature of dipolar interactions, hydrogen bonding and charge transfer in various technologically promising molecules and their polymorphs and between certain large systems like carbon nanotubes (CNTs) and metal clusters, focusing particularly on the structural variation, electrical and electronic properties of such species. Through various structural modifications, we have tried to modulate the extent of charge transfer by tweaking the strength of hydrogen bonding and other weak interactions like dipole-dipole interactions in these systems. Our findings support that such interactions are particularly important in modulating carrier mobilities in, and linear and non-linear optical responses of these classes of systems. We also find that Coulombic charge transfer between metal clusters and CNT in the metal-CNT composites result in semiconductor to metal transition.

The thesis is divided into five chapters:

The first chapter provides a brief introduction to non linear optics (NLO), the theory of Davydov Splitting and carrier (electron and hole) mobilities from the standpoint of Marcus' theory and Quantum-Classical equations. Computational methodologies together with mathematical expressions for the optical and transport properties discussed in the preceding chapters have also been illustrated in detail.

In the second chapter, we investigate the effect of intramolecular dipolar interactions in governing the NLO responses of free base porphyrin. Free base porphyrin has four pyrrole rings arranged in a coplanar arrangement in such a fashion that the dipole moments of the pyrrole rings trans to each other cancel, resulting in a net zero dipole moment of the overall molecule. On the other hand, for N-confused porphyrin, a synthetic molecule, one of the pyrrole rings is such that its N atom is located outside the macrocyclic cavity. For this molecule, the dipole moment of the pyrrole ring trans to the one confused, no longer cancels, resulting in a non-zero ground state dipole moment. We describe in this chapter how systematically distorting one pyrrole ring out of the co-

planar condition results in a non-zero dipole moment of the molecule, together with its NLO responses.

In the third chapter, we consider co-operative phenomena in Magnesium complexes of structurally similar molecules like Bacteriochlorin, Chlorin and Porphyrin to understand the nature of long range dipole-dipole interactions, and how such phenomena affect the light absorption of oligomers of such systems. We find that monomers of these molecules in the Light Harvesting Complexes (LHCs) are not planar, the Mg atom being around 0.4 - 0.6 Å out of the plane of the porphyrinoid structural moiety. We find that the cross sections of optical absorption are larger for the non-planar conformations than the corresponding planar conformations of all the systems. We also estimate the differences in light absorption cross-sections of the oligomers of these systems, particularly considering relative geometrical orientations similar to those found in the LHCs.

In the fourth chapter, we consider linear hydrogen bonded chains of urea and thio-urea and their derivatives to understand the effect of the varying nature of bonding on the NLO responses and charge mobilities in such linear chains. While molecules of Urea, N,N'-Dimethyl Urea, Thiourea and N,N'-Dimethyl Thiourea are held in their respective linear chains by hydrogen bonding, N,N,N',N' Tetramethyl Urea and N,N,N',N' Tetramethyl Thiourea are held together in linear chains by dipolar interactions. We attempt to elucidate the contribution of electrostatic forces and mixing of low-energy states in the intermolecular interactions in these systems. We find that the linear polarizability (α) increases linearly with increasing chain length; however the first order non-linear optical response (β) shows an oscillatory behavior. We elucidate such behavior of β from a simple two-state picture.

Finally, in the fifth chapter, we consider the nature of interactions between metallic and semiconducting CNTs and metal clusters in elucidating the semiconductor-metal transitions of these composites. We consider the noble metals Au and Pt, and present our results from calculations on various clusters and chains of the metals physisorbed onto CNTs. We find that the semiconducting CNTs upon interaction with the physisorbed metal clusters become metallic. Metallic CNTs, however, fail to show transition to semiconductors upon adsorption of metal clusters onto them.

Chapter I

I. Introduction:

This introductory chapter is divided into the following three sections:

1. **Introduction to Non-Linear Optical Phenomenon in molecules and materials**
2. **Introduction to the Exciton Theory of Molecular Interactions**
3. **Introduction to the Charge Carrier Mobilities in Organic Molecular Solids**

1.1 Introduction to Non-linear Optical Phenomena in Molecules and Materials

A molecule undergoes distortion when exposed to an external electric field. The atoms develop a separation of charges that leads to the formation of instantaneous dipoles which tend to counteract the external electric field, which leads to charge separation. In the case where there is an electromagnetic radiation, its oscillating electric field component creates dipolar oscillation in the system. The system then emits light of frequency as that of the oscillating dipole. Since there can be an out-of-plane component of this induced electromagnetic wave, there occurs a phase shift in the emerging wave. This phase shift is the refractive index of the medium.

Under the influence of this external oscillating electric field, the material becomes polarized, with an induced dipole moment. Each constituent molecule acts as a dipole, with a dipole moment, P_i. The dipole moment vector per unit volume P is given by,

$$P = \sum_i P_i \qquad (1.1.1)$$

where, the summation is over the dipoles in the unit volume. The induced polarization in the material depends upon the strength of the (oscillating) electric field. For a weak field one can write the polarization as,

$$P = \chi E \qquad (1.1.2)$$

where, χ is called the polarizability of the medium. The polarizability is related to the dielectric constant (ε) of the medium by,

$$\varepsilon = 1 + 4\pi\chi \tag{1.1.3}$$

If we consider the polarization of a molecule or an atom, rather than that of the material as a whole, the (molecular) polarization can be written as,

$$\mu_i = \alpha E \tag{1.1.4}$$

where, α corresponds to the polarizability of the molecule. The polarizability of the total system is directly proportional to the number of charges present in it.

The wavelike properties of light are described by an oscillating electromagnetic field, *E(r,t)* . Consequently, the material response *P*, and its linear susceptibility are also time and space dependent properties. Thus the equation (1.1.2) modifies to,

$$P(r,t) = \sum_{r_i} \chi_{rr_i} E(r_i,t) \tag{1.1.5}$$

Thus it can be seen that the polarization can be induced in a different direction to that of the electric field. This occurs due to the fact that the polarizability is a tensorial quantity.

Nonlinear optical processes

After the invention of lasers [1], the field of optics took a new turn, especially towards its nonlinear aspects. This is because the intensity of the lasers being high, the non-linear aspects of polarization by light become more prominent. The bulk polarization P, for strong external field is then defined by a phenomenological power series expansion in terms of the external applied electric field as [2-4]:

$$P = \chi^{(1)}E + \chi^{(2)}EE + \chi^{(3)}EEE + ... \tag{1.1.6}$$

where, $\chi^{(n)}$ is the n^{th} order susceptibility of the medium and E represents the total electric field experienced by the system. The n^{th} order susceptibility is a tensor quantity of rank (n+1) which has 3^{n+1} elements [5]. Thus, $\chi^{(1)}$ is a second rank tensor with nine elements, $\chi^{(2)}$ is a third rank tensor with twenty seven elements, $\chi^{(3)}$ is a fourth order tensor with eighty one elements, and so on. This number is of course drastically reduced by symmetry requirements as all the elements are not linearly independent, and in most practical materials much fewer elements are required to describe the tensor. Thus, on the

application of a strong electric field, the optical characteristics of a medium which depend on the susceptibility, such as dielectric permittivity and refractive index etc., all become a function of the field [6-9].

Although optoelectronic effects like Pockel's [10] and Kerr's [11] effects were known much before lasers came into practice, the possibility of exploiting a monochromatic light beam for the production of non-linear optical phenomenon was first experimentally shown by Frenken *et al* [12]. They observed ultraviolet light at twice the frequency of ruby laser (λ = 6493 Å), when the light was made to travel through a quartz crystal. Also about at the same time there were examples of multi-photon absorption processes through which one could access high energy states which are otherwise forbidden by dipolar transitions, with relatively low energy photons [13].

These experiments attracted huge attention from the science community and marked the beginning of a rich field called *Nonlinear optics* [14, 15]. The field experienced a tremendous growth with the development of newer lasers [16, 17]. The developments of lasers are due to the seminal works of Townes, Basov, and Prokhorov (Nobel Prize 1964) [18] and N. Bloembergen (Nobel Prize 1981) [19]. In short, lasers are sources of coherent light, characterized by a high degree of monochromaticity, high directionality, and high intensity or brightness. With dye lasers it is possible to range over the entire spectrum of visible light and even to the near IR region.

The manifestation of the non-linear optical behavior can be clearly seen by substituting a sinusoidal field $E = E_0 + E_1 \cos \omega t$ in the place of the static electric field in equation(1.1.6), to get:

$$P = (E_0 + E_1 \cos \omega t)\chi^{(1)} + (E_0 + E_1 \cos \omega t)^2 \chi^{(2)} + (E_0 + E_1 \cos \omega t)^3 \chi^{(3)} + \ldots \quad (1.1.7)$$

Rearranging the above equation,

$$\begin{aligned} P = {} & (\chi^{(1)} E_0 + \chi^{(2)} {E_0}^2 + \chi^{(3)} {E_0}^3) \\ & + (\chi^{(1)} E_1 + 2\chi^{(2)} E_0 E_1 + 3\chi^{(3)} {E_0}^2 E_1) \cos \omega t \\ & + (\chi^{(2)} {E_1}^2 + 3\chi^{(3)} E_0 {E_1}^2) \cos^2 \omega t \\ & + (\chi^{(3)} {E_1}^3) \cos^3 \omega t \end{aligned} \quad (1.1.8)$$

Using the relations $\cos^2 \omega t = (1 + \cos 2\omega t)/2$, $\cos^3 \omega t = (\cos 3\omega t + 3\cos \omega t)/4$ one gets:

$$
\begin{aligned}
P = {} & \chi^{(1)}[E_0 + E_1 \cos\omega t] \\
& + \chi^{(2)}[{E_0}^2 + \frac{1}{2}{E_1}^2 + 2E_0E_1\cos\omega t + \frac{1}{2}{E_1}^2\cos 2\omega t] \\
& + \chi^{(3)}[{E_0}^3 + \frac{3}{2}E_0{E_1}^2 + 3{E_0}^2E_1\cos\omega t + \frac{3}{4}{E_1}^3\cos\omega t \\
& \quad + \frac{3}{2}E_0{E_1}^2\cos 2\omega t + \frac{3}{4}{E_1}^3\cos 3\omega t] + \ldots
\end{aligned}
\tag{1.1.9}
$$

The first terms in the brackets for all $\chi^{(n)}$ are constant factors. They give rise to a dc field across the medium.

Second-Order Optical Processes

Now let us consider the processes associated with the $\chi^{(2)}$ in details. From equation(1.1.9),

$$
P^{(2)} = \chi^{(2)}[{E_0}^2 + \frac{1}{2}{E_1}^2 + 2E_0E_1\cos\omega t + \frac{1}{2}{E_1}^2\cos 2\omega t] \tag{1.1.10}
$$

The coefficient E_0E_1 corresponds to the linear electro-optic effect and is represented as $\chi^{(2)}(-\omega;\omega,0)$. The sign attached to a frequency is negative if the photon is emitted and is positive if a photon is absorbed. The last term which is multiplied to the squared ac electric field and has a frequency 2ω in equation (1.1.10) is called the second harmonic generation. Considering that two coherent light waves of unequal frequencies ω_1 and ω_2 are traveling in the medium, the 2nd and 4th terms from equation (1.1.10) become:

$$
\chi^{(2)}\frac{1}{2}{E_1}^2[\cos(\omega_1 - \omega_2)t + \cos(\omega_1 + \omega_2)t] \tag{1.1.11}
$$

Thus, one has two new frequencies $(\omega_1 + \omega_2)$ and $(\omega_1 - \omega_2)$. This phenomenon is known as *optical mixing*. While $(\omega_1 + \omega_2)$ is called sum-frequency generation (SFG), $(\omega_1 - \omega_2)$ is called the difference frequency generation (DFG). The SHG process, actually, is a special case of SFG where the frequencies of both the photons are equal, i.e. $\omega_1 = \omega_2$.

A solution or glass, in its natural form being random, does not exhibit any second order effect. For biological systems, important second order effects are associated with interference and electric field poling. Surface induced SHG from a biological membrane

provides a powerful method for SH imaging for selectively probing interactions and dynamics involving membranes [20]. The electric field induced SHG, also called EFISH provides an excellent probe for membrane potentials and has been found to be very promising for use in bio-imaging [21, 22].

Symmetry requirement for Second Order Processes

In 1962, it was proposed by Kleinman that in many non-linear processes, where all the interacting frequencies are far away from resonances, energy is simply exchanged between the fields and not dissipated in the medium [23, 24]. This amounts to susceptibility tensors being invariant under any permutation of their Cartesian indices. For instance, in the $\chi^{(2)}$, the symmetry relations give rise to:

$$\chi^2_{ijk} = \chi^2_{ikj} = \chi^2_{jik} = \chi^2_{jki} = \chi^2_{kij} = \chi^2_{kji} \qquad (1.1.12)$$

Thus due to Kleinman symmetry relations, the number of independent components of $\chi^{(2)}$ reduces from 27 to 10.

For a medium to exhibit frequency conversion processes mediated by $\chi^{(2)}$, the medium must have non-zero $\chi^{(2)}$. This condition requires that at a molecular level the non-linear coefficient β must be non-zero. Furthermore, the orientationally averaged sum of β at all sites that give rise to macroscopic $\chi^{(2)}$ should not be zero. These two conditions lead to the following symmetry requirements for the realization of $\chi^{(2)} \neq 0$:

1. For non-centrosymmetric molecules (i.e. molecules with without any inversion symmetry), β being an odd rank (3^{rd} rank) tensor, is not zero.
2. The molecules in the bulk are arranged in a non-centrosymmetric structure. Only then the overall $\chi^{(2)}$ is non-zero.

A molecular design often uses systems like D-(linkers)-A, where the Ds and As are usually polar moieties, and are very efficient in increasing the dipole moment of the total systems drastically. The linkers may be composed of π-conjugated chains, dipolar aggregates or hydrogen bonded molecules. Classic examples of systems where the linkers are π-conjugated chains are linear chains of para-nitroaniline. Linear chains of

dipolar systems, as well as hydrogen bonded chains have been extensively considered for the realization of high values of second order polarizability coefficients [25, 26].

Calculation of Non-linear Optical Polarizabilities

For the calculation of microscopic nonlinearities, there are many approaches. The three most extensively used methods will be introduced here. These are *Finite field approach, Sum-Over-States approach,* and *Correction Vector Method*.

Finite field approach:

The finite field approach expands the energy of the system in terms of the static field, F as:

$$E(F) = E(0) - \mu_i F_i - \frac{1}{2}\alpha_{ij}[F_i F_j] - \frac{1}{6}\beta_{ijk}[F_i F_j F_k] - \frac{1}{24}\gamma_{ijkl}[F_i F_j F_k F_l]... \quad (1.1.13)$$

The optical response functions are μ, α, β and γ are the 1st, 2nd, 3rd, and 4th order derivatives of the energy with respect to the static field respectively. These derivatives are calculated numerically using a five point formula, where the energies at five different field conditions; F = 0, F = F, F = 2F, F = -F and F = -2F, and a truncated series of the above expansion is used to derive the various order derivatives [27, 28]. For example,

$$\alpha_{ii} = \frac{[\frac{5}{2}E(0) - \frac{4}{3}[E(F_i) - E(-F_i)] + \frac{1}{12}[E(2F_i) - E(-2F_i)]}{F_i^2} \quad (1.1.14)$$

$$\beta_{iii} = \frac{[E(F_i) - E(-F_i) - \frac{1}{2}[E(2F_i) - E(-2F_i)]}{F_i^3} \quad (1.1.15)$$

Although this method has been quite popular, it suffers from the following limitations:
The numerical n-point formula for calculation of the energy derivatives is valid only at very low field strengths like 0.001 Volt. The energies need to be extremely accurate for the calculation of the derivatives. As the molecular integrals in quantum chemical

calculations are seldom more accurate than 10^{-21} eV, the finite field procedure for the calculation of hyperpolarizabilities may be not be reliable enough.

Sum-Over-States Approach:

The sum over states (SOS) approach has its basis in a perturbation theory method developed by Ward and Orr to account for the effects of an externally applied electromagnetic field on the motion of the electrons [29, 30]. Under the influence of the oscillating field the electrons will be perturbed and the resulting polarization in the molecule can be obtained by the inclusion of the field as a perturbation

$$H^1 = -e(Er)\sin\omega t \tag{1.1.16}$$

to the Hamiltonian and collecting terms of appropriate orders in the electric field. In this expression, E is the amplitude of the field and r is a coordinate associated with the position of the electrons and is calculated from

$$r = \sum_a r_a \tag{1.1.17}$$

in which a is summed over all the electrons and

$$-e.r = \mu \tag{1.1.18}$$

The polarizabilities and hyperpolarizabilities are expressed as an infinite sum over various excited states in which the numerators contain dipolar integrals of the type

$$\langle m|\mu_{p=i,j,k}|n\rangle \tag{1.1.19}$$

where $m \neq n$. It corresponds to the transition dipole moment between the two states m and n. The expression for the polarizability is then given by,

$$\alpha_{ij}(\omega) = \sum_m \frac{e^2}{\hbar}\left[\frac{\langle g|\mu_i|m\rangle\langle m|\mu_j|g\rangle}{(\omega_{mg}-\omega)} + \frac{\langle g|\mu_j|m\rangle\langle m|\mu_i|g\rangle}{(\omega_{mg}+\omega)}\right] \tag{1.1.20}$$

In this expression ‘g’ refers to the ground state and ‘m’ refers to excited state with $\omega_{mg} = \omega_m - \omega_g$. The first hyperpolarizability term $\beta[-(\omega_p+\omega_q);\omega_p,\omega_q]$, which is responsible for the SHG, is given by,

$$\beta_{ijk}[-(\omega_p+\omega_q);\omega_p,\omega_q] = P\sum_{mn}\frac{e^3}{2\hbar^2}[\frac{\langle g|\mu_i|n\rangle\langle n|\mu_j|m\rangle\langle m|\mu_k|g\rangle}{(\omega_{ng}-\omega_p-\omega_q)(\omega_{mg}-\omega_p)} + \frac{\langle g|\mu_j|n\rangle\langle n|\mu_i|m\rangle\langle m|\mu_k|g\rangle}{(\omega_{ng}+\omega_q)(\omega_{mg}-\omega_p)} + \frac{\langle g|\mu_j|n\rangle\langle n|\mu_k|m\rangle\langle m|\mu_i|g\rangle}{(\omega_{ng}+\omega_q)(\omega_{mg}+\omega_p+\omega_q)}] \quad (1.1.21)$$

The symbol P indicates that the summations must be performed over all permutations of the Cartesian indices i, j and k, with the electric field frequencies ω_p and ω_q. This summation generates terms that are products of the transition dipole moment matrix elements and also the sums and differences of the dipole moments between the ground states and the excited states, as well as between various excited states. The above expression simplifies to an interestingly simple equation if one considers the properties of the molecule to be approximated by the simple two-state model. The two-state model can be appreciated from a Davydov approach, as discussed in the next section of the current chapter.

Correction-vector Method:

In practice the SOS method can be expected to give valid results if the systems are such that the convergence is rapid, especially considering the fact that the excited states are added as a perturbative expansion. For the case of linear polarizability, this criterion is met, as the small number of excitations associated with charge transfer across the system is the main contributor to the linear polarizability of the system. However for the calculations of hyperpolarizabilities, a slow convergence poses a problem for the computation of a large number of excitations. This makes the calculation of hyperpolarizabilities extremely slow.

Another method developed by Soos and Ramashesa [31], for the computation of NLO coefficients, involves the variational calculation of the first and second order correction vectors $\phi_i^{(1)}(\omega_1)$ and $\phi_{ij}^{(2)}(\omega_1,\omega_2)$ to the unperturbed ground state in the presence of perturbation. These vectors can be solved from the two inhomogeneous linear equations as:

$$(H - E_0 + \omega_1 + i\varepsilon)\left|\phi_i^{(1)}(\omega_1)\right\rangle = \tilde{\mu}_i \left|G\right\rangle \quad (1.1.22)$$

$$(H - E_0 + \omega_2 + i\varepsilon)\left|\phi_{ij}^{(2)}(\omega_1)\right\rangle = \tilde{\mu}_j \left|\phi_i^{(1)}(\omega_1)\right\rangle \quad (1.1.23)$$

where, H is the unperturbed Hamiltonian, E_0 is the ground state energy, ω_1 and ω_2 are frequencies, and $\tilde{\mu}_i$ is the component of the dipole displacement operator, $\tilde{\mu}_i = \hat{\mu}_i - \langle G|\hat{\mu}_i|G\rangle$ and ε is the average lifetime of the excited states. Once the correction vectors are calculated, the NLO coefficients can be readily determined as:

$$\alpha_{ij}(\omega) = \left\langle \phi_i^{(1)}(\omega_1)\right| \hat{\mu}_j \left|G\right\rangle + \left\langle \phi_i^{(1)}(-\omega_1)\right| \hat{\mu}_j \left|G\right\rangle \quad (1.1.24)$$

$$\beta_{ijk}(\omega_1, \omega_2) = P_{ijk}[\left\langle \phi_i^{(1)}(-\omega_1 - \omega_2)\right| \hat{\mu}_j \left|\phi_k^{(1)}(\omega_2)\right\rangle] \quad (1.1.25)$$

where P_{ijk} are permutation operators. The tumbling average quantities $\bar{\alpha}, \bar{\beta}$ are defined as:

$$\bar{\alpha} = \frac{1}{3}\sum_i (\alpha_{ii})$$
$$\bar{\beta} = \sqrt{\sum_i \beta_i \beta_i^*} \quad ; \quad \beta_i = \frac{1}{3}\sum_i (\beta_{ijj} + \beta_{jij} + \beta_{jji}) \quad (1.1.26)$$

where the sums are over the coordinates *x, y, z,* and β_i^* refers to the conjugate of the β_i vector. The advantage of defining the tumbling average NLO coefficients is that it allows for the comparison of the calculated results with the values from experiments. It maybe noteworthy to mention that low values of electric field (typically, electric field of up to 0.5 volt/nm) do not perturb the nuclear geometry of the system or the lattice and are sufficient for the polarization of electronic states and thus can be safely incorporated in theoretical calculations [32].

1.2 Introduction to the Exciton Theory of Molecular Interactions

The development of materials with large NLO responses is of great technical, industrial and synthetic importance particularly from the standpoint of optical materials that are used in the propagation of light. In this regard, the response of materials to an external electric field has received tremendous focus, from the lasers to optical switches. Some of the best NLO responses are showed by organic π-conjugated materials [33]. Another added advantage of using organic systems is that they are easy to synthesize, and integrate into a device, and very importantly properly orienting them into the device is very easy [34]. The 'orientation' is very crucial in realizing the full potential of these materials.

When we talk about the importance of orientation, we mean that by varying the orientation of the molecules in the materials or aggregates, we can manipulate the electronic states of the system towards realization of higher NLO responses. It would thus be of fundamental interest to understand theoretically the role of changing orientation in molecular aggregates on the energy shift and polarization of local environments. In the following section we present the exciton theory based on the Davydov splitting for molecular aggregates considering different orientations of the monomers.

Exciton model for the molecular aggregates:

We discuss here a basic model to explain the electronic excitations of one-dimensional molecular aggregates. The exciton theory is the theory of interaction between the excitonic states formed as a result of electron correlation. In self assembled aggregates with low packing densities, the excitons are considered to be Frenkel excitons where the electron and hole of a mono-excitation are located on the same molecular site. To develop a simple theory, composite molecules are considered, which includes van der Waals dimers, trimers and higher order aggregates. As has been shown [35], if the direct

overlap between the chromophoric MOs is negligible, then the exciton interactions can be expressed in the direct product basis of the chromophoric MOs.

The zeroth order Hamiltonian for the mth molecule alone in an aggregate can be written as

$$H_m = \sum_k |k_m\rangle (E^{k,m}) \langle k_m| \tag{1.2.1}$$

where, k_m specifies the kth electronic state of the m^{th} molecule. The wavefunction for the N number of molecules (in an aggregate) can be approximated by a linear combination of product functions $|k_1, k_2, ..., k_m, ...k_N\rangle$ where the k$_m$'s are the kth electronic states for the m^{th} molecule. If the electronic exchange interactions are considered, the excitations will be the admixtures of charge transfers states which correspond to Wannier type excitons. However it is assumed here that intermolecular distances are too large to make electron exchange effects quite negligible, at least in low order. The ground state of N molecules is then the tensorial product of the molecular ground states.

$$|G\rangle = |G_1, G_2, ..., G_m, ...G_N\rangle \tag{1.2.2}$$

Each molecular excitation gives rise to a band of N degenerate product states in the zeroth order. For excitation 'e' in the mth molecule, it reads

$$|m, e\rangle = |G_1, G_2, ..., G_{m-1}, e_m, G_{m+1}, ...G_N\rangle \tag{1.2.3}$$

In general the spatial structure of an aggregate is not well defined. However, translational symmetry can be assumed to be valid in case of a molecular crystalline system. Here, the case of a perfect molecular aggregate is considered. The exciton coupling interaction term is denoted as $H_{m,n}$ for the interaction between the monomers, m and n. the energy expressions are derived with the general $H_{m,n}$ terms. For the N monomers, energy matrix for an excitation e, for the perturbation $H_{m,n}$ will have the general form

$$[E_{mn}] = E_G(N-1) + \begin{pmatrix} E_e & H_{1,2} & H_{1,3} & \cdots & H_{1,N} \\ H_{2,1} & E_e & H_{2,3} & \cdots & H_{2,N} \\ H_{3,1} & H_{3,2} & E_e & \cdots & H_{3,N} \\ \vdots & \vdots & \vdots & \vdots & \vdots \\ H_{N,1} & H_{N,2} & H_{N,3} & \cdots & E_e \end{pmatrix} \tag{1.2.4}$$

where, E_G and E_e are the ground state energy and energy of the excitation 'e' respectively. The matrix is assumed to be symmetric. However the above equation can be solved for a number of limited cases. Imposing either periodic or open-boundary condition in a one-dimensional case, the energies of the N perturbed states can be written as,

$$E(q) = (N-1)E_G + E_e + 2H_{m,m+1}\cos q + 2H_{m,m+2}\cos 2q + 2H_{m,m+3}\cos 3q + ... \quad (1.2.5)$$

where, the energies are written in momentum space, *q*. We note here that for both periodic and open boundary conditions, the *q* space energies are same, although the wavefunctions are completely different.

An analytical solution of the above expression can be obtained only for the nearest neighbor case. Assuming $H_{m,m+1}$ as the strongest coupling, and therefore, neglecting all other types of coupling, the width of the excitation band *e* can be estimated to be $4H_{m,m+1}$ for periodic and $4H_{m,m+1}\cos(\pi / N+1)$ for the open chain case. However if all other $(|m-n|>1)H_{m,n}$ couplings are considered, the width will be increased by 25% of the nearest neighbor values. Moreover, the allowed transition is different for two different boundary conditions. For an open chain, the allowed transitions are to the states with $q = \pi/(N+1), 2\pi/(N+1), ..., N\pi/(N+1)$. For the periodic chain, however, the transitions are to the momentum states with $q = 0, \pi/N, 2\pi/N, ..., (N-1)\pi/N$ values. In the subsequent discussion, we consider the expressions for the coupling element $H_{m,n}$, between *m* and *n*, and then discuss the consequences of the arrangement of monomer molecules on the allowed electric dipole transitions.

For dipolar molecules, the strongly allowed transition would be to the lowest exciton state and the coupling interactions can be approximated at large distances by a point-dipole model. Assuming all molecules to be the same, the coupling interactions can be written as,

$$H_{m,n} = \frac{\vec{M}_{ij} \bullet \vec{M}_{ij}}{r_{mn}^3} - \frac{3(\vec{M}_{ij} \bullet \vec{r}_{mn})(\vec{M}_{ij} \bullet \vec{r}_{mn})}{r_{mn}^5} \quad (1.2.6)$$

where, $\vec{M}_{ij}$ is the transition dipole moment from state *i* to state *j* of the monomer and $\vec{r}_{mn}$ is the vectorial distance between the molecular centers *m* and *n*. It is to be noted that both

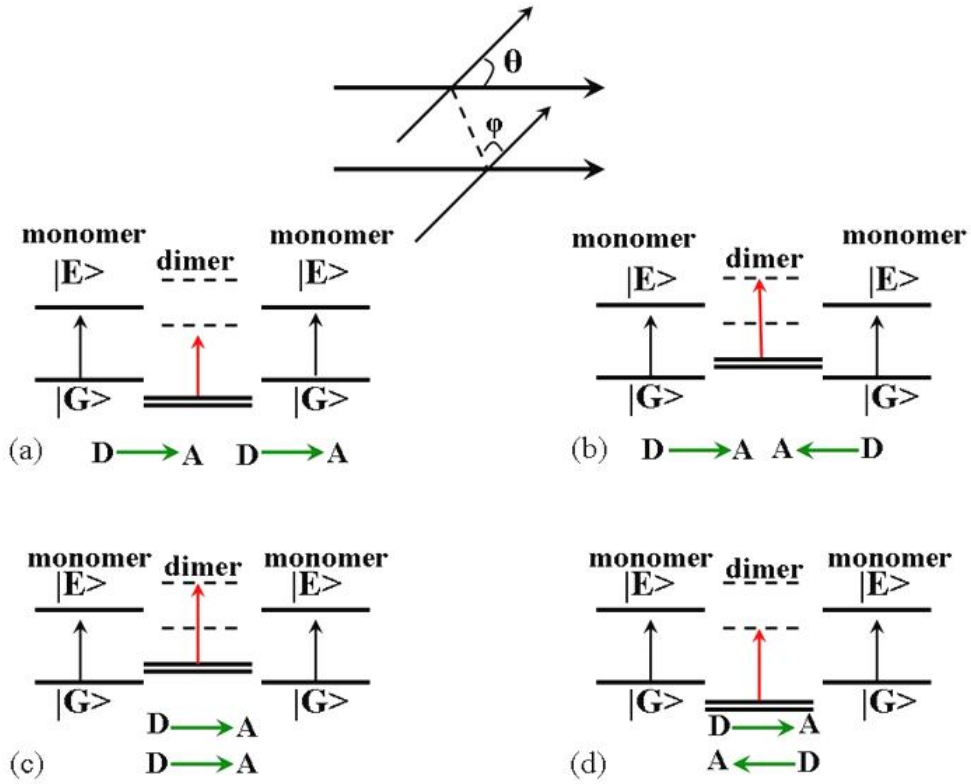

Figure 1.2.1: schematic representation of excitonic splitting due to dipole-dipole interactions for various molecular orientations. The arrows indicate the vector quantities. ϕ is the angle between the dipoles and θ is the angle between the dipole and its molecular axis. Different orientations of the monomers are shown in the dimeric system, with $D \to A$ representing the dipolar axis. Each molecule has tow levels, $|G\rangle$ and $|E\rangle$. The arrows between the states indicate the allowed transitions. The split states of the composite systems are indicated by dashed lines.

the transition dipole moment and the molecular axis, being vectorial quantities, the magnitude of interaction will depend crucially on the relative orientations of the dipolar molecules as well as on the axis joining their centers. We shall present here a quasi-classical vector treatment to this interaction as we assume electrostatic interaction between the transition moments.

Excitation Spectra in Molecular aggregates:

A number of cases can be analyzed where the dipolar monomers are arranged in various orientations. Let us assume that in the aggregate the chromophores are arranged as shown in figure 1.2.1. The directions shown there correspond to the polarization axis of the corresponding chromophores. The aggregate is constructed such that the chromophores are oriented with an angle ϕ between them and an angle θ created between each monomer with its molecular axis. It is quite simple to derive the splitting energy in this case, from equation (1.2.6),

$$\Delta E = 2\frac{M_{gs}^2}{r_{mn}^3}(\cos\phi - 3\cos^2\theta) \qquad (1.2.7)$$

Therefore a singlet excited state of the monomer molecule would split according to the angles (θ,ϕ). Let us now derive the splitting patterns for the dimer. The ground state and the excited state in the two monomers can be expressed as $|g_1\rangle, |e_1\rangle$ and $|g_2\rangle, |e_2\rangle$ respectively. On the formation of the head-to-tail arrangement of the dimer, $\theta,\phi = 0,0$, as shown in figure 1.2.1.a, the ground state of the dimer $|G\rangle = |g_1 \bullet g_2\rangle$ is stabilized by a favorable dipole-dipole attractive term while the excited state splits into $|E_1\rangle = \frac{1}{\sqrt{2}}[|e_1 \bullet g_2\rangle + |g_1 \bullet e_2\rangle]$ and $|E_2\rangle = \frac{1}{\sqrt{2}}[|e_1 \bullet g_2\rangle - |g_1 \bullet e_2\rangle]$. Since the dipolar interaction is attractive for the head to tail arrangement, $|E_1\rangle$ is lower in energy than $|E_2\rangle$. The dipole-allowed transition is $|G\rangle \rightarrow |E_1\rangle$ while $|G\rangle \rightarrow |E_2\rangle$ is forbidden. Clearly the transition energy is smaller for the allowed transition when compared to that of the transition for the monomers. Thus a red shift is observed in the absorption spectra.

Interestingly, for the repulsive head-to-head dipolar arrangement, the ground state is destabilized, and the excited states are given as $|E_1\rangle = -\frac{1}{\sqrt{2}}[|e_1 \bullet g_2\rangle + |g_1 \bullet e_2\rangle]$ and $|E_2\rangle = -\frac{1}{\sqrt{2}}[|e_1 \bullet g_2\rangle - |g_1 \bullet e_2\rangle]$. In this case $|E_1\rangle$ is greater in energy than $|E_2\rangle$. Thus the allowed transition $|G\rangle \rightarrow |E_1\rangle$ involves larger energy and the absorption maximum will be blue shifted.

We consider next, another arrangement of dipoles that one commonly comes across while perusing crystal structures of various molecules. These are the stacked parallel or anti-parallel arrangements, as shown in figure 1.2.1.b. For the parallel arrangement, the ground state of the dimer $|G\rangle = |g_1 \bullet g_2\rangle$ is destabilized due to unfavorable interactions, while the excited state splits into two: $|E_1\rangle = \frac{1}{\sqrt{2}}[|e_1 \bullet g_2\rangle + |g_1 \bullet e_2\rangle]$ and $|E_2\rangle = \frac{1}{\sqrt{2}}[|e_1 \bullet g_2\rangle - |g_1 \bullet e_2\rangle]$. However, now due to dipole-dipole repulsion $|E_1\rangle$ is destabilized in comparison to $|E_2\rangle$. On the other hand, when we consider stacked anti-parallel arrangement, both $|G\rangle$ and $|E_1\rangle$ are stabilized, and the transition corresponds to $|G\rangle \rightarrow |E_1\rangle$.

However what we must remember is that the linear and the stacked arrangements are specific cases, and should be easily derived from a generalized case, where the dipolar arrangement is not linear. For such generalized cases, both the states $|E_1\rangle$ and $|E_2\rangle$ are accessible from the ground state, with varying oscillator strengths depending on the transition electric dipoles.

1.3 Introduction to the Charge Carrier Mobilities in Organic Molecular Solids

The study of charge transport in organic semiconductors and bio-molecules alike has been a subject of great interest since the past two decades [36]. This interest arises not only from the technological viewpoint which involves the application of this knowledge to further the development of devices like Field Effect Transistors (FETs) [37], and Organic Light Emitting Diodes (OLEDs) [38], but also in understanding the role of charge carriers in governing the biological functions of DNA, Metal-DNA complexes [39], as well as complex biological photo-active systems like Porphyrins and bacterial membrane proteins [40]. The discovery of organic molecules exhibiting electroluminescence [41] has further fuelled the interest in these quantities.

In any conductor, the specific electrical conductivity, σ, is defined by Ohm's law:

$$j = \sigma E \tag{1.3.1}$$

where, j is the current density and E is the applied electric field. Typical values of σ range from $10^{-30}\ \Omega^{-1}cm^{-1}$ to $10^{10}\ \Omega^{-1}cm^{-1}$. Schematically shown in figure 1.3.1, organic semiconductors have σ values in the lower region of the schematic.

In the simplest case of any conducting solid, the current is due to only a single type of charge carrier with a charge q (which is equal to e, the electronic charge, for electron conductors). The density of these carriers is then denoted as n_e. If the charge carriers then move with a drift velocity v_D, an electric current flows with the current density, given by,

$$j = qn_e v_D \tag{1.3.2}$$

$v_D = \langle v \rangle$ is the mean value of the velocity of all the charge carriers. In an electric field we have,

$$v_D = \frac{\sigma}{qn_e} E \tag{1.3.3}$$

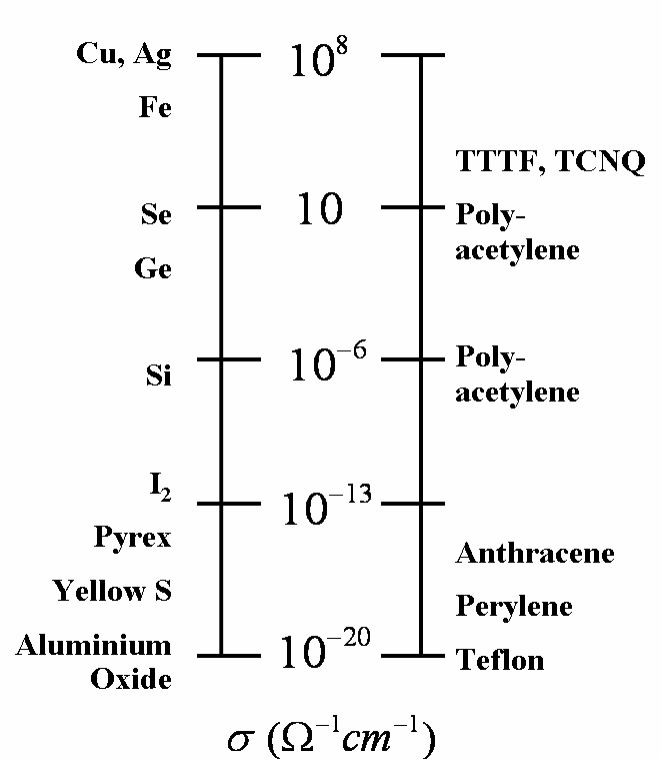

Figure 1.3.1: Typical specific electrical conductivities of some common materials.

The proportionality constant in the relation between v_D and E is called the charge carrier mobility μ. Thus,

$$v_D = \mu E \tag{1.3.4}$$

It is important to note here that the quantity μ is independent of the electric field, and hence intrinsic to a particular material. As the drift velocity, v_D, is an average over all the charge carriers, the choice of a good conductor should be such that the electron and hole mobilities be similar in magnitude. To this regard, materials like amorphous Si prove to be very promising, particularly because the magnitudes of both the electron and hole mobilities are comparable, and individually high, thus adding up to the total mobility of the system.

In general, due to the amorphous nature of organic solids, charge densities within the materials are strongly localized on the atomic positions. In materials governed by positional and energetic disorder, charge transport occurs via hopping [42] between the

localized sites. The description of hopping transport can be adequately simplified by employing the concept of transport energy, E_t [43]. Charge carriers in shallow energy sites ($Ei < E_t$) will hop to sites with lower energy ($Ei < E$) that are close by. For charge carriers at lower energy sites ($Ei > E_t$), the most probable hop upwards in energy is a hop to a site with $E \sim E_t$, regardless of the value of Ei. This means that hopping transport processes within the system are dependent on E_t [44]. In organic semiconductors, the transport energy plays the role of the mobility edge, which in inorganic non-crystalline semiconductors, is the energy separating the delocalized sites from the localized sites in the conduction or valence bands.

Thus, organic conductors have mobilities that are very less when compared to the typical values of inorganic systems like amorphous Si. However, the advantage of using organic conductors is that they are light weight and considerably easy to synthesize. Further, recent research demonstrates the use of polymers of thiophene derivatives to have charge carrier mobilities comparable to that of amorphous Si [45]. However, the challenge to increase the values of charge carrier mobilities to at least half the value as that for inorganic systems still remains for both technologists and scientists alike. To this regard, molecular modeling can provide insights for the selection and fine-tuning of the materials [46].

Single crystals of organic conductors provide pathways of hopping through intermolecular weak forces such as π stacking and subtle interactions such as C-H$\cdots\pi$ interactions. In fact, these weak intermolecular forces effectively control the packing of molecules in crystals and thin films [47]. Even very small variation of these forces leads to the formation of different polymorphs [48]. The geometry of the crystal plays a very important role in governing the strength of these weak interactions. Hence, the extent to which these interactions provide hopping pathways is greatly altered by the geometry of the crystal. The charge carrier mobilities, especially for that of the electron, are extremely sensitive to the presence of traps and disorders in the solid state [49]. Generally, for most π conjugated organic systems, the hole conductance values are at least an order more than that for the electron. For a few systems like perylene and some related structures, however, the values of electron mobilities are larger than the hole mobilities [50].

Methodology for the calculation of Charge Carrier Mobilities in Organic Molecular Solids:

Charge hopping in most organic and inorganic semiconductors can be adequately modeled by the Marcus Theory of Non-Adiabatic electron transfer reactions. In order to understand the foundation of such a theory, we first need to understand what is adiabatic and diabatic (more commonly called non-adiabatic) electron transfer. According to the IUPAC gold book [51], electron transfer process in which the reacting system has to cross over between different electronic surfaces while passing from reactants to products, is called a diabatic process. For non-adiabatic electron transfer, the electronic transmission factor is much lesser than unity. On the other hand, adiabatic electron transfer processes are those in which there is no change of electronic state or multiplicity. In such a process, no quantum jump occurs from one electronic state (say, the reactant state, in which the electron density is more localized on the donor end of the complex) to the other (the product state, in which the electron density is more localized on the acceptor end of the complex, in this case); instead the electron lingers at the barrier, and the curves smooth out to form a continuum, with a quasi state at the top of the activation barrier. DeVault's explanation [52] is: "Briefly, since nuclear motion is generally much slower than electronic motion, one can approximate the electronic part of the wavefunction of a molecular system by solving for it with nuclei fixed in position. The electronic energy eigenvalues obtained this way, when plotted as a function of the nuclear positions, form adiabatic surfaces which form potential energy surfaces for nuclear motion. However, when the nuclei are allowed to move, the wavefunctions arrived at by this approximation are no longer exactly eigenfunctions and they can change spontaneously from one to another. The matrix elements causing the changes are made from the terms neglected in the approximation and are called 'non-adiabaticity operator'. This operator involves derivatives of both electronic and nuclear wavefunctions with respect to nuclear coordinates". The reactions which are non-adiabatic are usually for systems that have weakly coupled donor and acceptor electronic states.

To a reasonable approximation, each hopping process can be understood as a non adiabatic electron transfer reaction. For such cases we utilize the Markus theory to calculate the rate of charge transfer (W) between neighboring molecules.

$$W = \frac{2H_{mn}^2}{h}\left(\frac{\pi^3}{\lambda k_B T}\right)^{\frac{1}{2}} \exp\left(-\frac{\lambda}{4k_B T}\right) \tag{1.3.5}$$

where, H_{mn} is the coupling element between the a pair (*m,n*) of molecules, and λ is the reorganizational energy, k_B is the Boltzmann constant, and T is the temperature (300 K for our calculations). The reorganization energy, λ, is defined as the change in the free energy if the reactant state were to distort to the equilibrium configuration of the product state without transfer of the charge.

From equation (1.3.5), it is clear that the rate of hopping (W) would be high if the reorganization energy (λ) is low, and intermolecular coupling (H_{mn}) is high.

Between any pair of molecules, the diffusion coefficient is related to the hopping rate as,

$$D = \frac{1}{2d}\sum_i r_i^2 W_i^2 \tag{1.3.6}$$

where, d is the dimensionality of the system, r is the distance between the pairs of molecules considered, and W_i is the probability of the charge carrier hop to the i^{th} neighbor, normalized over the total hopping rate ($\sum_i W_i$).

The drift mobility, μ, due to hopping can then be evaluated from the Einstein relation for a given temperature, as,

$$\mu = \frac{e}{k_B T} D \tag{1.3.7}$$

where, e is the electronic charge.

The reorganizational energy (λ) contains both inner-sphere (λ_i) and outer sphere (λ_o) components; $\lambda = \lambda_i + \lambda_o$. Generally, the λ value depends on fast changes in the molecular geometry (the inner sphere contribution) and slow variations in the solvent polarizations of the surrounding medium (the outer sphere contribution). In the case of gas-phase calculations, however, the latter contribution is generally neglected, so that the changes in the molecular geometry (as the system proceeds from the reactant state to the

product state) become the dominant factor. The reorganizational energy depends on the charge carrier considered. For hole conductors, the reorganizational energy is calculated as,

$$\lambda_{hole} = (E_{+}^{*} - E_{+}) + (E_{cation}^{*} - E) \quad (1.3.8)$$

where, E is the optimized ground state energy, E_{+} is the optimized energy of the cationic molecule, E_{cation}^{*} is the energy of the neutral molecule in cationic geometry, and E_{+}^{*} is the energy of the cationic molecule in neutral geometry. Similarly, for the electron conductors, the reorganizational energy is calculated as,

$$\lambda_{electron} = (E_{-}^{*} - E_{-}) + (E_{anion}^{*} - E) \quad (1.3.9)$$

where, E is the optimized ground state energy, E_{-} is the optimized energy of the anionic molecule, E_{anion}^{*} is the energy of the neutral molecule in anionic geometry, and E_{-}^{*} is the energy of the anionic molecule in neutral geometry. However it is very important to note that the reorganizational energy of a particular molecule, be it either an electron conductor or a hole conductor, in the gas phase, is very different from that of the molecule in the crystal. This is because for the molecule in the crystal structure, there are many neighboring interactions that perturb the electronic structure of the molecule sufficiently to yield completely different reorganizational energy values.

At the molecular level, one of the key parameters for the calculation of charge carrier mobilities is the electron transfer element H_{mn}, which expresses the ease with which the charge carrier may be transferred between two interacting molecular systems. For most organic semiconductors, it is sufficient to consider the frontier orbitals of the interacting molecular species. In such a case, for calculating the electron transfer matrix element, H_{mn}, between two adjacent molecules, we use Markus-Hush two-state model [53], where HOMO and LUMO of both the monomers constituting the dimer are considered. Due to electrostatic interactions between the monomers, which are labeled as the donor and acceptor , the double degeneracy of both the HOMO and LUMO is lifted, giving four levels corresponding to HOMO-1, HOMO, LUMO, LUMO+1 of the dimer. The transfer matrix element for the hole and electron conductors in a homonuclear system (same site energies) are calculated as,

$$H_{mn}^{hole} = \frac{1}{2}\left(E_{HOMO}^{\text{dimer}} - E_{HOMO-1}^{\text{dimer}}\right)$$
$$H_{mn}^{elect} = \frac{1}{2}\left(E_{LUMO+1}^{\text{dimer}} - E_{LUMO}^{\text{dimer}}\right) \quad (1.3.10)$$

From the standpoint of this theory, it is assumed that the role of the intermolecular interactions between the dimers considered is to provide virtual orbitals that create an effective electronic coupling between them. This reduces the problem of the whole system to an effective two-state Hamiltonian consisting of only donor and acceptor states. It is noteworthy to mention here that, at low temperatures, for weak (non-bonded) interactions between molecular species in a crystal, the charge transport can be described by a band like regime similar to that of inorganic semiconductors [54]. Just as in molecular species, where the electron and hole mobilities are directly proportional to the splitting of the monomer LUMO and the HOMO levels respectively, in infinite aggregates of weakly interacting molecular species, higher the LUMO and HOMO bandwidths, the higher the electron and hole mobilities. The splitting of the monomer HOMO and LUMO levels for small molecular species and larger aggregates are shown schematically in figure 1.3.2. From this theoretical background, we calculate the charge carrier mobilities in the systems as and when discussed in the later chapters of this thesis.

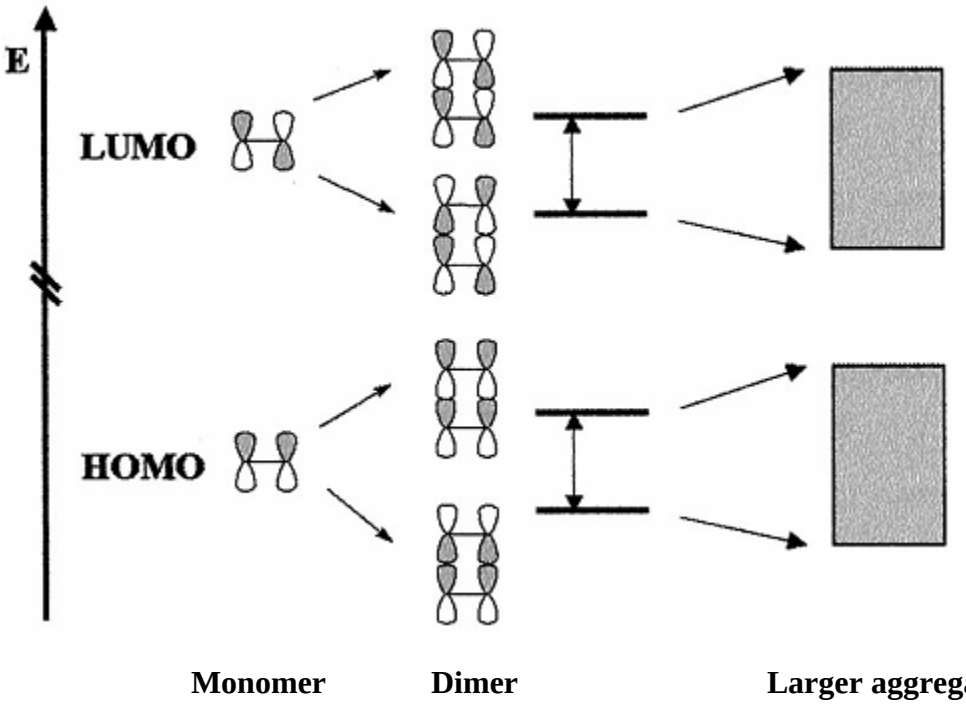

Figure 1.3.2: Schematic diagram of the splitting of HOMO-LUMO levels indicated for two molecules of ethane in stacked orientation, as well as for a large number of molecules in an infinite aggregate resulting in bands. Note that, the extent of splitting depends on the orientation and proximity of the stacked molecules, and the energies of splitting shown here are not to scale.

References:

[1] Maiman, T. H., *Nature*, 1960, **187**, 493.

[2] *Nonlinear Optical Properties of Organic Molecules and Crystals*, Chemla D. S., Zyss J., Academic Press, 1987.

[3] *Introduction to Nonlinear Optical Effects in Molecules and Polymers*, P. N. Prasad P. N., Williams D. J., Wiley (New York), 1991.

[4] *Lasers and Nonlinear Optics*, Laud B. B., New Age Intl., 1991.

[5] *Nonlinear Optical Materials*, ACS Symposium series, 628, Karna S. P. and Yeats A. T., (Eds.), Washington D. C., 1996.

[6] *Optical Nonlinearities in Chemistry*, Burland D. M., (Ed.), *Chem. Rev*., 1994, **94** (special vol.).

[7] *Nonlinear Optics*, Boyd R., 2nd edition, Academic Press, 2003.

[8] Williams D. J., *Angew. Chem. Intl. Ed*., 1984, **23**, 690.

[9] Marks T. J., Ratner M. A., *Angew. Chem. Intl. Ed*., 1995, **34**, 155.

[10] Pockels F., zu Göttingen A. d. G. d. W., Math. Phys. Klasse, 1893, **39**, 1.

[11] Kerr J., *Phil. Mag*., 1875, **50**, 337.

[12] Franken P. A., Hill A. E., Peters C. W., Weinrich G., *Phys. Rev. Lett*., 1961, **7**, 118.

[13] Goppert-Mayer M., *Annu. Phys*., 1931, **9**, 273; Kaiser W., Garett C. G. B., *Phys. Rev. Lett*., 1961, **7**, 229.

[14] Bloembergen N., Shen Y. R., *Phys. Rev. Lett*., 1964, **12**, 504.

[15] *Topics in Non-Linear Optics*, Selected papers of Bloembergen N., Indian Academy of Science, 1982.

[16] Hagen W. F., Magnante P. C., *J. App. Phys*., 1969, **40**, 219.

[17] Kleinmann D. A., *Phys. Rev*., 1962, **125**, 87.

[18] www.nobelprize.org/nobel_prizes/physics/laureates/1964/

[19] www.nobelprize.org/nobel_prizes/physics/laureates/1981/

[20] Eisenthal K. B., Yan E. C. Y., *Biophys. J*., 2000, **79**, 898.

[21] Fine S., Hansen W. P., *Appl. Oct*., 1971, **10**, 2350.

[22] Bouevitch O., Lewis A., Pinevsky L., Wuskell J. P., Loew L. M., *Biophys. J*., 1993, **65**, 672.

[23] Kleinmann D., *Phys. Rev*., 1962, **125**, 87.

[24] Kleinmann D., *Phys. Rev*., 1962, **128**, 1761.

[25] Moliner V., Escribano P., Peris E., *New J. Chem*., 1998, **387**.

[26] Castet F., Champagne B., *J. Phys. Chem. A*., 2001, **105**, 1366.

[27] Kurtz H. A., Stewart J. J. P., Dieter K. M., *J. Comput. Chem*., 1990, **11**, 82.

[28] Sophy K. B., Pal S., *J. Chem. Phys*., 2003, **118**, 10861.

[29] Ward J., *Rev. Mod. Phys*., 1965, **37**, 1.

[30] Orr B. J., Ward J. F., *Mol. Phys*., 1971, **20**, 513.

[31] Ramasesha S., Soos Z. G., *Chem. Phys. Lett*., 1988, **153**, 171; Soos Z. G., Ramasesha S., J. *Chem., Phys*., 1989, **90**, 1067.

[32] Champagne B., *Chem. Phys. Lett.*, 1996, **261**, 57.

[33] Polymers for Second-Order Nonlinear Optics, Lindsay G. A., Singer K. D. (Eds.), ACS Symposium Series 601, Washington D.C., 1995.

[34] Ball P., *Nature*, 2007, **445**, 363.

[35] *Theory of Molecular Excitons*, Davydov A. S., McGraw-Hill, New York, 1962.

[36] Burroughes J. H., Bradley D. D. C., Brown A. R., Marks R. N., Mackey K., Friend R. H., Burns P. L., Holmes A. B., *Nature*, 1990, **347**, 539; F. Garnier F., R. Hajlaoui R., A. Yassar A., Srivastava P., *Science*, 1994, **265**, 1684; Katz, *J. Mater. Chem*., 1997, **7**, 369; Scherf U., List E. J. W., *Adv. Mater*., 2002, **14**, 477.

[37] *Handbook of Oligo- and Polythiophenes*, Katz H. E., Dodabalapur A. and Bao Z. (Eds.), Wiley-VCH, Weinheim, Germany, 1999.

[38] Umeda T., Tokito S., Kumaki D., *J. Appl. Phys*., 2007, **101**, 4517.

[39] Kwok H.L., *Nanobiotechnology : IEE Proceedings*, 2004, **151**, 193.

[40] *Microwave charge carrier hall mobility measurements on cytochrome-oxidase prepared from heavy beef heart mitochondria* , Journal of Bioenergetics and Biomembranes, Springer Netherlands, 2005, **3**.

[41] Bernanose A., *Br. J. Appl. Phys*., 1955 , **6**, S54-S55; Frederiksen P., Bjørnholm T., Madsen H. G., Bechgaard K., *J. Mater. Chem*., 1994, **4**, 675.

[42] Conwell E. M., *Phys. Rev*., 1956, **103**, 51; Mott N. F., *Canadian J. Phys*., 1956, **34**, 1356.

[43] Grunewald M., Thomas P., phys. stat. sol. (b), 1979, **94**, 125.

[44] Baranovskii S. D., Faber T., Hensel F., Thomas P., *J. Phys.: Condens. Matter*, 1997, **9**, 2699.

[45] McCulloch I., Heeney M., Bailey C., Genevicius K., MacDonald I., Shkunov M., Sparrowe D., Tierney S., Wagner R., Zhang W., Chabinyc M. L., Kline R. J., McGehee M. D., Toney M. F., *N. Mat*., 2006, **5**, 328.

[46] Kafer D., Witte G., *Phys. Chem. Chem. Phys*., 2005, **7**, 2850; Sundar V. C., Zaumseil J., Podzorov V., Menard E., Willett R. L., Someya T., Gershenson M. E., Rogers J. A., *Science*, 2004, **303**, 1644.

[47] Debije M. G., Chen Z., Piris J., Neder R. B., Watson M. M., Mullend K., Wurthnerb F., *J. Mater. Chem.*, 2005, **15**, 1270.

[48] Bernstein J., *J. Phys. D: Appl. Phys*., 1993, **26**, B66.

[49] Ellman B., Nene S., Semyonov A. N., Twieg R., J., *Adv. Mater*., 2006, **18**, 99; Ellman B., *J. Chem. Phys*., 2006, **125**, 074702.

[50] Jones B. A., Ahrens M. J., Yoon M. H., Facchetti A., Marks T. J., Wasielewski M. R., *Angew. Chem., Int. Ed*., 2004, **43**, 6363; Hammond R. B., Roberts K. J., Smith E. D. L., Docherty R., *J. Phys. Chem. A*, 1999, **103**, 7762 and references therein.

[51] Gold Book, PAC, 1996, **68**, 2223.

[52] DeVault, D., *Q. Rev. Biophys*., 1980, **13**, 387.

[53] Grimme S., J. Comput. Chem., 2004, **25**, 1463.

[54] J. L. Bredas, J. P. Calbert, D. A. Silva Filho, J. Cornil, *Proc. Natl. Acad. Sci. USA*, 2002, **99**, 5804.

Chapter II

II. The Role of Intramolecular Dipolar Interactions in fine-tuning the Linear and Non-linear Optical Responses in Porphyrins

Introduction:

Porphyrins have been molecules of long and sustained interest in chemistry and biology because of their central role in photosynthesis, biological redox processes and oxygen transport [1-5]. The diverse applications for this molecule with seemingly small changes around the side-chains of the core tetrapyrrole moiety (chlorophyll-a and chlorophyll-b) has remained unexplained till date [6-11]. Similarly, the origin of cooperative phenomenon in oxygen-binding processes in hemoglobin and myoglobin is yet to be understood from a molecular viewpoint [12-14]. Interestingly, the basic structure of the porphyrin skeleton remains preserved across the full phylogenic tree with minor genetic mutations from the anaerobic to the aerobic world. Apart from the biological importance of this molecule, there has been a tremendous interest in porphyrin-based derivatives for molecular materials [15-20]. Assemblies of porphyrins have been shown to exhibit promising applications in molecular wires for one-dimensional electronic conduction, photonic-wires, ferroelectric bistability and non-linear optical responses [21-23]. The second-harmonic generation from porphyrins with varied donor-acceptor strengths has been studied in great details in the last decade from both theoretical and experimental standpoints [24-27]. Similarly, the absorption and emission spectra of porphyrins have been a subject of detailed quantum-chemical modeling from both semi-empirical as well as ab-initio treatments [28-36].

However, recent progress in the synthesis of porphyrin based molecules has led to isolation of many porphyrin-derivatives that are either conformational or configurational isomers of the parent molecule. The most-common of such systems belong to the class of molecules called N-confused porphyrin [NCP] wherein the N-end of a pyrrole ring is situated outside the central cavity and instead a C-H group points towards central cavity [37-40]. The porphyrin molecule has four dipoles (the pyrrole rings) pointing to the

central cavity. In the free base porphyrin, H_2Por, two trans pyrrole rings each have a proton attached to them, whereas the other two do not. If the porphyrin chelates to a divalent metal, all pyrrole rings become identical, and the most stable structure has D4h symmetry. The M-Por molecule then maybe considered as a system where four dipoles are situated on the vertices of a square, as shown in figure 2.1. The overall dipole moments of both the H_2Por and M-Por are zero because in either case all the in-plane dipole moments of the pyrrole rings cancel each other.

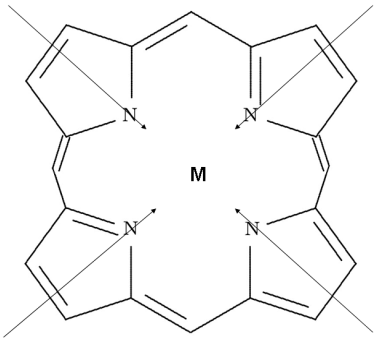

Figure 2.1: Metal Porphyrin [M-Por] indicating the dipole moments of the four pyrrole rings constituting the central cavity of the Porphyrin macrocycle.

Thus, we find it interesting to study the variation in the opto-electrical response functions in porphyrin with changing the conformation and configuration in the pyrrole rings in this chapter. Changing the orientation of the pyrrole rings leads to variations in the inter-dipolar interactions. We present the results on our systematic study on the role of dipolar interactions in controlling the linear and non-linear responses in porphyrins.

Results and Discussion:

The geometry optimized structures for porphyrin and N-confused (Ncp) porphyrin are shown in figure 2.2. All the calculations are performed at B3LYP/6-31+G(d) level with removal of the vibrational instabilities through additional frequency calculations. Porphyrin is perfectly planar (figure 2.2(A)) while the structure of NCP is puckered with the N-cp ring being distorted from the plane of the other three pyrrole rings by 32.9 degrees (figure 2.2 (C) and (D)). It is important to note that NCP is a configurational

isomer of porphyrin and it cannot be realized from a simple dipolar rotation of one pyrrole ring of the parent porphyrin. However, one can realize interesting conformations in porphyrin through conformational twists as shown in the scheme figure 2.2 (A) to figure 2.2 (B). The parent porphyrin structure is associated with a dihedral twist (φ) of 0 degrees while the perpendicular orientation of the ring is realized through a dihedral twist of φ=90 degrees (figure 2.2 (B)).

The rotation of the pyrrole ring (as shown in figure 2.2 (A)) leads to a situation where the dipole moments of the pyrrole rings no longer cancel each other completely. This results in the molecule developing a dipole moment. However, this also results in a destabilization of the molecule. We show the variation in the ground-state energy of porphyrin with increase in the distortion angle (ϕ), as shown in figure 2.3 (A). For a distortion of 90 degrees, the structure is destabilized by 10 kcal/mol. We have verified that additional distortion in the system leads to steric interaction of the rotating pyrrole ring with the two central N-H groups in the cavity. Thus, further rotation of the pyrrole ring above 90 degrees will be unpractical. Figure 2.3 (B) shows the variation in the ground state dipole moment of the porphyrin ring with increase in the distortion. The computed magnitude of the dipole-moment (at B3LYP/6-31+G(d) level) increases with increase in distortion. However, such distortion also involves increase in the dipole-moment in the system through simple-dipolar addition. For the ground-state structure of porphyrin, the dipole-moment of the system is zero due to anti-parallel orientation of the dipoles of the pyrrole rings (inter-dipolar angle between opposite rings along the X and Y axes is 180 degrees). With distortions, the inter-dipolar angle reduces from 180 degrees to 90 degrees for the opposite rings along the Y-axis while the inter-dipolar angle between the pyrrole rings along X-axis remains fixed at 180 degrees. Thus, a simple classical dipolar picture predicts that the total ground state dipole-moment for the system can be predicted from a vector sum of the two dipoles along the Y-axis with changing inter-dipolar angles (ϕ).

$$\mu_{effective}^2 = 2\mu_1^2[1+\cos(180-\phi)] \qquad (2.1)$$

where, μ_1 is dipole-moment of a single pyrrole ring. The dipole-moment of a single pyrrole ring is computed to be 1.858 Debye. The variation in the additive magnitude of

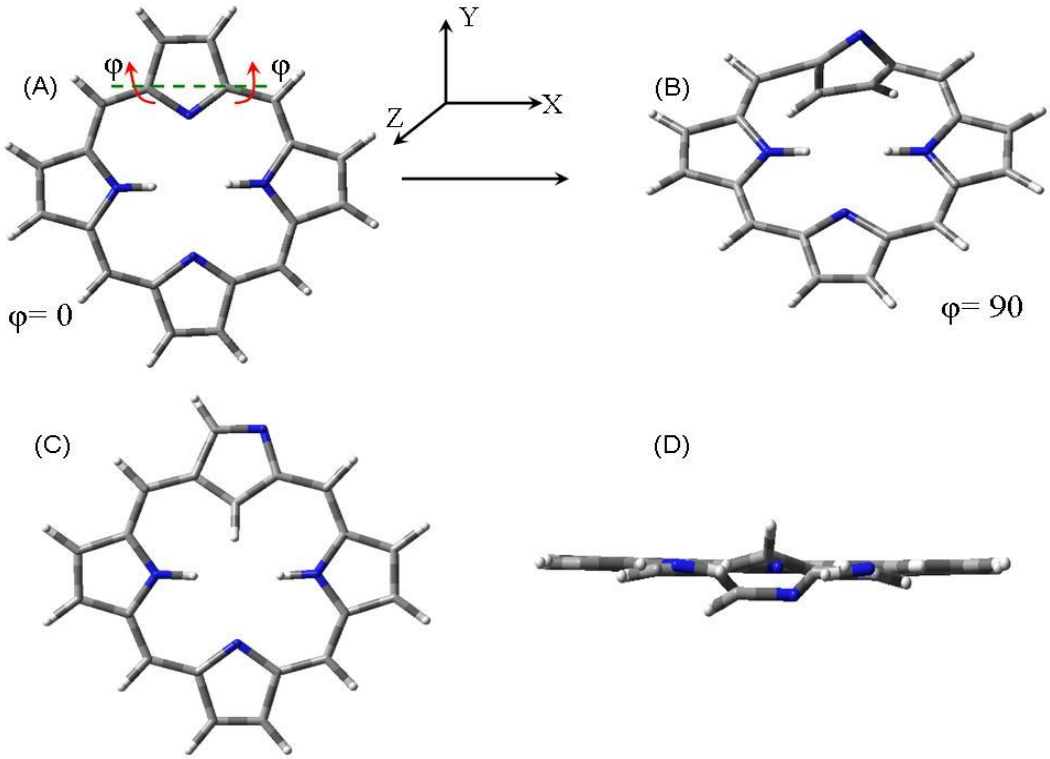

Figure 2.2: (A) Geometry optimized structure for porphyrin. ϕ represents the dihedral angle of distortion. (B) Distorted structure of porphyrin with ϕ = 90. (C) Molecular structure of NCP and (D) Molecular structure of NCP (side-view).

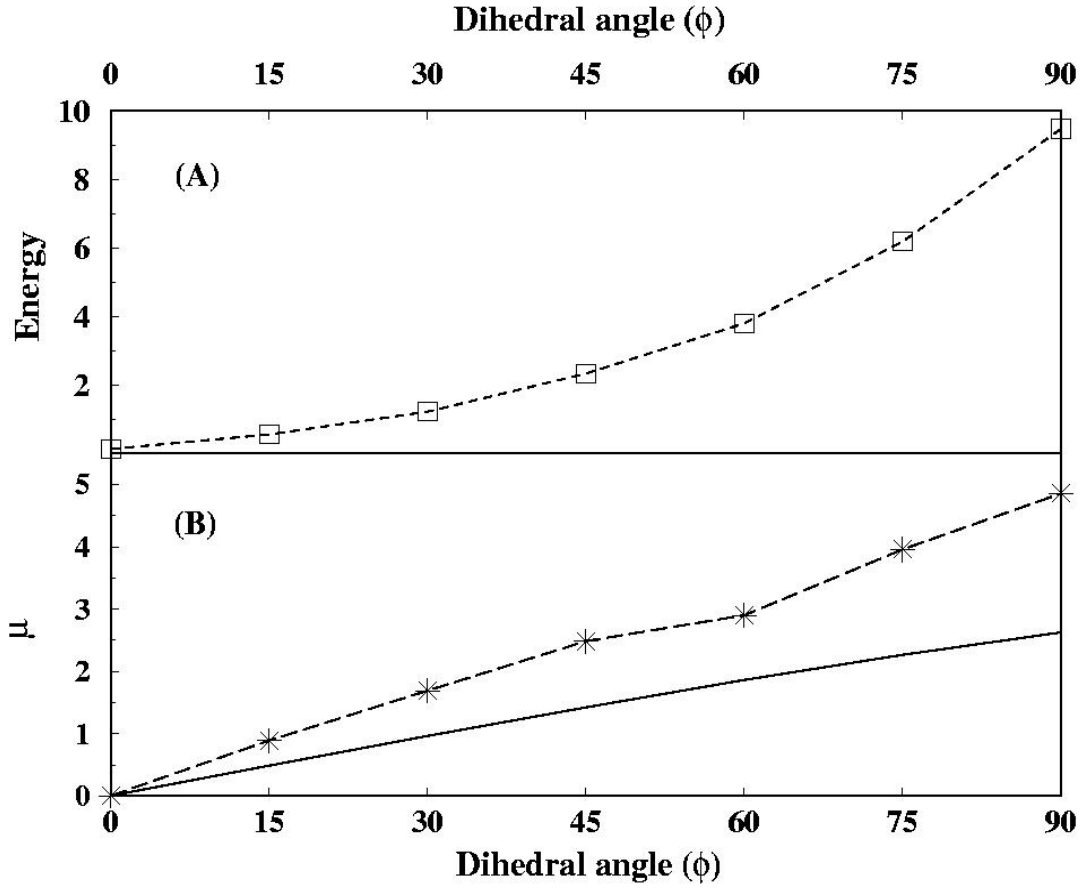

Figure 2.3: (A) Variation in the energy (in kcal/mol) for porphyrin with increase in the distortion angle (ϕ). (B) Variation in the calculated ground state dipole moment (in Debye), dotted line with stars; and variation in the additive vector sum of the dipole moment (in Debye), solid line, with increase in the distortion angle (ϕ).

the dipole moment is shown as a solid line in figure 2.3 (B). The calculated magnitude of the dipole-moment exceeds the analytical value, more so for larger distortion.

For a more detailed understanding of the non-classical origin of enhanced dipole-moment, we have analyzed the Mülliken charges on the N-atom of the pyrrole ring being distorted. For ϕ=0, both N-atoms in the two pyrrole rings along the Y-axis have $q = +0.472e$. However, with progressive distortions, negative charge is built over the N-atom of the distorted ring and for ϕ=90, while the charge on the planar N-atom of the pyrrole ring remains unchanged, the N-atom on the distorted pyrrole ring has $q = -0.622e$. The variation in charge on the N atom with successive distortions is shown in figure 2.4. Such a large localization of electrons over the N of the distorted ring is a direct consequence of the fact that distortion leads to non-parallel orientation of the p_z orbitals. Such non-parallel orientation of the π orbitals leads to charge-separation which accounts for enhanced dipole-moment.

Next, we consider the variation of the linear and non-linear optical responses with the gradual conformational changes described above. The change in the linear and non-linear optical responses is directly related to the change in the ground state dipole moment. In figure 2.5, we show the variation in the magnitudes of the dynamic linear and non-linear optical coefficients of porphyrin with increase in the distortion angle. All the calculations were performed at dynamic electric field strength of 0.0428 a.u corresponding to the Nd:YaG laser (1064 nm) [41, 42]. As can be seen, the magnitude of the polarizability (in figure 2.5 (A)) increases with increase in the distortion. The variation in the various response functions associated with 1st hyperpolarizability like static component (in figure 2.5 (B)), second harmonic coefficient (in figure 2.5 (C)) and optical rectification (OR) /electro-optical Pockel's effect (EOPE) (in figure 2.5 (D)) show almost identical behavior. While the static component as well as the OR/EOPE steadily increase with distortion and increases substantially at ϕ=90, the SHG coefficient which shows an odd-even oscillation also exhibits a large increase at ϕ=90.

For a clear understanding of the variation in the optical response functions, we have analyzed the HOMO-LUMO gap in the system with increase in the distortion (figure 2.6). As can be seen from figure 2.6 (A), the gap decreases steadily with increase

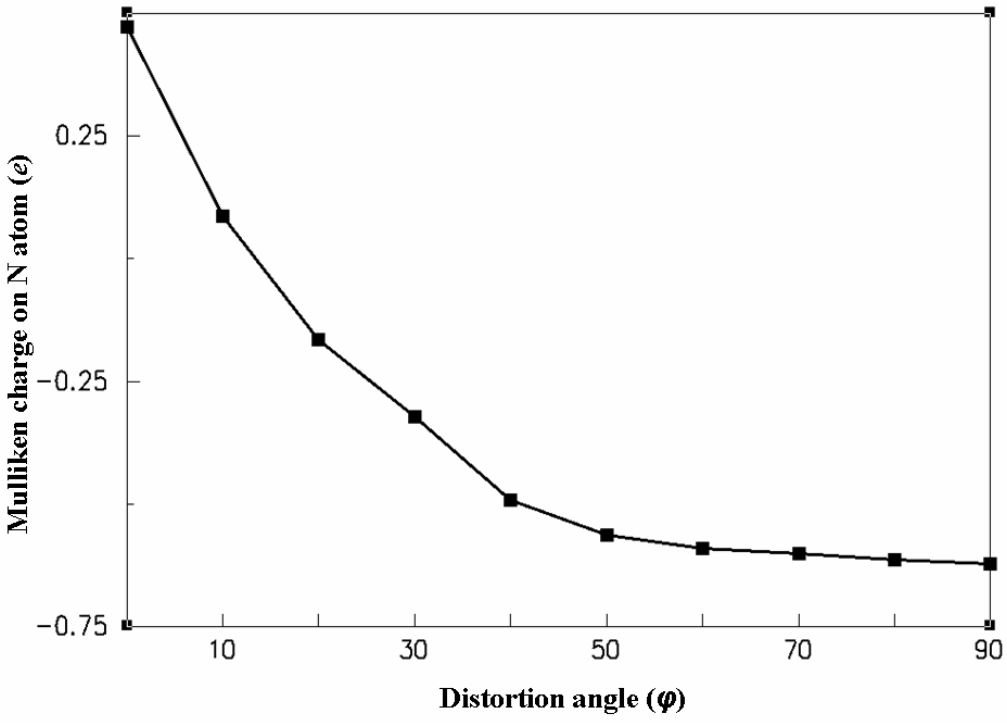

Figure 2.4: Variation of the Mulliken charge (*e*) on the N atom of the pyrrole ring being distorted from $\phi = 0^0$ to $\phi = 90^0$.

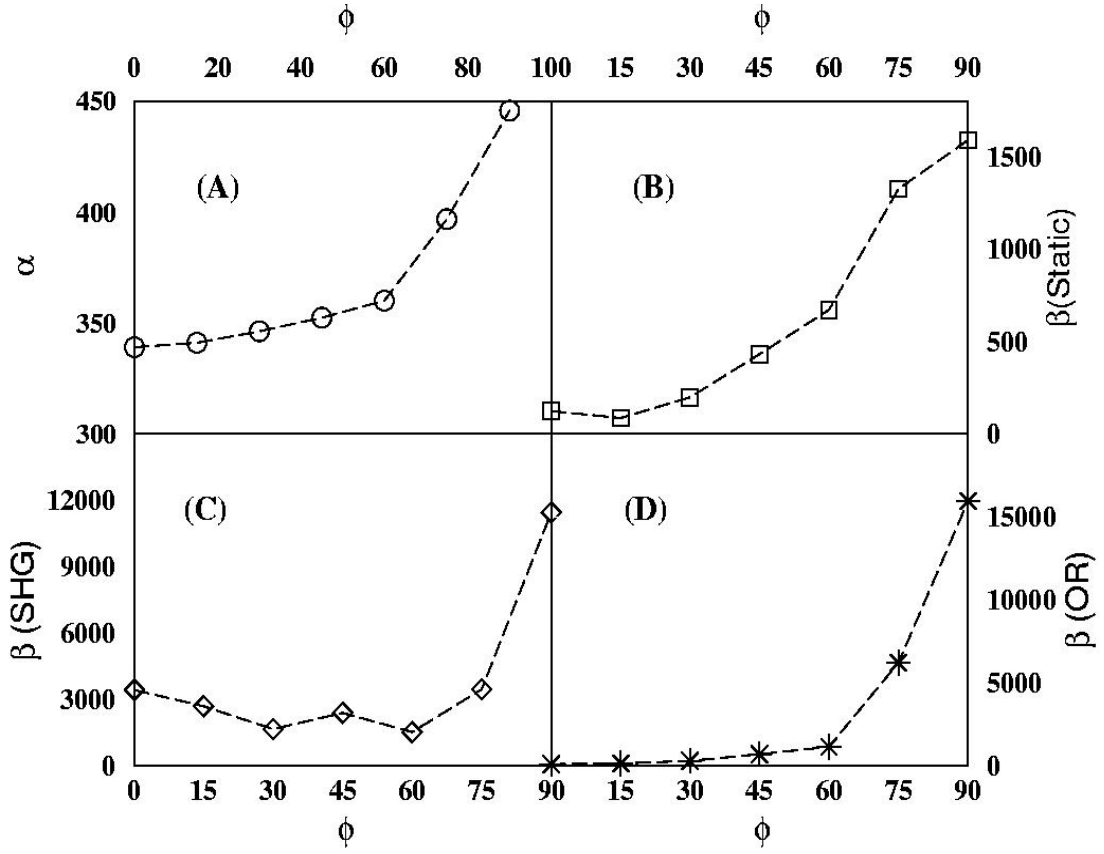

Figure 2.5: Variation in the polarizability (A) (in a.u), static 1st hyperpolarizability (B) (in a.u), second harmonic generation (C) (in a.u) and optical rectification (D) (in a.u) for porphyrin with increase in the distortion angle (ϕ).

in the distortion. For ϕ=90, the gap decreases to the lowest value of 1.0 eV. The origin of the reduction in the gap for the system can be understood by studying the variation in the exciton splitting from a simple dipolar interaction model, as discussed in chapter 1 of the current thesis. The excitonic splitting for two dipoles with an inter-dipolar angle (ω) is given by,

$$\Delta E = 2\mu_1\mu_2\left(\cos\omega - 3\cos\theta_1\cos\theta_2\right)/\, r_{12}^3 \tag{2.2}$$

where, μ_1 and μ_2 are transition dipole of the monomers, r_{12} is the distance between the centre-of-masses of the dipolar molecules and θ_1 and θ_2 are angles made by the transition dipoles with the r_{12} vector [43-47]. TD-DFT calculation at the B3LYP/6-31+G(d,p) level reveals that a single pyrrole molecule (non-protonated) has a transition dipole moment of 0.646 a.u. Substituting this in equation (2.2) and noting that $\omega = 180 - \phi$, we obtain the variation in the splitting energy, as shown in figure 2.6 (B).

However, as discussed in chapter 1, it is important to note that for ϕ=0, the dipole-allowed transition occurs to higher energy excited state from the ground-state. As one of the pyrrole rings is distorted from the plane of the porphyrin molecule, the gap due to the excitonic splitting decreases. This effectively reduces the gap for the system (shown schematically as a red arrow). From the standpoint of the two-state model discussed in chapter I, the 1st hyperpolarizability, β, is given as,

$$\beta_{two-level} = \frac{2e^2}{2\hbar^3}\frac{\omega_{ge} f_{ge} \Delta\mu_{ge}}{(\omega_{ge}{}^2 - \omega^2)(\omega_{ge}{}^2 - 4\omega^2)} \tag{2.3}$$

where, ω_{ge} is the optical transition energy, f_{ge} is the associated oscillator strength, and $\Delta\mu_{ge}$ is the difference between the ground- and excited-state dipole moments.

It is evident from equation (2.3) that, both the linear polarization term, α, as well as the 1st hyperpolarizability, β, are inversely proportional to the gap for the system. Thus, with increase in the distortion, which leads to a reduction in the gap should lead to an enhancement in α and β. This is almost the case as seen from figure 2.4, where both polarizability and the various 1st hyperpolarizability terms increase with increase in the distortion. However, it is important to note that the sudden increase in polarizability and the 1st hyperpolarizability at large distortion angles is a direct consequence of the large

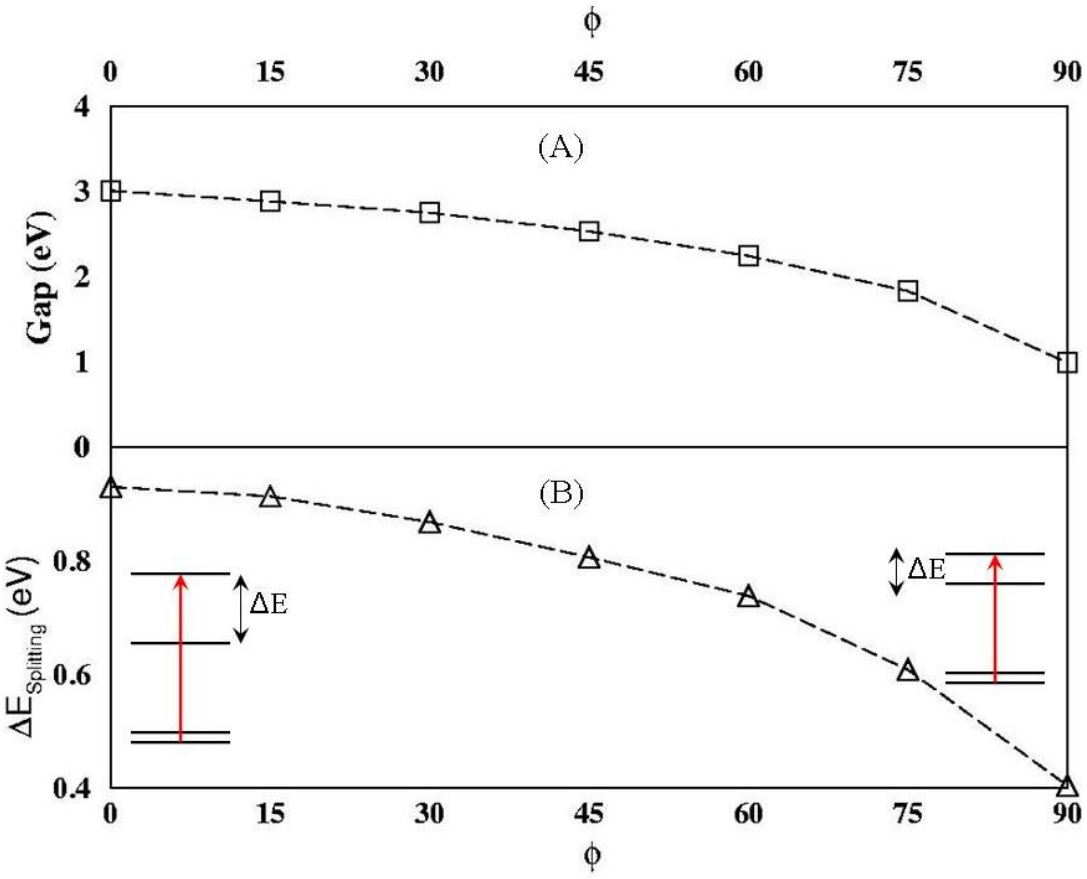

Figure 2.6: (A) Variation in the HOMO-LUMO gap (A) (in eV) and excitonic splitting (B) (in eV) of the system with increase in the distortion angle (ϕ).

charge localization over the distorted pyrrole ring (at ϕ=90) which is not considered within the excitonic dipolar splitting model.

In conclusion, we have shown that a distortion in the structure of porphyrin that leads to movement of one of the pyrrole ring from the plane of the molecule leads to an enhancement in the linear and non-linear optical response functions. However, such distortions lead to destabilization for system as well. Thus, additional supramolecular forces like π-stacking maybe required to stabilize such a porphyrin structure with distorted conformers. In contrast, our additional calculations (at frequency=0.0428 a.u) for the configurational isomer, N-confused porphyrin reveals that $\alpha = 340.86$ au, $\beta_{static} = 101.53$ au, $\beta_{SHG} = 836.54$ au and $\beta_{EOPE} = 107.67$ au. Thus, both conformational as well as configurational isomers of porphyrins can serve as additional materials for design of NLO devices.

The structural modifications involving such distortion of pyrrole ring from planarity in not from a purely synthetic viewpoint. Although additional forces like π-π interactions and crystal packing forces maybe required for stabilizing such conformations, we observe that magnesium complexes of molecules closely related to Porphyrin, namely, Chlorin and Bacterichlorin, present in light harvesting complexes of photosynthetic organisms, exhibit conformations in which all of the four pyrrole rings are distorted from planarity. Thus, not only will it be very interesting to study the role such distortions in further enhancing the NLO responses, but also to elucidate its role on the light absorbing properties of such photo-active pigments, correlating their properties in the microscopic (molecular) level to the macromolecular level. These will be subsequently discussed in the following chapter.

References:

[1] L. R. Milgrom, *The Colours of Life: An Introduction to the Chemistry of Porphyrins and Related Compounds*, Oxford University Press, Oxford, 1997.

[2] I. Okura, *Photosensitization of Porphyrins and Phthalocyanines*, Kodansha Ltd. Tokyo, 2000.

[3] E. Alessio, *Non-Covalent Multi-Porphyrin Assemblies: Synthesis and Properties*, Springer, Berlin, 2006.

[4] D. K. Lavallee, *The Chemistry and Biochemistry of N-Substituted Porphyrins*, J. Wiley & Sons, NY, 1987.

[5] A. B. P. Lever, H. B. Gray, *Iron Porphyrins*, Wiley-VCH, Weinheim, 1989.

[6] R. Huber, EMBO J. 8 2125 (1989).

[7] J. Deisenhofer, H. Michel, ibid. 8, 2149 (1989).

[8] T. Ritz, A. Damjanovic, K. Schulten, *ChemPhysChem* **3**, 243 (2002).

[9] M. K. Sener, S. Park, D. Lu, A. Damjanovic, T. Ritz, P. Fromme, K. Schulten, *J. Chem. Phys.*, **120,** 11183 (2004).

[10] Z.Katiliene, E. Katilius, G. H. Uyeda, J. C. Williams, N. W. Woodbury, *J. Phys. Chem. B* **108**, 3863 (2004).

[11] D. Gust, T. A. Moore, A. L. Moore, *Acc. Chem. Res.* **34** 40 (2001).

[12] S. Franzen, K. Fritsch, S. H. Brewer, *J. Phys. Chem. B* **106,** 11641 (2002)

[13] P. M. Kozlowski, T. G. Spiro, M. Z. Zgierski, *J. Phys. Chem. B* **104,** 10659 (2000).

[14] B. D. Dunietz, A. Dreuw, M. Head-Gorden, .*J. Phys. Chem. B* **107,** 5623 (2003).

[15] W. Su, T. M. Cooper, Chem. Mater. 10, 1212 (1998).

[16] C. Y. Liu, H. L. Pan, H. Tang, M. A. Fox, A. J. Bard, J. Phys. Chem. 99, 7632 (1995).

[17] B. R. Patel, K. S. Suslick, *J. Am. Chem. Soc.* **120**, 11802 (1998).

[18] J-H. Fuhrhop, C. Demoulin, C. Boettcher, J. Koning, U. Siggel, *J. Am. Chem. Soc.* **114**, 4159 (1992).

[19] V. V. Borovkov, J. M. Lintuluoto, M. Fujiki, Y. Inoue, *J. Am. Chem. Soc.* **122**, 4403 (2000).

[20] Y. Kobuke, H. Miyaji, *J. Am. Chem. Soc.* **116**, 4111 (1994).

[21] C. T. Chen, K. S. Suslick, *Coord. Chem. Rev.* **128**, 293 (1993).

[22] M. J. Crossley, P. L. Burn, *J. Chem. Soc. Chem. Commun*. 1561 (1991).

[23] J. P.Collman, J. T. McDevitt, G. T. Yee, C. R. Leidner, L. G. McCullough, W. A. Little, J. B. Torrance, *Proc. Natl. Acad. Sci. USA*, **83**, 4581 (1998).

[24] K. S. Suslick, C. T. Chen, G. R. Meredith, L. T. Cheng, *J. Am. Chem. Soc.* **114**, 6928 (1992).

[25] A. Sen, P. C. Ray, P. K. Das, V. Krishnan, *J. Phys. Chem.* **100**, 19611 (1996).

[26] Z. Peng, Z. Bao, L. Yu, *J. Am. Chem. Soc.* **116**, 6003 (1994).

[27] H. Chou, C-T. Chem, K. F. Stork, P. W. Bohm, K. S. Suslick, *J. Phys. Chem.* **98**, 383 (1994).

[28] N. C. Maiti, S. Mazumdar, N. Periasamy, *J. Phys. Chem. B* **102,** 1528 (1998).

[29] J. M. Kroon, R. B. M. Koehorst, M. van Dijk, G. M. Sanders, E. J. R. Sudholter, *J. Mater. Chem*. **7**, 615 (1997).

[30] A. Osuka, K. Maruyama, *J. Am. Chem. Soc*. **110**, 4454 (1988).

[31] J. M. Ribo, J. M. Bofill, J. Crusats, R. Rubires, *Chem. Eur. J*., **7** 2733 (2001).

[32] M. Gouterman, *J. Mol. Spectr*. **6**, 138 (1961).

[33] M. Gouterman, G. H. Wagniere, *J. Mol. Spectr*. **11**, 108 (1963).

[34] H. C. Longuet-Higgins, C. W. Rector, J. R. Platt, *J. Chem. Phys*. **18**, 1174 (1950).

[35] A. Ghosh, *Acc. Chem. Res.* **31**, 189 (1998).

[36] A. Ghosh, P. G. Gassman, Almlof, J. Am. Chem. Soc. **116**, 1932 (1994).

[37] H. Furuta, T. Asano, T. Ogawa, *J. Am. Chem. Soc.* **116**, 767 (1994).

[38] P. J. Chmielewski, L. Latos-Grazynski, K. Rachlewicz, T. Glowiak, *Angew. Chem., Int. Ed. Engl.* **33**, 779 (1994).

[39] A. Srinivasan, H. Furuta, *Acc. Chem. Res.* **38**, 10 (2005).

[40] H. Furuta, H. Maeda, A. Osuka, *Chem. Commun.* 1795 (2002).

[41] G. te Velde, F.M. Bickelhaupt, S.J.A. van Gisbergen, C. Fonseca Guerra, E.J. Baerends, J.G. Snijders, T. Ziegler, *J. Comput. Chem.* **22**, 93 (2001).

[42] S.J.A. van Gisbergen, J.G. Snijders, E. J. Baerends, *Comp. Phys. Commun*. **118**, 119 (1999).

[43] A. Datta, S. K. Pati, *J. Chem. Phys.*, 118, 2003, **118**, 8420 (2003).

[44] A. Datta, S. K. Pati, *J. Phys. Chem. A*, **108**, 320 (2004).

[45] A. Datta, S. K. Pati, *Chemistry- A Eur. J*. **11**, 4961 (2005).

[46] A. Datta, F. Tarenziani, A. Painelli, *ChemPhysChem*, **10**, 2961 (2006).

[47] A. Datta, S. K. Pati, *Chemical Society Reviews*, **35**, 1305 (2006).

Chapter III

III. Understanding the role of Intermolecular Interactions and Co-operative Phenomena in Magnesium complexes of Bacteriochlorin, Chlorin and Porphyrin

Introduction:

Porphyrins have been studied with much interest widely due to their active participation in almost every part of the living system, ranging from redox processes to photosynthesis and oxygen transport [1]. Apart from the biological importance of this molecule, there has been a tremendous interest in porphyrin-based derivatives for molecular materials [2, 3]. Assemblies of porphyrins have been shown to exhibit promising applications in molecular wires for one-dimensional electronic conduction, photonic-wires, ferroelectric bistability and non-linear optical responses [4, 5]. The second-harmonic generation from porphyrins with varied donor-acceptor strengths has been studied in great detail in the last decade by both theoretical and experimental methods [6, 7]. The absorption and emission spectra of porphyrins and porphyrin based materials have been a subject of detailed quantum-chemical modeling from both semi-empirical as well as *ab-initio* treatments [8-11].

Nature employs various forms of this widely prevalent molecule which on being classified chronologically has a particular evolutionary aspect tagged to it [12]. While various functions like electron and oxygen transport and catalysis of certain redox processes all involve porphyrin or certain modifications of it, perhaps the most studied systems are the light harvesting complexes [13], or LHCs. If one focuses on the so called evolutionary aspect of time, a definite structural difference among the active centers of various LHCs of various organisms is noticeable. Within the whole phylogenetic tree of photosynthetic organisms, the porphyrinoid active centers reveal intriguing differences; reduction of one pyrrole ring in the porphyrin molecule results in chlorin (Chl), reduction of another pyrrole trans to the former results in bacteriochlorin (BChl).

Although the compounds existent in nature involve an active centre (the metallo-porphyrin centre) linked to various kinds of side chains and functionalities [14, 15], their impact on the low-energy properties is less, and are more important from a structural consideration. Further, theoretically modeling such a complex molecule is very difficult, as they differ hugely with respect to these side chains and functionalities, and computationally very costly too, as the length of these side chains are too large to involve in a purely quantum calculation. In the Bacterial Light Harvesting Complexes, is believed that the symmetrical distribution cooperatively affects the light absorbing properties of each individual Mg-Chl / Mg-BChl molecule [16, 17].

It should thus be an interesting question as to whether there is a variation in efficiency of absorption as we, keeping the metal (here, Mg) constant, vary the molecule of interest from Porphyrin to Chlorin to Bacteriochlorin. Also concerning how these molecules exhibit configurationally different forms in nature, it was observed that many LHCs were not planar, the metal being around 0.4-0.6 Å out of the plane, which may not be just a structural variation. The four pyrrole rings in these tetra-pyrrole macrocycles, then, distort out of the plane to point toward the metal atom. It should thus be noteworthy a study whether such a non planar structure and efficiency of absorption can be correlated. As has been discussed in chapter 2 of the current thesis, distortions of one pyrrole ring from planar conformation significantly increases the non-linear optical responses of the porphyrin molecule. Thus, it may also be of significant technological interest, to study how the non linear optical behavior of such metallo-porphyrins varies with such structural modifications.

Although, recently there has been a huge interest in modified porphyrins, the so called core modified porphyrins [18], as well as synthetically derived porphyrins [19], there has also been quite a few advances toward how the spectra change with distortion of the porphyrin ring from planarity [20]. Whether this non planar structure is a simple conformational variation due to neighboring chemical environmental factors or is not, is still a matter of debate. Extensive works done [21] may have overlooked the fact as to what changes arise on bringing out the metal from planarity and distorting the pyrrole rings significantly to point toward the metal. In this chapter, we compare the variation in the opto-electronic and electronic transport properties of magnesium complexes of

Porphyrin, Bacteriochlorin and Chlorin, as well as the variation of the extent of intermolecular interaction between them as we distort the metal atom from being co-planar with the macrocycle to a non-planar conformation.

There is abundant spectroscopic data on porphyrins, chlorins and bacteriochlorins. Spectral data range from experiments carried out on all these molecules; such as in the ground state, in solutions, and within various protein environments as found in nature [22]. Generalizations are also possible from these abundances of data [23], assuming all three molecules fall into the normal type as classified by Gouterman with only π-π^* transitions [10].

It is known that single crystals of organic conductors provide pathways of charge hopping through intermolecular weak forces such as π-stacking and σ-π alternation [24, 25]. It is these forces that govern the packing of molecules in crystals and thin films. Very slight geometrical variations in the structures lead to the formation of different polymorphs. Thus, we believe that it will be very interesting to study systematically the variations in the electron and hole mobilities in various arrays of Por, BChl and Chl from the standpoint of how they are oriented in the crystal and how such orientation influences co-operatively, the charge carrier mobilities in them.

In this chapter we present a systematic study, that aims in answering how structural modifications, either synthetic or natural in origin, can lead to changes in the absorption spectra, keeping in mind that in the living world, certain photosynthetic bacteria employ very efficient light harvesting mechanisms. We also present in this chapter the results from our work on how co-operative phenomena alter the absorption of light by BChl and Chl molecules.

Results and discussion:

All calculations were performed with a TZP quality basis set, with all electrons being involved in a GGA-PW91 level DFT calculation, through the ADF 2007.01 package [26]. Fragment analyses and TDDFT studies were also performed at the same level, using the same package.

We generate non-planar structures of Mg complexes of Por, BChl and Chl by distorting the Mg atom 0.4 Å out of the plane of each molecule. This was done as follows: Firstly, the planar magnesium complexes of Por, BChl and Chl were oriented in such a way so that they became oriented in the xy plane. Subsequently, the Mg atoms are brought out of the plane of the macrocycle, and the pyrrole rings were distorted so that the N atoms on the pyrrole ring point toward the Mg atom. We observe various changes as we go from the planar to the non-planar structure. Optimization of these structures leads to the obvious outcome, where the Mg atom becomes co-planar with the porphyrin ring. From TDDFT studies we obtain absorption spectra for both planar and non-planar variants of Mg-Por, Mg-Chl and Mg-BChl molecules. From these spectra, we find that for the planar Mg-Por, two Q bands (Q_x and Q_y) are at 330 nm and 355 nm, respectively, whereas the Soret band being the most intense is positioned at 285 nm. The N, L, M bands are not visible. For the planar conformation of Mg-Chl, the Q bands are positioned at 525 nm and 537 nm; the Soret band is accompanied by a shoulder, the most intense peak is at 370 nm. For the planar conformation of Mg-BChl, there is a huge gap between the Q_x and Q_y bands; they are located at 530 nm and 650 nm, respectively. The Soret band has a prominent shoulder, the main peak being located at 360 nm. Hence, we find that, for the planar conformations of the magnesium complexes of Por, BChl, and Chl, experimental data were well reproduced [23], the deviations from the latter being negligible, especially considering the fact that these calculations were performed without any solvent being incorporated, and experimental data always concern a solvent which is known to shift absorption maxima of pi conjugated systems considerably.

There was an overall red shift in the absorption maxima as we go from the planar to the non-planar structures of Mg-Por and Mg-Chl. We find that, for the non-planar Mg-

Por the Soret band is located at 375 nm and the Q bands are red shifted to 540 nm. The Soret band of the non-planar Mg-Chl is located at 380 nm and the Q bands are located at 542 nm and 554 nm. However, for Mg-BChl, there is actually a blue shift in both the Soret band (maxima is at 342 nm) and the Q band (maxima is at 630 nm).

The corresponding oscillator strengths for the planar and non-planar structures of porphyrin, chlorin and bacteriochlorin are summarized table 3.1.

Table 3.1: Comparison of the absorption spectra of planar and non-planar structures of Por, Chl and BChl. ω indicates the frequency of absorption (eV), f indicates the corresponding oscillator strength. Figures in parenthesis are for the planar conformation of the system

Systems	**Bands**					
	Soret		**Q**		**N, L, M**	
	ω	f	ω	f	ω	f
Por	3.30 (4.34)	0.31 (2.04)	2.27 (3.50)	0.003 (0.09)	--	--
Chl	3.24 (3.32)	0.22 (0.51)	2.23 (2.31)	0.093 (0.06)	3.57, 3.70 (4.1, 4.3, 4.65)	0.02, 0.06 (0.21, 0.06, 0.004)
BChl	3.61 (3.48)	0.48 (0.56)	1.97 (1.92)	0.20 (0.21)	3.84 (3.65,3.81)	0.02 (0.22, 0.158)

.

It appears that, if the MOs are plotted for any of these structures; there are four orbitals that can well be separated from the other levels. These four orbitals are what Gouterman had originally referred to in his papers and classical reviews as the ‘Four orbital picture’. From a comparison of these four orbitals we can explain how the distortion of the Mg atom out of planarity results in a red shift in the spectra of Mg-Por and Mg-Chl.

A qualitative explanation of the phenomenon can be linked to the fact that the Mg 2px orbitals conjugate to the HOMO (b1) of the porphyrin, which in turn stabilizes it. As the Mg atom is brought out of the plane, the aforesaid conjugation is no longer possible, and the HOMO considerably rises in energy. Whereas a rise in energy is also observed for the HOMO-1 orbital, this rise is not significant as it is symmetry allowed to interact only with one lobe of the 2px orbital. Hence the red shift in the Q band of Por and Chl. We find that for Mg-BChl, however the HOMO and HOMO-1 are lowered in energy as

we go from the planar to the non-planar structure. The decrease in the HOMO is more than the decrease in the LUMO, and so for the BChl we observe a blue shift in the Q bands as we go from the planar to the non-planar structure.

We compared the efficiency in absorption for chlorin, porphyrin, and bacteriochlorin, separately for the planar as well as the non-planar geometry, to understand how the change in the total energy absorbed differs between these two different geometrical variations. Mg-Chl is the most efficient in absorption of visible light. As we move from a planar structure to the corresponding pyramidal one, the efficiency of all three species increases, as is evident from the areas under the curve, computed in the visible range of 380-750 nm. On comparison we found that the order of efficiency in both the planar and non-planar variants was Chl > BChl > Por. Figures indicating the areas under the absorption curves are representative of the efficiency of absorption [system (planar, non-planar): BChl (0.30, 0.51), Chl (0.51, 0.54), Por (0.04, 0.39)]. The non-planar Chl molecule absorbs light most efficiently.

In terms of dipolar contributions, it is quite obvious that there is a huge change in dipole moments of the ground states as we move from the planar to the non-planar structure. As the GS dipole moment for the planar porphyrin molecule is zero, we observe the highest increase in absorption efficiency on achieving a non-planar structure; whereas there are slighter increases for the chlorin and the bacteriochlorin. The frequency dependent second harmonic susceptibility β_{SHG} was calculated at a frequency of 0.0428 hartree corresponding to a wavelength of 1064nm of the Nd:YaG laser. The magnitudes of the second harmonic generation are presented in table 3.2.

Table 3.2: Comparison of the non-linear frequency dependent second harmonic susceptibility β_{SHG} and its dependence on the optical gap (ΔE), oscillator strength corresponding to ΔE (***f***) and the ground state dipole moment (μ_G) for planar and non-planar variants of Por, Chl and BChl. Figures in parenthesis are for the planar conformation of the system.

Systems	***f***	$\Delta E_{HOMO-LUMO}$**(eV)**	μ_G	β_{SHG}
Por	0.0038 (0.0023)	2.04 (1.981)	1.212 (0.0)	110.0 (3.03)
Chl	0.093 (0.062)	1.744 (1.899)	2.76 (2.22)	2479.5 (2030)
BChl	0.202 (0.201)	1.276 (1.189)	1.210 (0.98)	638.0 (3.4)

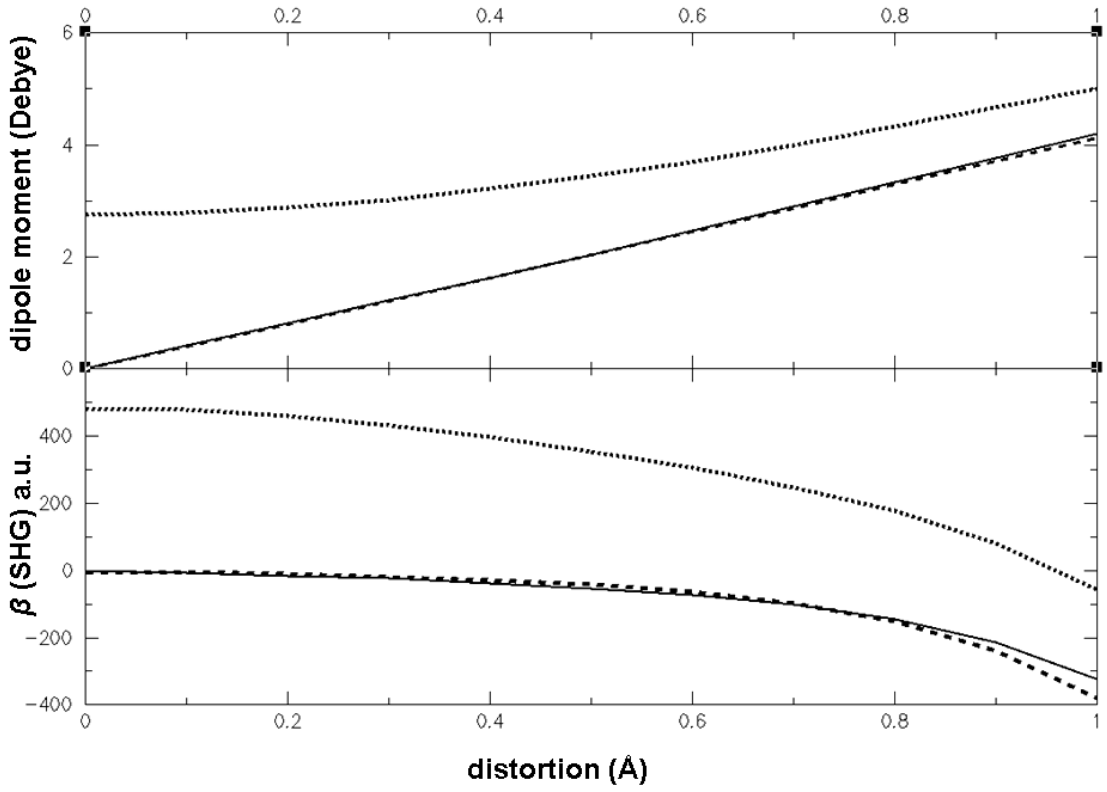

Figure 3.1: Variation of dipole moment (a) and SHG hyperpolarizability (b) of Mg-BChl (dashed line), Mg-Chl (dotted line) and Mg-Por (solid line) with subsequent distortion of the Mg atom out of planarity.

A simple two-level model derived from a more general perturbation expression for the first hyperpolarizability of NLO chromophores can be assessed from the equation,

$$\beta_{two-level} = \frac{2e^2}{2\hbar^3} \frac{\omega_{ge} f_{ge} \Delta\mu_{ge}}{(\omega_{ge}{}^2 - \omega^2)(\omega_{ge}{}^2 - 4\omega^2)} \qquad (3.1)$$

where, the first hyperpolarizability depends on the optical transition energy, the associated oscillator strength (*f*ge), and the difference between the ground- and excited-state dipole moments ($\Delta\mu_{ge}$).

We performed a gradual study on all three structures by distorting the Mg from planarity to non-planarity and noting how the non-linear optical properties change. The Mg atom was moved from planarity to a distance of 1Å in steps of 0.1 Å along the z-axis, where the porphyrin, chlorin and the bacteriochlorin moiety in the original planar structure were confined in the xy plane. We find that, with gradual distortion, the NLO response (β_{static} and β_{SHG} corresponding to a frequency of 1094nm) decreases with increasing distortion. Although the value of beta, as inferred from the two-state model, varies directly with dipole moment, it is the variation in the HOMO-LUMO gap that brings about such a drastic decrease in the NLO response. From the expression of beta, it is evident that, as the optical gap (energy difference between the ground state and the 1st dipole allowed state) increases, (which, here, are implemented by bringing out the Mg atom out of co-planarity) the magnitude for β decreases. It is noteworthy that as the β is governed by ω^{-2} and Δμ, the effect of an increasing ω is outweighs the effect of an increasing Δμ. With subsequent distortion, the rate of decrease in the NLO response for Chl is the most and that for BChl and Por being almost comparable. This is due to the fact that for Por and BChl the ground state dipole-moment is 0, whereas for Chl, an asymmetric molecule there is a finite dipole moment. With increasing distortion, the dipole moment increases significantly for BChl and Por and by a lesser amount for Chl, as shown in figure 3.1.

Co-operative phenomena are important from the viewpoint of how these molecules exist in nature. The structure of light harvesting complexes in both plants and bacteria illustrate a highly symmetrical gross structure [27]. Light harvesting complexes in nature are cylindrical in shape, and it is believed that such cylindrical arrangement leads to more efficient light absorption. However the arrangement of Chl molecules in

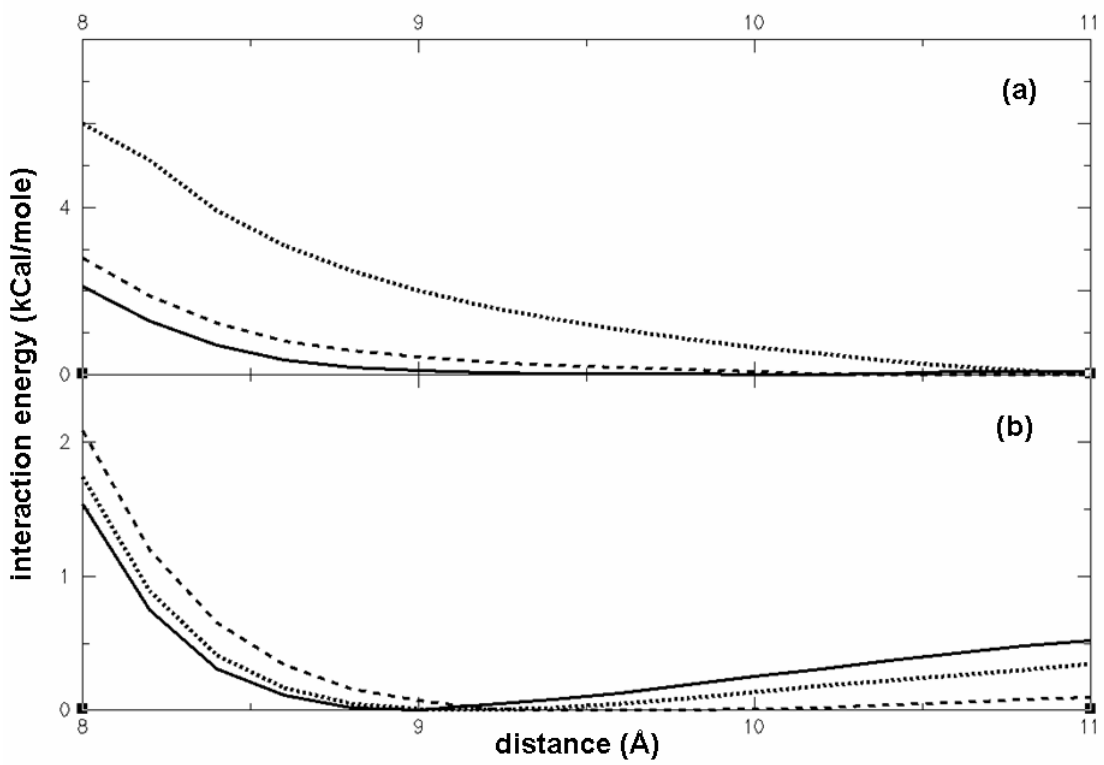

Figure 3.2: Variation of interaction energy with distance (d) in dimers of Mg-BChl (dashed line), Mg-Chl (dotted line) and Mg-Por (solid line), in (a) planar and (b) non-planar configurations. The intermolecular distance (d) is the distance between the Mg centers of each monomer. Interaction energies have been scaled according to minimum energies for each dimer species.

plant light harvesting complexes is very different from the arrangement of BChl molecules in bacterial light harvesting complexes. Whereas the bacteriochlorin moieties in the LH2 complex from Rhodopseudomonas acidophila [28] are particularly symmetrically arranged, revealing a highly ordered orientation, no such correlation is observed from the crystal structures of plant light harvesting complexes. It is also known that bacteria employ much more efficient light harvesting systems than plants. Earlier work suggests that photo-excitation in LHCs operate between two different kinds of BChl molecules in a co-operative manner [29].

It should thus be interesting to see how one molecule of each of Mg-BChl, Mg-Chl and Mg-Por interacts with another. We consider dimers of Mg-BChl, Mg-Chl and Mg-Por obtained from crystal structures of the aforesaid bacterial light harvesting complexes, with suitable modifications as mentioned in the supporting information section of the current chapter. To have a better understanding of the distance and orientation dependent interactions between these molecules, we observe the variation of interaction energy with distance between the monomers, considering both non-planar and planar conformations of the monomers, as shown in figure 3.2

It is evident from the comparison of the interaction energy between BChl, Chl, and Por that there exists a long range stabilizing interaction between the monomers that constitute the dimer. However, this kind of stabilizing interaction is different between the three species. For the dimer constituted of non-planar monomers, the interaction energy goes through a minimum as we increase the distance (d) from 8 Å to 11 Å. The corresponding minima are 9.0 Å, 9.2 Å and 9.6 Å for Mg-Por, Mg-Chl and Mg-BChl respectively.

If we however consider the planar variants of these three molecules in a similar kind of orientation, the comparison of the interaction energy yields interesting findings (figure 3.2b). As compared to the case where we considered dimers constituted of non-planar variants of Mg-BChl, Mg-Chl and Mg-Por, the steep decrease in interaction energy indicating predominance of repulsive interactions at low values of d is similar. However, what is noteworthy is that the dimer fails to show any particular favorable distance where the stabilizing interaction energy is maximum. The energy vs. d curve becomes somewhat flat, but continues to indicate a decrease in the interaction energy as

we keep on increasing d above 9.00 Å. This may have far reaching consequences especially from the viewpoint that, if the dimeric system fails to converge to an optimum, then there will be no favorable coupling between the monomers, as the monomers will favour larger and larger distance from each other. We will then fail to see any co-operative effect whatsoever.

As a result of such interactions between the non-planar structures of monomers of Mg-Por, Mg-Chl and Mg-BChl in a dimer, both the HOMO and LUMO of the monomers gets split, which effectively reduce the optical gap. The gaps (in eV) reduce to 1.03, 1.44, and 1.74 for BChl, Chl and Por respectively from 1.22, 1.63 and 1.74, respectively, in the monomers.

We adopt a Davydov picture to understand the nature of dipolar interaction between two monomers. This essentially is an exciton-exciton interaction, which leads to splitting of the first excited state (given by ΔE). If such an interaction is treated purely quasi-classically, the splitting energy is given by,

$$\Delta E = 2\frac{\mu_{g\to s}^2}{d^3}(\cos\phi - 3\cos^2\theta) \qquad (3.2)$$

where, $\mu_{g\to s}$ is the transition dipole from the ground state to the excited state of a single monomer, θ is the angle between the transition dipole moment and the molecular axes of a monomer, and ϕ is the angle between the transition dipole moments of the two interacting monomers.

To understand how dipolar interactions between two monomers in dimers of Mg-Chl and Mg-BChl, ΔE (i.e the energy difference between the LUMO and LUMO+1) was plotted as a function of Mg-Mg distance (d). It may be mentioned here that according to the Davydov description of excitonic splitting, the splitting of HOMO is very less and in most case is neglected, and the study of the variation of the $\Delta E_{(\text{LUMO-LUMO+1})}$ with d suffices. The scenario for Mg-Por is however different. For the monomer of Por, the LUMO is two-fold degenerate for the planar configuration, and very closely spaced in energy for the non-planar configuration. Interactions between two monomers lead to symmetry restricted splitting, and the ΔE corresponds to the gap between LUMO and LUMO+2 for the non-planar Por, and LUMO and LUMO+3 for the planar porphyrin. However, at d greater than 10.2 Å, there is not enough interaction between the monomers

and the ΔE corresponds to the gap between LUMO and LUMO+1 for the non-planar porphyrin, and LUMO+1 and LUMO+3 for the planar porphyrin. For the non-planar structures, the dipole moments of Por, Chl and BChl vary considerably and hence the difference in the splitting energies. However for the planar structures the variation in the dipole moment between Por, Chl and BChl is less and the difference in the splitting is less prominent. In the calculations above, the relative orientation of the monomers in the dimers were kept constant, so that an analogy could be drawn between the three. From the trend in the variation of the interaction energy, it can be concluded that the intermolecular interaction between monomers of Mg-BChl, Mg-Chl and Mg-Por, essentially being dipolar interactions, can be well described by the exciton model.

However to understand how these co-operative phenomena affect the absorption phenomena of extended porphyrinoid arrays as present in LHCs, we consider various oligomers of Mg-BChl, Mg-Chl and Mg-Por. As the electronic origin of the Q band is the lowest excited singlet state, essentially it corresponds to the HOMO→LUMO transition. The Soret band on the other hand corresponds to contributions from (HOMO-1) → LUMO and HOMO → (LUMO+1) transitions. From the fragment analyses we find that the contributions of the monomer occupied-MOs toward the occupied-MOs of the arrays (dimer onwards) are many-fold. In other words HOMO, HOMO-1 and HOMO-2 of the monomers constituents have significant contributions toward the HOMO of the oligomers. The same situation occurs for the unoccupied-MOs as well. Thus as we go from the dimer to hexamers, we find that the intensity of the Soret band decreases considerably and is almost zero trimer onwards. The intensity of the Q band, on the other hand increases in intensity along with considerable red shift. The overall effect of this change is that the area under the curve computed in the visible range (380nm-750nm) increases. This effect is most prominent in the BChl arrays, and least for the Por arrays. This results in a huge broadening of the spectral curve. Areas under the curve show beyond doubt that with increasing number of monomers the efficiency of Mg-BChl absorption increases. However for Mg-Chl and Mg-Por, the absolute efficiency has an oscillation pattern with almost no average increase. This maybe a direct consequence of the fact that, whereas the structures of Mg-BChl were obtained from experimental data and hence depict the real system, the structures of Mg-Chl and Mg-Por were forcefully

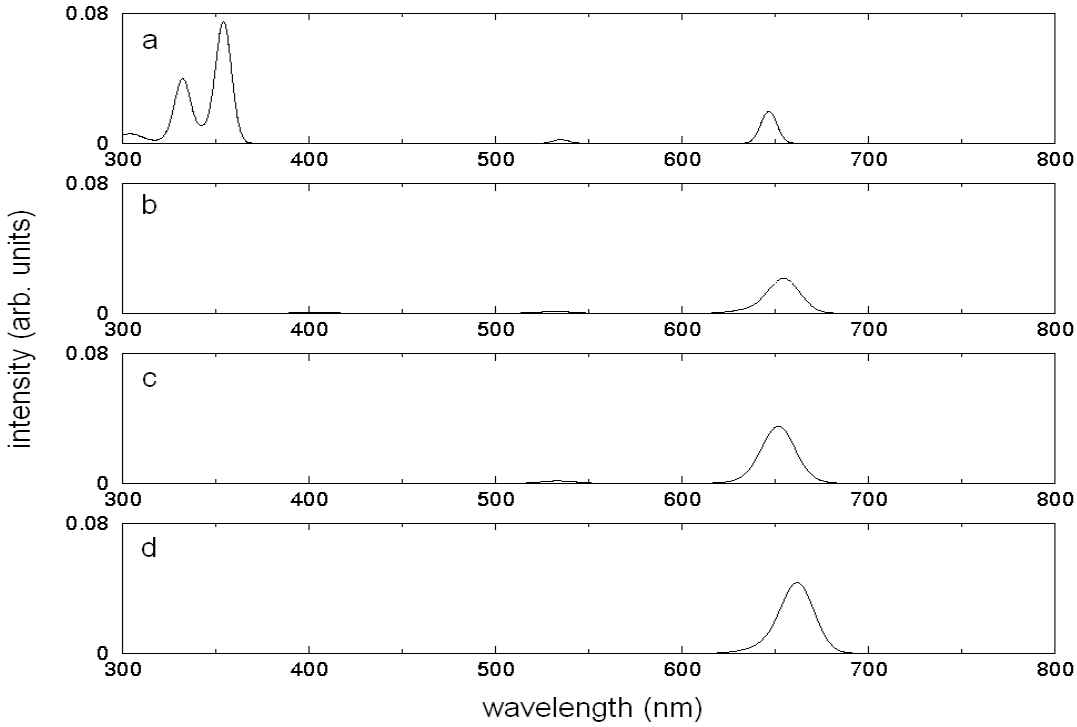

Figure 3.3: Comparison of absorption spectra of various oligomers of Mg-BChl generated from crystal structures of R. acidophila. Monomer (a), dimer (b), trimer (c), and tetramer (d).

put into an array that structurally mimics the relative orientation of Mg-BChl molecules in the light harvesting complex of Rhodopseudomonas acidophila. The disappearance of the Soret band and intensification of the Q band as we go from monomer to tetramer of Mg-BChl is shown in figure 3.3.

This interpretation can be extended to cyclic LHC systems as for that of R. acidophila. This analogy gives a clear idea as to why the Mg-BChl molecule, although structurally very similar to Mg-Chl and Mg-Por molecules, prove to be very different, and particularly intriguing in its display of the efficiency with which purple bacteria harvest light. Recalling the fact that for the single molecules, Mg-Chl, in both the planar and non-planar variants is by far the most efficient light absorber, it is quite intriguing that when co-operative phenomena come into play, Mg-BChl oligomers turn out to be more efficient than the others. This may also be an answer to the question as to why light harvesting systems of plants bear no such exquisite symmetrical arrays of porphyrinoids as do purple bacteria.

We further calculate the charge mobilities in aggregates of Mg-BChl, Mg-Chl and Mg-Por to understand the extent to which co-operative phenomena operate in such systems. The overall structures generated are in accordance to the methodology described in the supporting information section of the current chapter. To a reasonable approximation, each hopping process can be understood as a non adiabatic electron transfer reaction. For such cases we utilize the Markus theory to calculate the rate of charge transfer between neighboring molecules. For such calculations we adopt a methodology as described in the introductory chapter of the current thesis.

In order to study the variation of H_{mn}(hole) and H_{mn}(electron) with intermolecular distance, we vary the distance between the Mg centers in the molecules from 8.00 Å to 11.00 Å. It is very important to note that the coupling matrix elements decrease considerably with increasing distance, as shown in figure 3.4, and beyond a particular distance, it tends to zero, indicating that at such large distances the contact pairs do not contribute to the conductance of the molecule.

As mentioned in the supporting information section of the current chapter, the electron and hole mobility values for the Mg-BChl, Mg-Chl and Mg-Por systems were calculated keeping in consideration the intermolecular contacts at 9.15 and 9.44 Å. The

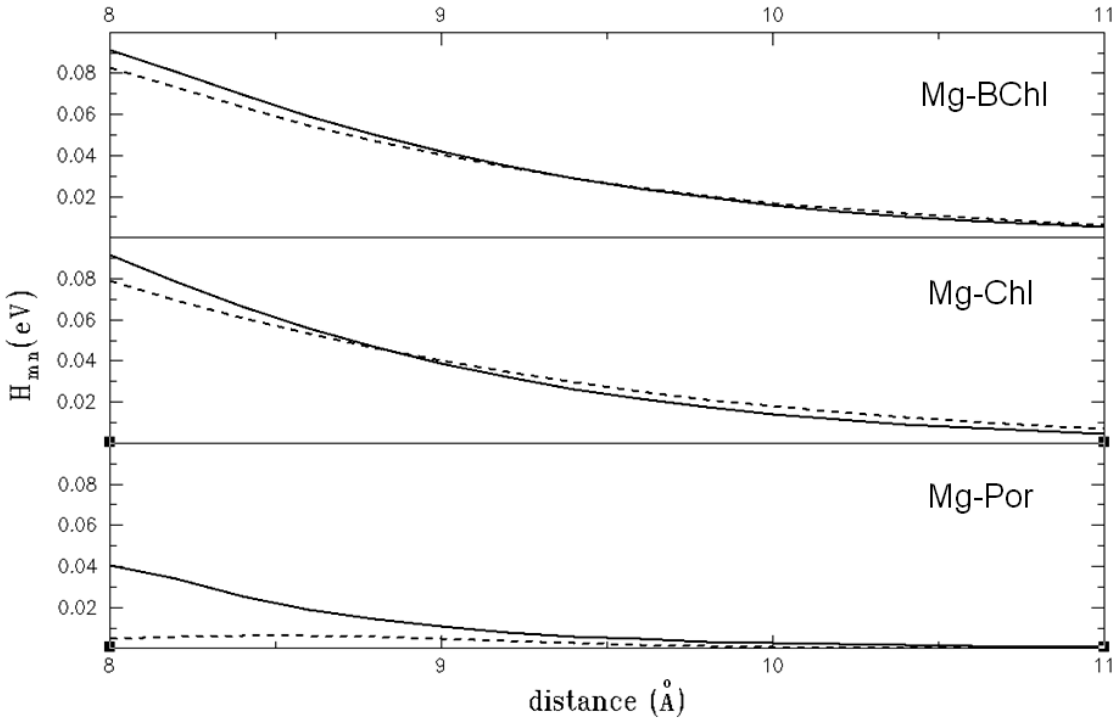

Figure 3.4: Comparison of H_{mn}(electron) [solid line] and H_{mn}(hole) [dashed line] for dimers of Mg-BChl, Mg-Chl and Mg-Por with varying intermolecular distance.

values are reported in table 3.3. It may be noteworthy to mention here that the relaxed geometries of Mg-BChl, Mg-Chl and Mg-Por maintain the symmetrical structures after addition or subtraction of charge, for realization of the cationic and anionic geometries of the same.

Table 3.3: Hole and electron mobilities (μ_{hole} and $\mu_{electron}$) for Mg-BChl, Mg-Chl and Mg-Por. Mobilities are reported in $cm^2\ V^{-1}\ s^{-1}$.

molecule	μ_{hole}	$\mu_{electron}$
Mg-BChl	0.116	0.071
Mg-Chl	0.152	0.078
Mg-Por	0.058	0.008

Although there is no direct correlation between photo-excitation and drift mobilities, it has been shown that for LHC complexes, photo-excitation results in charge separation, a phenomenon which is widely employed in nature to catalyze various photo activated reactions. We find from our calculations that, all the three systems are preferential hole conductors. On the other hand, both electron anh hole mobility values in Mg-BChl and Mg-Chl are almost one order higher than the corresponding values for Mg-Por. This may be an answer as to why, although these molecules are so similar, only BChl and Chl molecules are found in photo active pigments.

In conclusion, we show how long range co-operative phenomena operate in cyclic arrays of Mg-BChl, Mg-Chl and Mg-Por, and how such phenomena are responsible in altering the visible light absorption characteristics of such arrays. We further show how non-planar dimers of these molecules get stabilized through long-range interactions, especially when compared to dimers composed of planar monomers. Additionally, through this study we aim at understanding as to how, although structurally so similar, Mg-Por is so different from the other photoactive pigments Mg-BChl and Mg-Chl from a standpoint of efficiency of absorption, and charge transport.

Supporting Information:

Generation of oligomers of Mg-BChl, Mg-Chl and Mg-Por from crystal structures of Light Harvesting Complexes of R. Acidophila:

Crystal structures of the bacterial light harvesting complexes were appropriately modified to remove the side chains and functionalities. In the cases where they were covalently attached to the Mg-BChl moiety, the sites were passivated with H. To obtain oligomers of Mg-BChl, retaining the original relative orientation present in the crystal structure of the LHC, positions of the H atoms were fully relaxed, keeping the co-ordinates of all the other atoms frozen. Further, to obtain oligomers of Mg-Chl and Mg-Por with the same relative orientation, the appropriate carbon atoms on the pyrrole rings were functionalized or de-functionalized with H atoms, with the consequent relaxation of their positions. We consider a pair of adjacent monomers, in all three cases, and accordingly label them as the dimer composed of non-planar conformations of the Mg complexes of BChl, Chl and Por. The distance between the two Mg atoms in the dimer was then labeled as the intermolecular distance between the corresponding non-planar variants of the monomers.

Note that, in the crystal structures of the bacterial LHC considered, the non-planar Mg-BChl molecules maintain a slipped parallel orientation with respect to their nearest neighbors. It is also important to realize that the individual molecules adopt a particular distortion to accommodate the curvature of a perfect cylindrical structure consisting of a large array of Mg-BChl molecules. To generate dimers composed of planar Mg-BChl monomers, maintaining the same relative orientation as observed in the original structure, all atomic positions except two N atoms on a pair of trans pyrrole rings in each of the macrocycles, were fully relaxed. After full relaxation, we find that, the Mg-BChl macrocycles became planar. This structure was labeled as a dimer composed of planar Mg-BChl monomers with same relative orientation of the monomers, as present in the original crystal structure. To generate dimers of Mg-Chl and Mg-Por from the structure obtained above, a methodology described earlier in this section was adopted. Further, the

distance between the two Mg atoms in the dimer was labeled as the intermolecular distance between the corresponding planar variants of the monomers.

Methodology for calculating the coupling matrix elements (H_{mn}) between different molecular contacts:

We observe in the crystal structure, modified as mentioned above, that, each Mg-BChl molecule has 6 nearest neighbors. We present a simplified figure showing only the Mg atoms in figure S3.1. It is clear from figure S3.1 that, for the molecule under consideration, labeled '0', there are 6 nearest neighbors, labeled '1' – '6'. The corresponding intermolecular distances in each contact, indicated in red, and defined as the distance between the Mg centers of two molecules constituting the contact, are given in table ST3.1.

Figure S3.1: Schematic showing molecular contacts of a particular monomer in the modified crystal structure of LHC, as considered in our calculations.

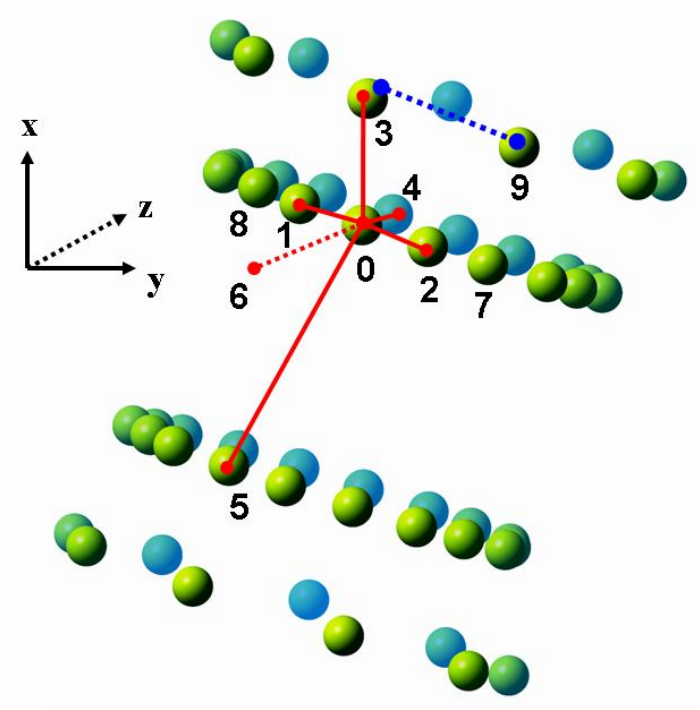

Table ST3.1: Intermolecular distances (Å) in various molecular contacts of the Mg-BChl oligomers. Numbers indicate atomic indices shown in figure S3.1.

	0-1	**0-2**	**0-3**	**0-4**	**0-5**	**0-6**
d	9.44	9.15	18.34	53.10	37.31	67.83

It is noteworthy to mention here that, for our adaptation of the crystal structure under consideration, there are two circular arrays of Mg-BChl molecules, the outer one and inner one having 9 and 18 Mg-BChl molecules, respectively. The distance between neighboring molecules within the outer ring, '3-9', as shown in blue, in figure S3.1, is 21.3 Å.

For a detailed understanding of the molecular contacts, we consider $2\times2\times2$ supercells of the above system and calculate the radial distribution function, g(r), maintaining a centre of distance of 11 Å as cut-off. We find two peaks, at 9.15 and 9.44 Å, corresponding to the molecular contacts labeled '0-1' and '0-2', respectively. To ensure that molecular contacts at distances greater than 11Å do not contribute significantly to the charge carrier mobilities in these systems, we evaluated the coupling constants (H_{mn}) at distances larger than 11Å, and found the magnitudes to be negligibly small. Thus, we can safely consider only the contacts '0-1' and '0-2' to be significant for our calculations of charge carrier mobilities. Further, we observe negligible magnitudes of H_{mn} due to contacts beyond the immediate neighbors, as indicated by '0-7' and '0-8'. In this context, it may be mentioned here that, there are no significant contacts between molecules in adjacent unit cells, the only means of electronic communications between such molecular contacts perhaps being the side chains and functionalities that we had neglected earlier.

References:

[1] *Porphyrins*, Dolphin D., 1978, Academic Press, Porphyrin and porphyrin compounds.

[2] (a) Su W., Cooper T. M., *Chem. Mater*., 1998, **10**, 1212. (b) Liu C. Y., Pan H. L., Tang H., Fox M. A., Bard A. J., *J. Phys. Chem*., 1995, **99**, 7632. (c) Patel B. R., Suslick K. S., *J. Am. Chem. Soc.*, 1998, **120**, 11802.

[3] (a) Fuhrhop J. H., Demoulin C., Boettcher C., Koning J., Siggel U., *J. Am. Chem. Soc*., 1992, **114**, 4159. (b) Borovkov V. V., Lintuluoto J. M., Fujiki M., Inoue Y., *J. Am. Chem. Soc.*,2000, **122**, 4403. (c) Kobuke Y., Miyaji H., *J. Am. Chem. Soc*., 1994, **116**, 4111.

[4] (a) Chen C. T., Suslick K. S., *Coord. Chem. Rev*., 1993, **128**, 293. (b) Crossley M. J., Burn P. L., *J. Chem. Soc. Chem. Commun*., 1991, 1561.

[5] Collman J. P., McDevitt J. T., Yee G. T., Leidner C. R., McCullough L. G., Little W. A., Torrance J. B., *Proc. Natl. Acad. Sci. USA*, 1998, **83**, 4581.

[6] (a) Suslick K. S., Chen C. T., Meredith G. R., Cheng L. T., *J. Am. Chem. Soc.*,1992, **114**, 6928. (b) Sen A., Ray P. C., Das P. K., Krishnan V., *J. Phys. Chem*., 1996, **100**, 19611.

[7] (a) Peng Z., Bao Z., Yu L., *J. Am. Chem. Soc.*, 1994, **116**, 6003. (b) Chou H., Chen C. T., Stork K. F., Bohm P. W., Suslick K. S., *J. Phys. Chem*., 1994, **98**, 383.

[8] (a) Maiti N. C., Mazumdar S., Periasamy N., *J. Phys. Chem. B*., 1998, **102,** 1528. (b) Kroon J. M., Koehorst R. B. M., van Dijk M., Sanders G. M., Sudholter E. J. R., *J. Mater. Chem*., 1997, **7**, 615.

[9] (a) Osuka A., Maruyama K., *J. Am. Chem. Soc.*, 1988, **110**, 4454. (b) Ribo J. M., Bofill J. M., Crusats J., Rubires R., *Chem. Eur. J.*, 2001, **7**, 2733.

[10] (a) Gouterman M., *J. Mol. Spectr*., 1961, **6**, 138. (b) Gouterman M., Wagniere G. H., *J. Mol. Spectr.*, 1963, **11**, 108. (c) Longuet-Higgins H. C., Rector C. W., Platt J. R., *J. Chem. Phys*., 1950, **18**, 1174.

[11] (a) Ghosh A., *Acc. Chem. Res*., 1998, **31**, 189. (b) Ghosh A., Gassman P. G., Almlof, *J. Am. Chem. Soc*., 1994, **116**, 1932.

[12] American Scientist, 87 (2), 126 (1999).

[13] (a) *The Chlorophylls*, Zuber, H., Brunisholz, R.A. (ed. Scheer, H.), 1993, **627**, CRC Press, Boca Raton; (b) *Wikipedia*, www. wikipedia.org/wiki/Light-harvesting_complex

[14] Fyfe P. K., Jones M. R., *Biochem. Soc. Trans*., 2005, **33**, 924.

[15] Liu Z., Yan H., Wang K., Kuang T., Zhang J., Gui L., An X., Chang W., *Nature*, 2004, **428**, 287.

[16] Ritz,T., Park, S., and Schulten, K., *J Phys. Chem. B*, 2001, **105** , 8259.

[17] *From simplicity to complexity and back: Function, architecture and mechanism of light harvesting systems in photosynthetic bacteria*, Schulten K., Frauenfelder H., Deisenhofer J.,

Wolynes P. G. (Eds.), Simplicity and Complexity in Proteins and Nucleic Acids, 1999, 227, Berlin, Dahlem University Press.

[18] (a) Anand, V. G., Pushpan, S. K., Venkatraman, S., Dey, A., Chandrashekar, T. K., Joshi, B. S., Roy, R., Teng, W., Senge, K. R., *J. Am. Chem. Soc*., 2001, **123**, 8620. (b) Core-Modified Expanded Porphyrins: New Generation Organic Materials Chandrashekar, T. K., Venkatraman, S., *Acc. Chem. Res.*, 2003, **36** , 676.

[19] Furuta, H., Maeda, H., Osuka, A., *J. Org. Chem.*, 2000, **65** , 5450.

[20] Parusel A. B. J., Wondimagegn T., Ghosh A., *J. Am. Chem. Soc*.,2000, **122**, 6371.

[21] (a) Linnanto, J., Korppi-Tommola, J., *J. Phys. Chem. A.*, 2001, **105**, 3855. (b) Linnanto, J., Korppi-Tommola, J., *Phys. Chem. Chem. Phys.*, 2000, **21**, 4962.

[22] Kozyrev A. N., Chen Y., Goswami L. N., Tabaczynski W. A., Pandey R. K., *J. Org. Chem*., 2006, **71**, 1949.

[23] *Photochemistry of polypyridine and porphyrin complexes*, Kalyanasundaram, K., Academic Press, 1992.

[24] French S. A., Catlow C. R. A., *J. Phys. Chem. Solids*., 2004, **65**, 39.

[25] Ohshiro T., Umezawa Y., *Proc. Natl. Acad. Sci*., 2006, **103**, 10.

[26] (a) G. te Velde, F.M. Bickelhaupt, S.J.A. van Gisbergen, C. Fonseca Guerra, E.J. Baerends, J.G. Snijders, T. Ziegler, 'Chemistry with ADF', *J. Comput. Chem.* **22**, 931-967, 2001. (b) C. Fonseca Guerra, J.G. Snijders, G. te Velde, and E.J. Baerends, *Theor. Chem. Acc*. **99**, 391, 1998. (c) ADF2007.01, SCM, Theoretical Chemistry, Vrije Universiteit, Amsterdam, The Netherlands, http://www.scm.com

[27] PDB Keywords: 1QSI, 1QZV, 1KZU.

[28] Prince, S.M., Papiz, M.Z., Freer, A.A., McDermott, G., Hawthornthwaite-Lawless A. M., Cogdell R.J., Isaacs N.W., *J.Mol.Biol*., 1997, **268**, 412.

[29] Damjanovic, A., Ritz, T., and Schulten, K., Physical Review E, **59**, 3293-3311, 1999.

Chapter IV

IV. The role of H-bonding and Dipole-Dipole Interactions on the Electrical Polarizations and Charge Mobilities in Linear Arrays of Urea, Thiourea and their Derivatives

Introduction:

The design of materials with large off-resonance nonlinear optical (NLO) responses has been a topic of active research, because of their potential applications in a number of advanced opto-electronic devices [1, 2]. On the other hand, materials with high charge carrier mobilities are of immense value in designing transistors and transport devices [3-5]. Larger systems like chromophore-macromolecule guest-host complexes, chromophore functionalized glassy macromolecules, cross-linked chromophore-macromolecules and intrinsically acentric self-assembled chromophoric superlattices have also been studied in great detail with a view to increase opto-electronic as well as transport characteristics [6]. To this regard, molecular crystals that allow easy polarization of their electron density are particularly interesting. Interactions like H-bonding, polarizations induced by dipole-dipole interactions, π-stacking etc. strongly influence the symmetry and hence orientation of a molecule in its crystal [7-9], which are crucial in realizing the various optical response functions [10]. While dipole-dipole interactions affect the NLO responses due to excitonic splitting [11a], the role of H-bonding on the NLO properties has only barely been investigated [11b]. Contributions of electrostatic energy, exchange repulsion energy, polarization energy and charge transfer energy, all account for the strength of H-bonding [12]. Although the charge transfer efficiency in H-bonded aggregates is less, the strong directional character of the H-bonds result in increased dipole moments of molecular aggregates [13], and thus H-Bonding is very important in controlling the NLO responses as it increases the transition dipole moment from the ground state to the optically allowed excited state [14].

For a proper understanding of the contribution of H-bonding and dipole-dipole interactions towards controlling the NLO responses and charge carrier mobilities, we

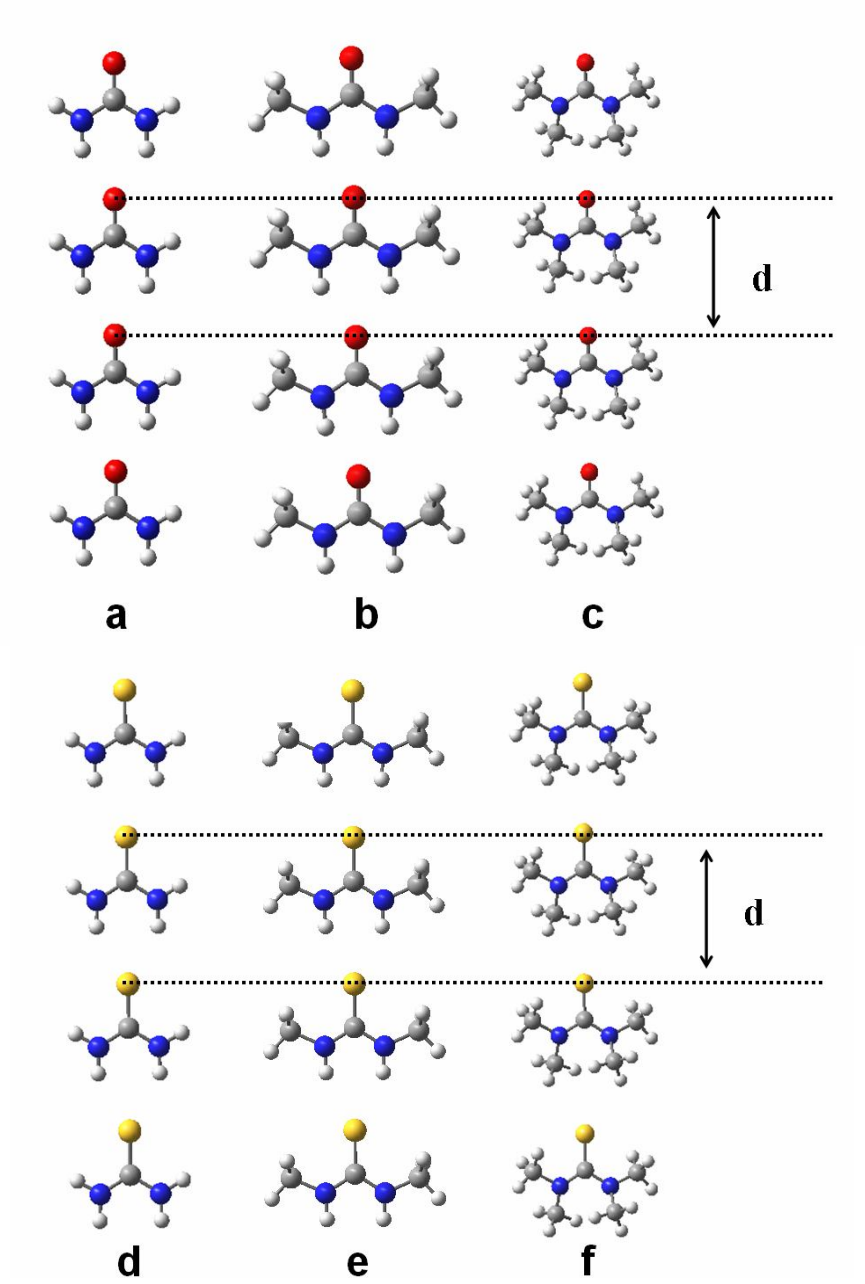

Figure 4.1: Linear chains of U (a), Me_2U (b), Me_4U (c), T (d), Me_2T (e) and Me_4T (f) indicating the intermolecular separation (d, in Å), as considered between two monomers in the linear aggregates.

consider linear chains of urea and thiourea and their dialkyl and tetra-alkyl derivatives. Whereas urea, thiourea, and their dialkyl derivatives are held in a head-to-tail arrangement through H-bonding, the tetra-alkyl analogues are held in a similar fashion through dipole-dipole interactions. Thus, it would be very interesting to study the effect of the varying nature of intermolecular interactions on the linear and first order non-linear polarizabilities as well as on the charge carrier mobilities of such linear chains. We also study how the intermolecular interactions in such systems [15] can be perturbed by the application of an external electric field, and comment on the charge carrier mobilities of such systems. We shall henceforth call urea, N,N'-dimethyl urea, N,N,N',N'-tetramethyl urea, thiourea, N,N'-dimethyl thiourea and N,N,N',N'-tetramethyl thiourea as U, Me_2U, Me_4U, T, Me_2T, Me_4T respectively for convenience.

Computational Details:

All optimizations have been performed using the ADF2006.01 package [16], at the TZ2P/GGA-PW91 level considering all electrons. Single point calculations to obtain the total energy of the system for the mobility calculations have been performed with the Gaussian 03 package [17] at the B3LYP/ 631-G (d,p) level. In the crystal structures of U, Me_2U, Me_4U, T, Me_2T, and Me_4T obtained from CCDC [18], the monomers are arranged linearly in columnar layers. We have extracted one pair of monomers from such a columnar layer in all the cases to generate the linear aggregates. To ensure that non-adjacent monomers have no significant effect on the geometry of a particular monomer, we have optimized linear chains of these molecules consisting of up to five monomers. The deviations of bond lengths in the individual monomers in the pentameric systems, when compared to that of the monomer located in the centre of the pentameric system, is negligible. Thus, we can safely extend the geometry of the central monomer in the pentameric system to realize chains of up to ten monomers to appreciably mimic an infinite system. In these chains, obtained as stated above, the exact distances (d, as shown in figure 4.1) between each monomer (measured as the distance between two central C atoms of neighboring molecules) are 4.75 Å, 4.67 Å, 6.26 Å, 5.61 Å, 5.64 Å and 6.96 Å

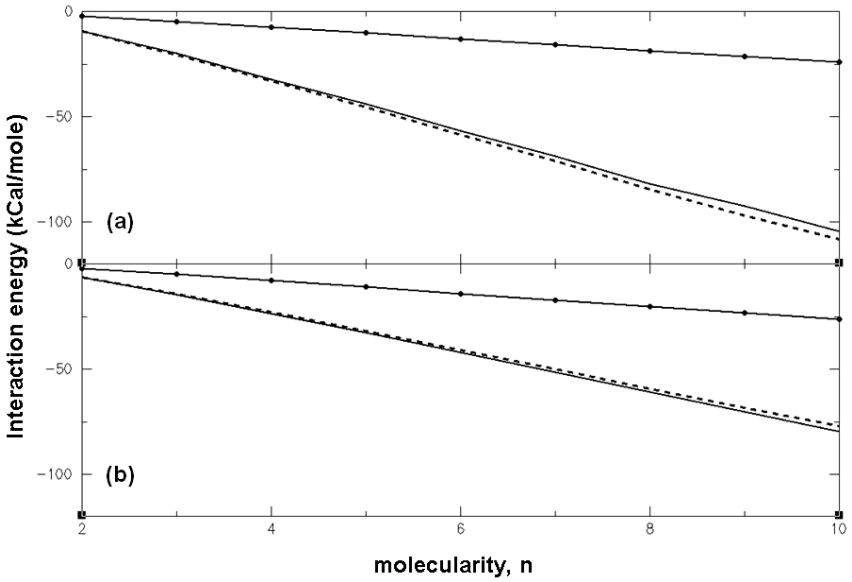

Figure 4.2: Variation of binding energy ΔE for different sizes of linear chains of (a) urea (solid line), N,N'-dimethyl urea (dashed line) and N,N,N',N'-tetramethyl urea (solid line with solid circles), and (b) thiourea (solid line), N,N'-dimethyl urea (dashed line) and N,N,N',N'-tetramethyl urea (solid line with solid circles).

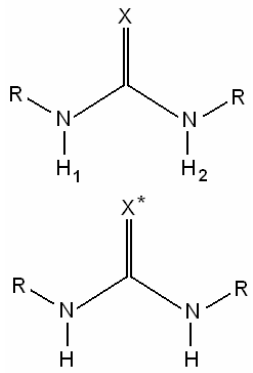

Figure 4.3: Schematic showing generalized dimer of the system. The H-bonds H_1-X^* and H_2-X^* form a triangle with the three atoms H_1, H_2, and X^*, respective side lengths of which are provided in the table (1) below.

Table 4.1: Side lengths of the triangle $H_1X^*H_2$.

system	H_1-H_2	H_1-X^*	H_2-X^*
U (X=O, R=H)	2.25	2.08	2.08
Me_2U (X=O, R=Me)	2.16	1.99	1.99
T (X=S, R=H)	2.34	2.49	2.49
Me_2T (X=S, R=Me)	2.17	2.46	2.46

for U, Me_2U, Me_4U, T, Me_2T, Me_4T, respectively. The distance between each monomer was kept constant for all chain lengths. For the calculation of electron and hole mobilities in these systems, we adopt a methodology [19] as mentioned in chapter 1 of the current thesis.

Results and Discussion:

To understand the electronic stabilization, we calculate the interaction energy for the linear chains as, $\Delta E_n = E_n - nE_1$ where E_n and E_1 are the energies of oligomers of molecularity *n* and 1 respectively. The variation of the interaction energy with increase in molecularity in the linear chains is shown in figure 4.2. As can be seen, the extent of stabilization for linear H-bonded chains of U and Me_2U and T and Me_2T are energetically similar, but larger than the corresponding stabilization energies of Me_4U and Me_4T, respectively. If we carefully examine the energy profile, we find interesting differences between U and Me_2U and between T and Me_2T that are negligible at lower molecularities (*n*), but become more apparent at larger values of *n*, particularly when $n > 6$. Linear aggregates of Me_2U are more stable than those of U, whereas, linear aggregates of T are more stable than that of Me_2T. This can be understood by considering the optimized structures of these systems, shown schematically in figure 4.3. The corresponding H atoms participating in the H-bonding (H_1 and H_2), and the heteroatom X^* (X=O, S) form a triangle, respective distances of which are presented in table 4.1. It is clear from table 4.1 that, H_1-H_2 distances for Me_2U and Me_2T are less than the H_1-H_2 distances for U and T, respectively. This is due to the steric class of interactions between the Me groups and the hydrogen atoms (H_1, H_2). For the oxygen analogues, this steric interaction brings the H atoms closer to the O atom (as shown in the table under the H_1-X^*, and H_2-X^* columns), and is thus favorable for the H-bonding. Hence, the intermolecular interactions in the aggregates of Me_2U are more stabilizing than those in the aggregates of U with the same number of monomer units. On the other hand, for the sulfur analogues, such proximity is unfavorable as it leads to steric congestion around the bulkier S atom, and this destabilization overrides the stabilization due to H-bonding at a closer proximity. Since the origin of such energy differences is steric in nature, the

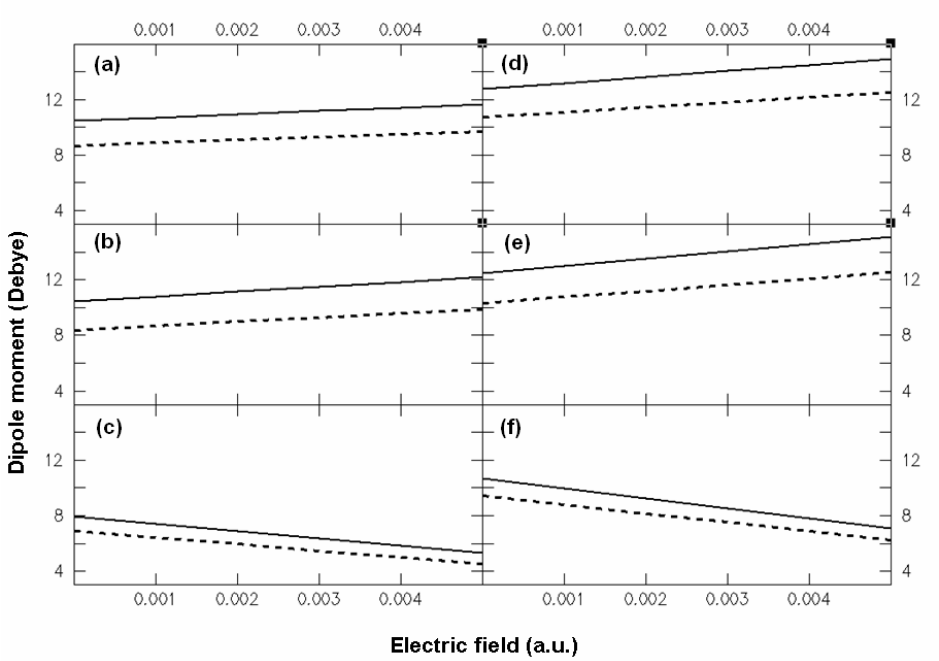

Figure 4.4: Variation of dipole moment of systems of (a) U, (b) Me_2U, (c) Me_4U, (d) T, (e) Me_2T, and (f) Me_4T with applied external electric field strength. Solid lines indicate dipole moments of dimeric systems, dashed lines indicate vector sum of dipole moments of the two monomers.

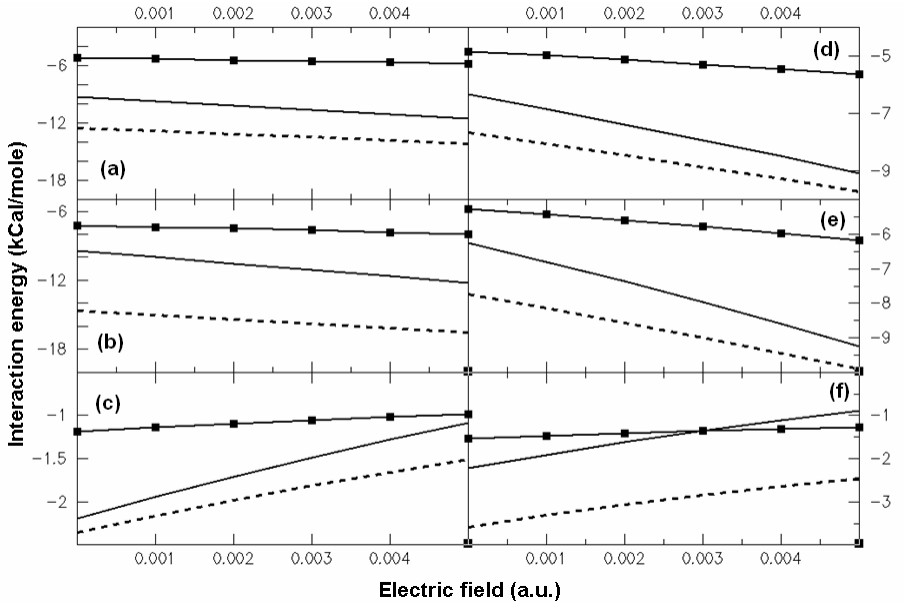

Figure 4.5: Variation in interaction energy terms of (a) U, (b) Me_2U, (c) Me_4U, (d) T, (e) Me_2T and (f) Me_4T with applied external electric field. Total energy (solid line), orbital interaction term (solid line with squares) and electrostatic interaction term (dashed line).

differences themselves are quite small. However, what is most noteworthy is that the extent of stabilization of linear chains of the tetra-alkyl derivatives through dipole-dipole interaction is much lesser when compared to the stabilization through H-bonding.

It has been shown that for linear chains of urea, H-bonding is mostly due to electrostatic (and polarization) interactions, rather than covalent interactions. The effects of electric fields on H-bonds for a qualitative understanding of the contribution of electrostatic and polarization interactions in different H-bonding environments have been studied [20]. It has been shown that high electric field strengths greatly alter the ground state geometry of H-bonded networks in water clusters [21]. External electric fields have also been shown to enhance charge-transfer efficiency in various systems like H-bonded acid-base complexes [22], organic molecular complexes [23, 24], as well as in organic molecule coated Au nanoparticles [25] and GaAs and ZnSe systems [26]. Thus, it would be very interesting to study the effect of electric field on the strengths of intermolecular interactions in such systems. To ensure that the geometry of the linear chains in the presence of the external electric field comparable to those in no-field condition, we have optimized the structures in external fields of 0.001 a.u. to 0.005 a.u, in steps of 0.001 a.u.

From a purely classical point of view, the dipole moment of the dimer is simply the summation of the dipole moment vectors of the non-interacting monomers. However, for molecular systems, the presence of a dipole next to another sufficiently perturbs the charge density throughout the backbone of the molecule and hence the dipole moment of the dimer may not equal to the sum of the dipole moments of the monomer. However, there is no thumb rule whatsoever that can predict the enhancement or reduction of dipole moment of the dimer. In figure 4.4, we compare the dipole moments of the dimeric systems with the sum of the dipole moments of the monomers and contrast between the variation of the dipole moments of U, Me_2U, Me_4U, T, Me_2T and Me_4T with the external electric field.

From figure 4.4, it is evident that the dipole moments of the dimers are in all cases more than the sum of the individual dipole moments of the monomers. However, what is interesting is that, while the dipole moments of the strongly H-bonded systems U, Me_2U, T, Me_2T increase with increase in the applied external field strength, that of the dimers of Me_4U and Me_4T decrease with the same. This can be understood by considering the

corresponding monomers. In the fully optimized structures of Me_4U and Me_4T, the C atoms of the lateral methyl groups are forced out of planarity from the nodal plane of the π bond to minimize the Me-Me steric interactions. Analysis of the Mulliken charges show that the lateral Me-N bond moments act opposite to the C=O bond moment, thus, decreasing the dipole moments of Me_4U and Me_4T drastically. As we increase the external field strength, the N atoms become more and more negatively charged, thereby increasing the lateral Me-N bond moment, consequently leading to the decrease in the dipole moment of the monomer. From figure 4.4, it is also evident that for strongly interacting systems like U, Me_2U, T and Me_2T, the enhancement in the dipole moments is more than that of Me_4U and Me_4T systems.

We further calculate the stabilization of the dimeric systems with varying electric field, as shown in figure 4.5. The stabilization energy of the dimer in presence of an electric field is defined as the stabilization energy of the dimer minus the sum of the energies of the monomers in the same electric field [27]. We find that for the H-bonded systems, viz. U, Me_2U, T and Me_2T, the interaction (stabilization) energy between the monomers increases with increase in the field strength, whereas for Me_4U and Me_4T the dimeric systems become unstable with increasing electric field. The energy of interaction between the monomers in the dimeric systems can be further broken down in terms of electrostatic (attractive) terms and orbital interaction terms through the Morukuma [12] analysis.

From the standpoint of the Kohn-Sham MO theory, one can decompose the total energy of a system into the bond energy between its fragments. The fragments maybe defined in such a case to obtain a relevant picture of the contributions of orbital, electrostatic, polarization and charge-transfer interactions toward the overall interactions between the fragments. Thus, this decomposition allows one to qualitatively investigate the role of the individual interactions (into which the interaction energy has been broken down) when a *supermolecule* is formed. The overall bond energy ΔE is broken down into the following terms:

$$\begin{aligned} \Delta E &= \Delta E_{prep} + \Delta E_{\text{int}} \\ &= (\Delta E_{prep,geo} + \Delta E_{prep,el}) + \Delta E_{\text{int}} \\ &= (\Delta E_{prep,geo} + \Delta E_{prep,el}) + \Delta E_{ES} + \Delta E_{EX} + \Delta E_{POL} + \Delta E_{CT} \end{aligned} \tag{4.1}$$

where, ΔE_{prep} is the energy required to deform the separated fragments from their equilibrium structure to the geometry they acquire in the overall molecule ($\Delta E_{prep,geo}$), and to excite them to their valence electronic configuration ($\Delta E_{perp,el}$). ΔE_{int} is the interaction energy between the fragments which is further broken down into four components, electrostatic (E_{ES}), exchange (E_{EX}), polarization (E_{POL}), and charge-transfer (E_{CT}), in accordance with the Kitaura-Morukuma scheme [12]. According to this scheme, the wavefunctions of the two isolated subunits of the complex φ_A and φ_B are computed separately. This pair of wavefunctions is taken as the starting point for an *ab initio* calculation of the complex.

$$\left|\varphi_1\right\rangle = \left|\varphi_A\varphi_B\right\rangle \tag{4.2}$$

It is noteworthy to realize here that, the electrons of A are antisymmetric within φ_A, and similarly for that of B. However, no exchange is allowed between φ_A and φ_B . The zeroth iteration of the SCF cycle yields an energy which differs from the total energy of the pair of isolated subunits by an amount E_{ES} since it permits the field of each monomer to interact with the density φ_A^2 of the partner molecule, without perturbing its density. The exchange energy is extracted by repeating the SCF procedure, however, this time permitting interchange of electrons between A and B:

$$\left|\varphi_2\right\rangle = A_{AB}\left|\varphi_A\varphi_B\right\rangle \tag{4.3}$$

where, A_{AB} denotes an antisymmetric combination of the wavefunctions. For the cases where one considers an H-bonded system, the interaction is in-between two closed shell systems. For such systems, the exchange interaction is repulsive in nature. This is similar to the classical picture of 'steric repulsion' between charge clouds. Starting with φ_1, and enforcing the restriction of no-exchange between electrons in the fragments A and B, convergence of the iterative SCF procedure permits the electrons in each subunit to relax in presence of its partner. The extra stabilization gained as a result of this relaxation is associated with the polarization of one subunit by the other. This is labeled as E_{POL}. A similar SCF relaxation, but now allowing the full anti-symmetrization of all electrons, yields the charge transfer energy E_{CT}. This arises due to transfer of electrons from the

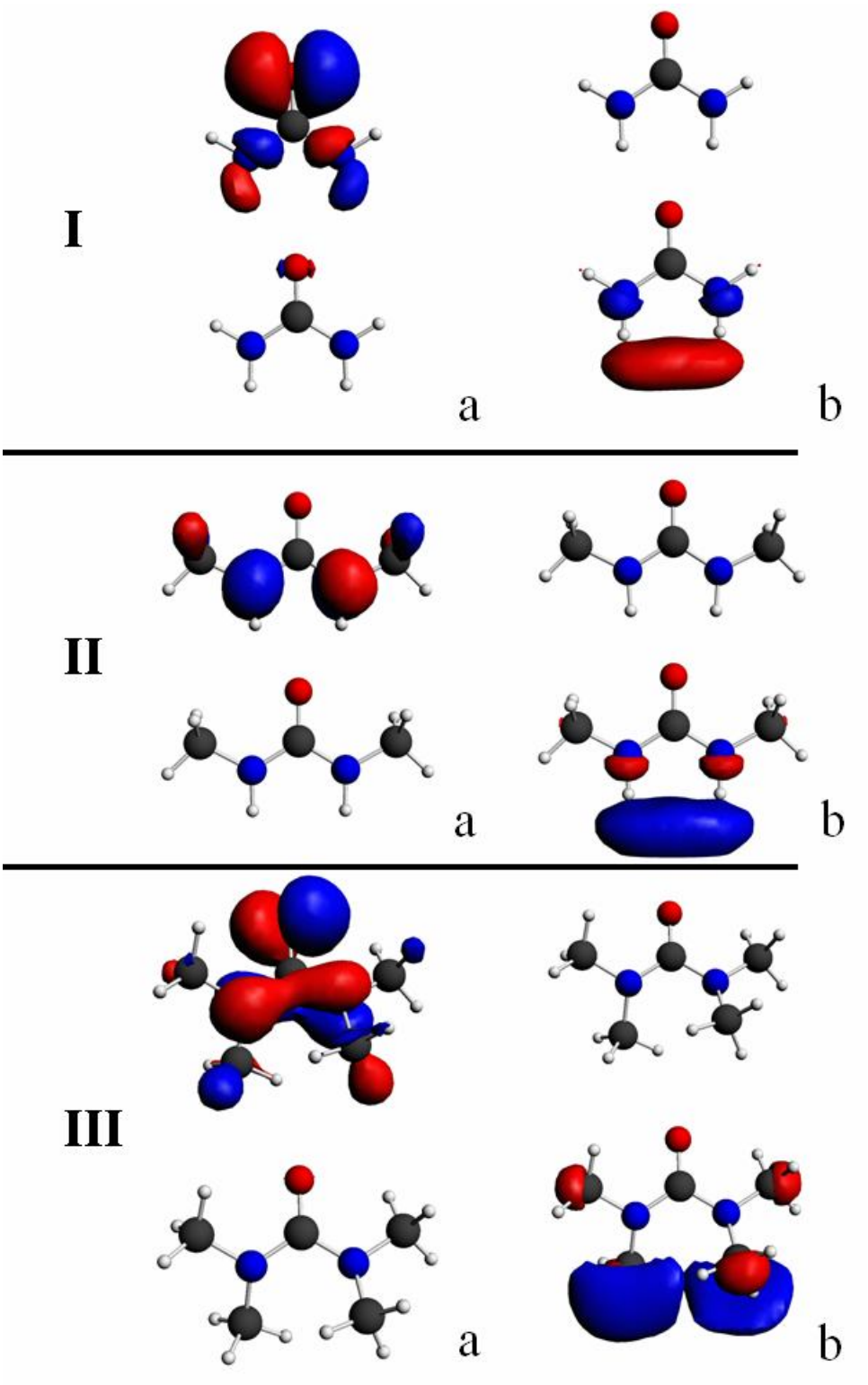

Figure 4.6 (i): HOMO-LUMO orbital plots for U (I), Me_2U (II), Me_4U (III). HOMO (a); LUMO (b).

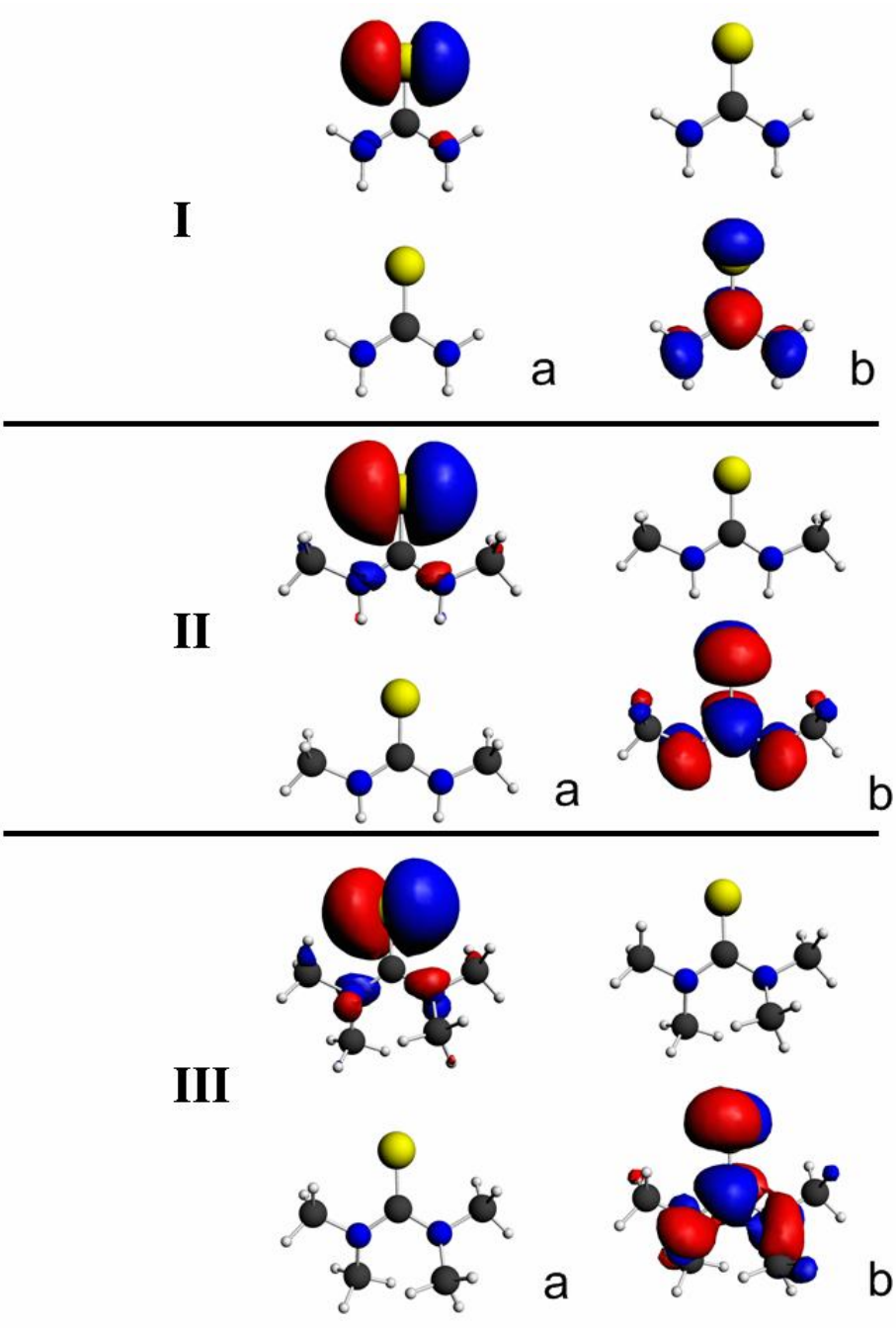

Figure 4.6 (ii): HOMO-LUMO orbital plots for T (I), Me_2T (II), Me_4T (III). HOMO (a); LUMO (b).

occupied MOs of one subunit to the unoccupied MOs of the other subunit. The HOMO and LOMO plots, clearly indicative of charge transfer in donor-acceptor systems, are shown in figure 4.6.

The comparison of the orbital interaction terms can be particularly informative as these terms account for the electron pair bonding, charge-transfer (HOMO-LUMO) and polarization interactions [28]. It is interesting to note that, for all these systems, the trend in the variation of the energy of interaction is governed primarily by the electrostatic energy term. As inferred from the variation of dipole moment with increasing external electric field, the electrostatic energy (stabilization) decreases for the case of Me_4U and Me_4T, whereas it increases for the rest. This is because the purely electrostatic interaction (stabilizing) energy term between two dipoles is proportional to the product of the dipole moments of the monomers, and inversely proportional to the cubic of their separation. However, what is noteworthy is that the orbital interaction terms are nearly constant for all the cases. The slight decrease in the orbital interaction terms with increasing field strength for the sulfur analogs is due to the fact that the C-S pi bonds are weaker than C-O pi bonds, and are relatively more polarizable, and hence more perturbed by the electric field.

To understand the effect of H-bonding and dipolar interactions on the linear and non-linear optical properties, we calculate the polarizability (α) and 1st frequency dependent hyperpolarizability, $\beta(\omega)$, with varying chain lengths of such linear systems. For the calculation of α and $\beta(\omega)$, we have used an external a.c field of 0.001 a.u [29]. We find that α increases linearly with increasing chain length for all systems. However the $\beta_n(\omega)$ shows remarkable features, as shown in figure 4.7.

We find that for the U and Me_4U, $\beta_n(\omega)$ increases up to n=2, then decreases, and an oscillatory pattern is obtained. However for Me_2U, $\beta_n(\omega)$ initially decreases up to n=2, and then increases drastically. The case for the sulfur analogs is, however, completely different. For T and Me_2T, $\beta_n(\omega)$ increases up to n=2, but then decreases up to n=7 and n=5, respectively, after which it increases again. However for Me_4T, we find that after n=2, $\beta_n(\omega)$ increases drastically up to n=10. To understand the effect of the intermolecular interaction in such systems on the magnitude of $\beta_n(\omega)$, we look at the

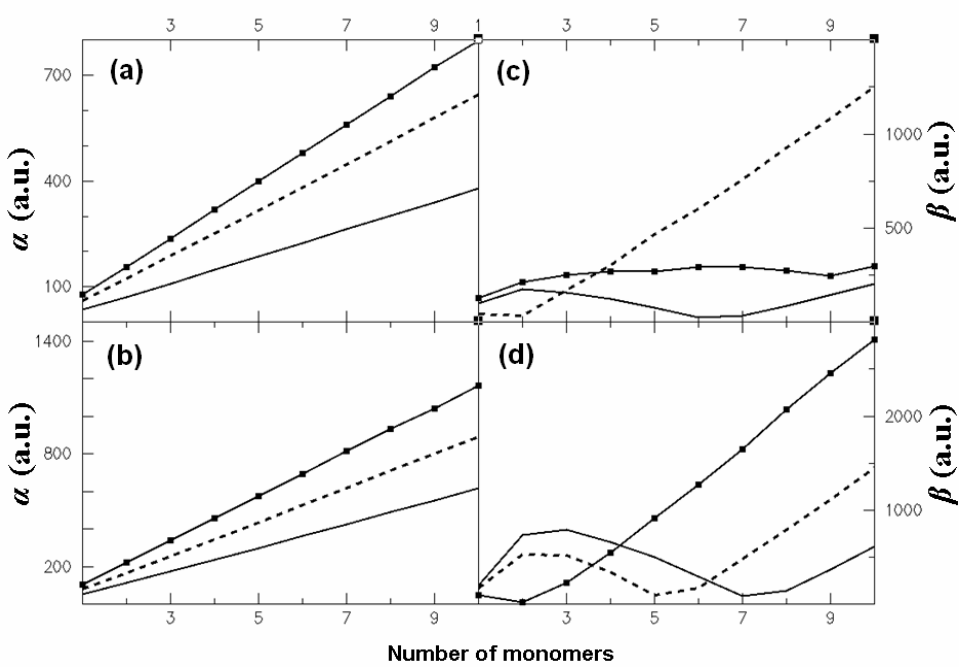

Figure 4.7: variation of α [O-analogues (a), S-analogues (b)] and β [O-analogues (a), S-analogues (b)] with increase in chain length. Solid line, dashed line, and solid line with squares indicate corresponding systems with increasing molecular weight, in the same order.

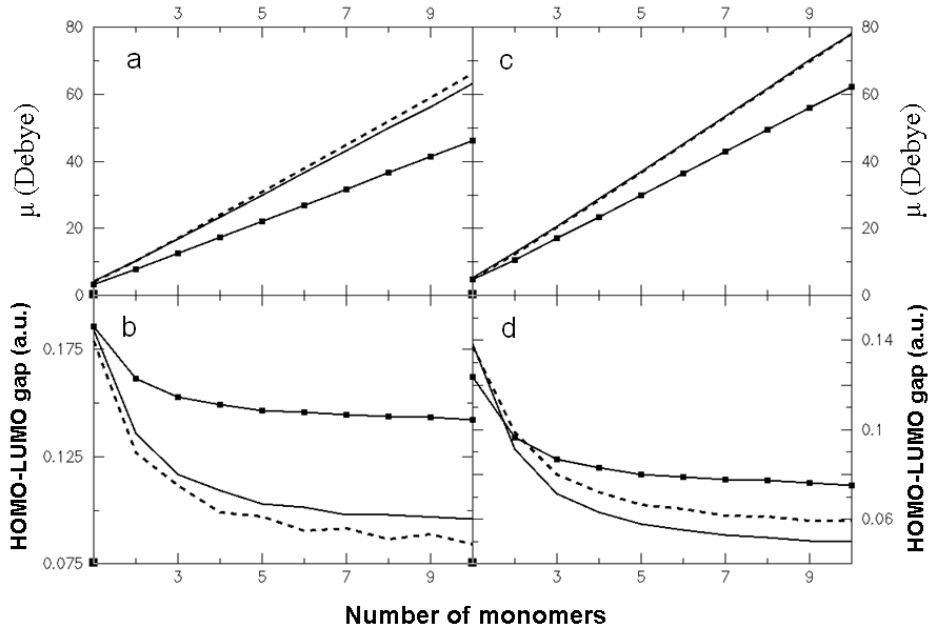

Figure 4.8: Variation of ground state dipole moment [O-analogues (a), S-analogues (c)] and optical gaps [O-analogues (b), S-analogues (d)] with increase in chain length. Solid line, dashed line, and solid line with squares indicate corresponding systems with increasing molecular weight, in the same order.

parameters that govern it carefully. Within the framework of the two-state model, the frequency dependent second harmonic generation can be written as [11],

$$\beta(\omega)_{two-level} = \frac{2e^2}{2\hbar^3} \frac{\omega_{ge} f_{ge} \Delta\mu_{ge}}{(\omega_{ge}{}^2 - \omega^2)(\omega_{ge}{}^2 - 4\omega^2)} \tag{4.4}$$

where, ω_{ge} is the optical transition energy, f_{ge} is the associated oscillator strength, and $\Delta\mu_{ge}$ is the difference between the ground- and excited-state dipole moments. To qualitatively understand the dependence of the magnitude of $\beta(\omega)$ on these microscopic parameters, we compare the variation of the optical energy gap and the ground state dipole moment with increasing molecularity (n) of the linear aggregates, as shown in figure 4.8.

We find that, while the dipole moment increases linearly with increase in chain length, the optical gap decreases sharply as we move to the dimer, and continues to decrease after that with increase in n, however, with a much lesser slope. From equation 4.4, the $\beta(\omega)$ value is directly proportional to $\Delta\mu_{ge}$ and inversely proportional to the optical gap, ω_{ge}. We find that the optical gaps of the linear chains of Me_4U are much higher than that of the other O-analogues. On the other hand, the optical gaps of the linear chains of the S-analogues are more or less comparable. The trend in the variation of the dipole moments with n is similar for both the O and S analogues. At n=10, the $\beta(\omega)$ value for Me_2U is the highest, owing to the lowest optical gap and the highest dipole moment. On the other hand at n=10, the $\beta(\omega)$ value for Me_4T is the highest, although both the dipole moment and optical gap indicate that Me_2T should have the highest $\beta(\omega)$ value. It should be noted here that the two-state model is a qualitative picture, and as has been given in equation (1.1.21) of chapter 1, the magnitude of $\beta(\omega)$ actually involves summing over all the intermediate states.

To estimate the effect of dipolar interactions and H-bonding on the charge carrier mobilities in U, Me_2U, Me_4U, T, Me_2T and Me_4T systems, we compare the electron and hole mobilities considering the crystals [18] of these molecules. To a reasonable approximation, each hopping process can be understood as a non adiabatic electron transfer reaction. For such cases, we utilize the Markus theory [30-32] to calculate the rate of charge transfer between neighboring molecules.

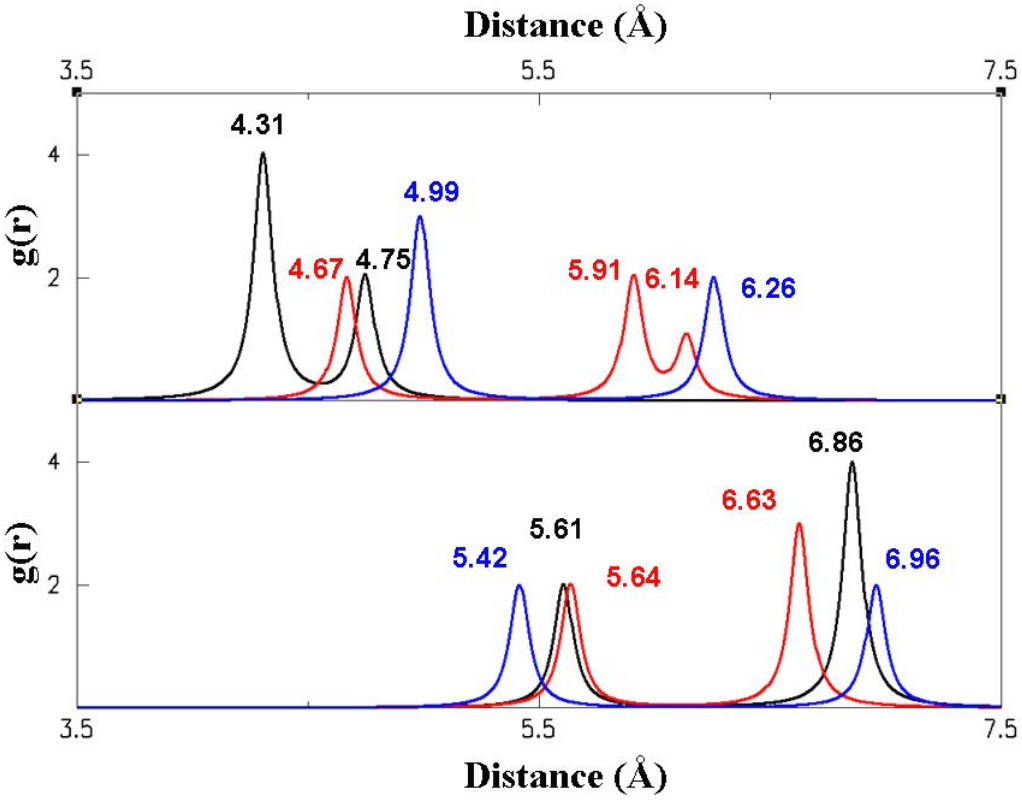

Figure 4.9: Radial distribution function for (a) U (black), Me_2U (red), and Me_4U (blue); and (b) T (black), Me_2T (red), and Me_4T (blue) in 2 x 2 x 2 supercells. Note that a Lorentzian broadening factor of 0.1 is used for smoothening the crystalline δ functions at the peak positions, x axis readings of which are indicated in the appropriate colors.

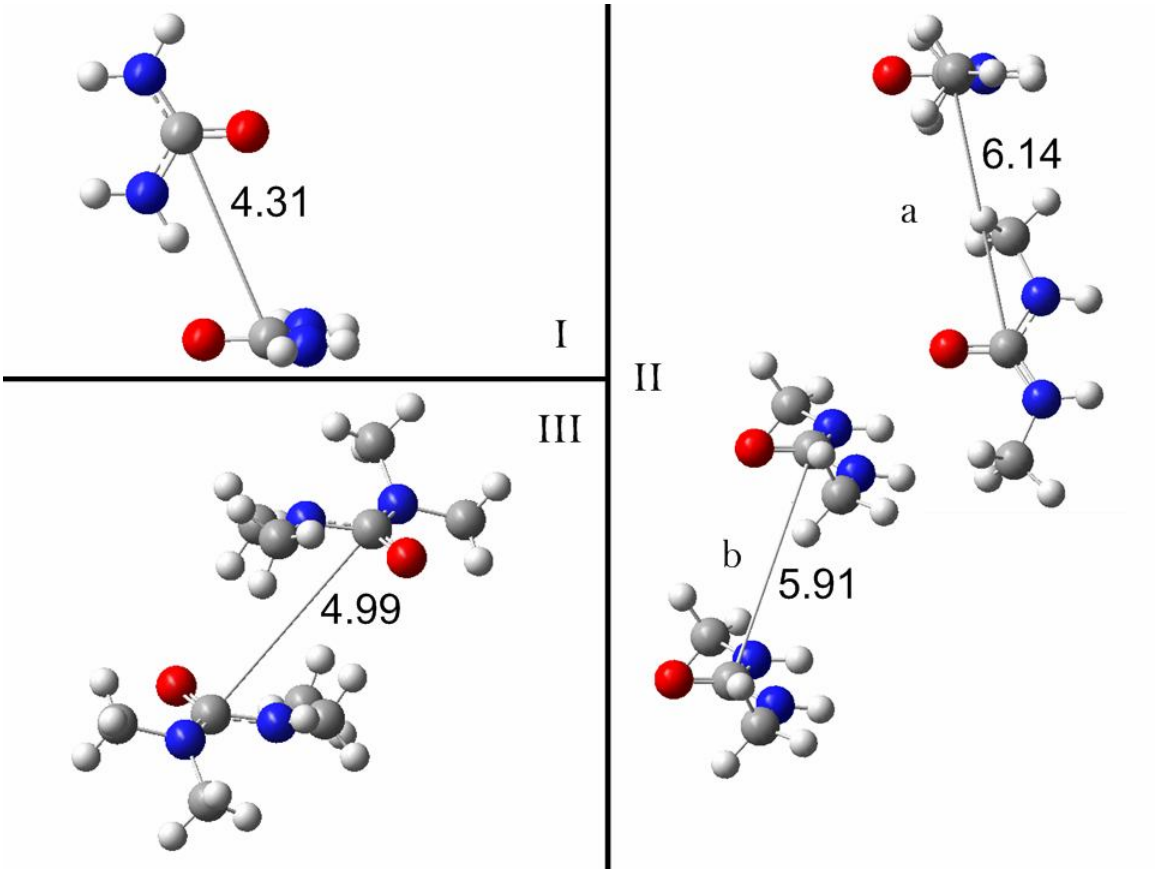

Figure 4.10 (a): Molecular contacts between the columnar layers in I (U), II (Me_2U) and III (Me_4U) indicating the intermolecular distances (in Å). IIa and IIb indicate two different molecular contacts for the Me_2U system.

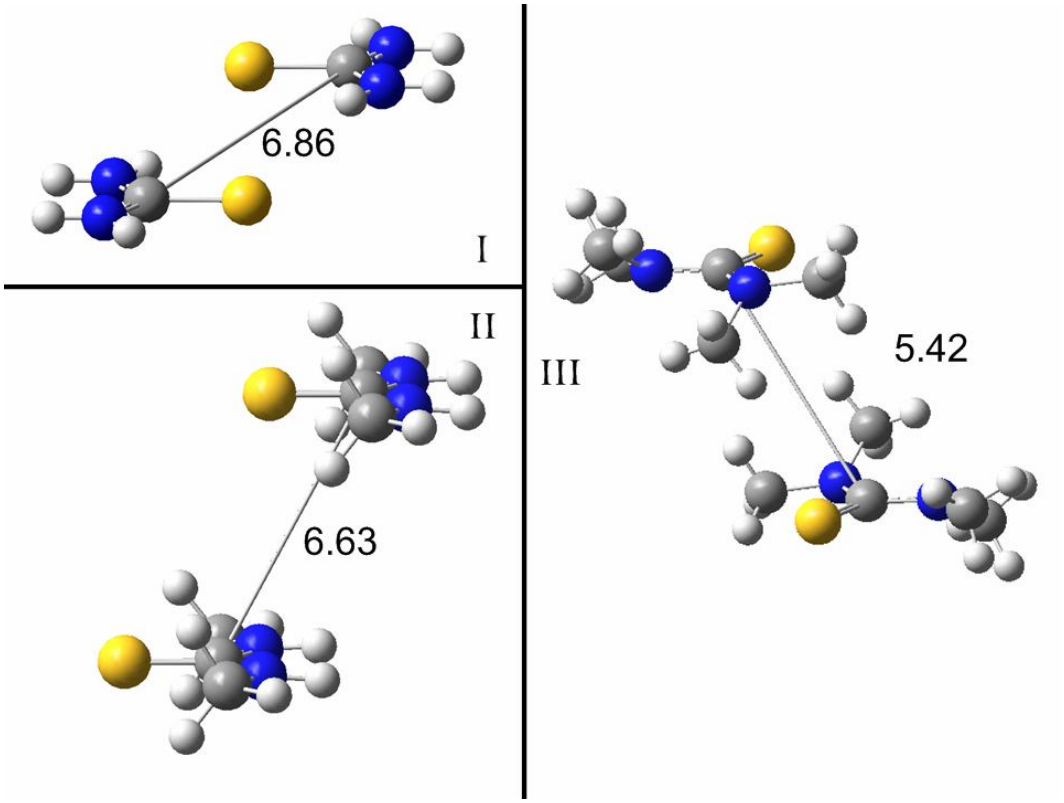

Figure 4.10 (b): Molecular contacts between the columnar layers in I (T), II (Me_2T) and III (Me_4T) indicating the intermolecular distances (in Å).

For a detailed understanding of the contribution of the different molecular contacts on the charge carrier mobilities in these systems, we consider $2\times2\times2$ supercells of the systems. We calculate the radial distribution function, g(r), maintaining a center of distance of 10.0 Å as cutoff, as shown in figure 4.9. We find from the g(r) plot that the most significant molecular contacts are at short distances ranging from 4.00 – 7.50 Å. We also find that in the crystal structures, the molecular contacts involve different relative orientations with respect to each other. As the relative orientation of the molecules are very important in realizing the proper magnitudes of the coupling matrix elements, and hence the electron and hole mobilities, we probed into the crystal structure to have a proper understanding of the types of molecular contacts present. We find that, in the crystal structures, apart from the linear packing of the molecules in the columnar layers (as mentioned before), there also exists parallel and anti parallel stacking. The different molecular contacts due to the stacking between different columnar layers, and the corresponding intermolecular distances are shown in figure 4.10. To ensure that molecular contacts at reasonably large distances do not contribute to the splitting of the HOMO and LUMO levels, we calculated the H_{mn} splitting as a function of intermolecular distances considering various orientations of the molecular contacts. We find that for the molecular contacts as observed in the crystal structures of U, Me_2U, Me_4U, T, Me_2T and Me_4T, the H_{mn} vanishes for values greater than 8.00 Å. The H_{mn} and the reorganization energies (λ) for the hole and electron for all the systems in different molecular contacts (linear and stacking orientations) are given in table 4.2. From these values, we calculate the values of the electron and hole mobilities (in $cm^2V^{-1}s^{-1}$) for the entire crystal systems are given in table 4.3.

Table 4.2: Comparison of the hole and electron H_{mn} and λ values for U, Me_2U, Me_4U, T, Me_2T and Me_4T. Units are in Hartrees. '***l***' and '***s***' indicate linear (intra-columnar) and stacking (inter-columnar) contacts, respectively.

system	Reorganization energy (λ)			H_{mn}	
	hole	electron		hole	electron
U	1.0299×10^{-2}	1.2969×10^{-3}	***l***	9.18×10^{-2}	7.70×10^{-3}
			s	4.93×10^{-2}	6.58×10^{-3}
Me_2U	7.4768×10^{-3}	1.9836×10^{-3}	***l***	4.85×10^{-2}	5.88×10^{-3}
			s	4.00×10^{-2}	6.05×10^{-3}
Me_4U	9.918×10^{-3}	1.709×10^{-3}	***l***	2.05×10^{-2}	5.29×10^{-3}
			s	1.74×10^{-2}	5.26×10^{-3}
T	7.081×10^{-3}	2.441×10^{-3}	***l***	3.92×10^{-2}	4.05×10^{-3}
			s	2.85×10^{-2}	1.83×10^{-3}
Me_2T	1.294×10^{-2}	2.258×10^{-3}	***l***	2.00×10^{-2}	3.56×10^{-3}
			s	9.12×10^{-3}	2.25×10^{-3}
Me_4T	2.166×10^{-2}	5.091×10^{-3}	***l***	8.69×10^{-2}	4.81×10^{-3}
			s	6.64×10^{-2}	5.07×10^{-3}

Table 4.3: Comparison of the hole and electron mobilities for U, Me_2U, Me_4U, T, Me_2T and Me_4T. Mobilities are reported in $cm^2\,V^{-1}\,s^{-1}$.

system	μ_{hole}	$\mu_{electron}$
U	0.226	0.042
Me_2U	0.174	0.028
Me_4U	0.018	0.027
T	0.165	0.009
Me_2T	0.171	0.008
Me_4T	0.013	0.007

Although we find that aggregates of urea and thiourea, and their methyl derivatives have poor charge carrier mobilities, especially when compared to organic semiconductors like naphthalene and perylene [19, 33-35], it is important to note that the strongly H-bonded systems (U, Me_2U, T and Me_2T) have hole mobility values higher than that for the electron.

As mentioned before, there are two types of molecular contacts that we observe from the crystal structures of these systems. Since, in this study, we focus on the

electrical polarizations and charge transfer efficiencies in linear chains of U, Me_2U, Me_4U, T, Me_2T and Me_4T, we find it interesting to decompose the total mobility values of the crystal in terms of the two classes of molecular contacts; viz. the linear contacts and the stacked anti-parallel contacts. These values are presented in table 4.4.

Table 4.4: Comparison of the hole and electron mobilities for U, Me_2U, Me_4U, T, Me_2T and Me_4T arising from different molecular contacts. Mobilities are reported in $cm^2 V^{-1} s^{-1}$.

system	Linear Contacts		Stacked Contacts	
	μ_{hole}	$\mu_{electron}$	μ_{hole}	$\mu_{electron}$
U	0.162	0.023	0.064	0.019
Me_2U	0.127	0.010	0.047	0.018
Me_4U	0.012	0.014	0.006	0.013
T	0.091	0.008	0.074	0.001
Me_2T	0.103	0.006	0.068	0.002
Me_4T	0.011	0.004	0.002	0.003

Thus, we find that, linear contacts in the crystal systems of U, Me_2U, Me_4U, T, Me_2T and Me_4T have much higher contribution to hole mobilities.

In conclusion, we have calculated the linear and non-linear polarizability of linear chains of urea and thiourea and their alkyl derivatives. We find that strongly H-bonded chains of urea, thiourea, and their dimethyl derivatives, where three-center-two-hydrogen bonds exist per intermolecular contacts are not a good choice for NLO materials. We also find that the strength of H-bonding greatly affects the magnitude of the NLO responses, even when the relative orientations of interacting molecules are similar. Thus, while the magnitude of $\beta(\omega)$ of strongly H-bonded linear aggregates of dimethyl urea increase with increase in chain length, that of urea (with similar strengths of H-bonding) decreases with the same. On the other hand, among the sulfur analogues, the magnitude of $\beta(\omega)$ for linear aggregates of tetramethyl thiourea show the highest rate of increase with increase in chain length. This arises due to the difference in the electronegativities of O and S, as well as due to the fact that C=S π bonds, being less stable than C=O π bonds, are more polarizable than the latter. Thus, although, the enhancement in dipole moments with increasing chain length considerably increases the linear polarizability, we find that the

trend in the $\beta(\omega)$ cannot be generalized. We further show that the dipole-dipole (i.e. electrostatic) interactions are the major contributory effect toward H-bonding in these systems. We also find that, with increasing electric fields induce stronger H-bonding in linear aggregates of U, Me_2U, T and Me_2T, whereas the strength of dipolar interaction in the linear aggregates of the dialkyl derivatives decreases with the same. We also compare the charge carrier mobilities in linear aggregates of such systems. We find that although the overall charge carrier mobilities of the linear aggregates of urea, thiourea and their methyl derivatives are low, H-bonded systems have higher hole mobility values in comparison to that for the electron. We also compare the role of orientation in fine-tuning the electron and hole mobilities in these systems.

References:

[1] M. Halter, Y. Liao, R. M. Plocinik, D. C. Coffey, S. Bhattacharjee, U. Mazur, G. J. Simpson, G. H. Robinson, S. L. Keller, *Chem. Mater*., 2008, **25**, 1778.

[2] S. Pal, S. K. Pati , *Computing Letters*, 2008, **3**, 367.

[3] Schoonbeck F. S., van Esch J. H., Wegewijs B., Rep D. B. A., de Haas M. P., Klapwijk T. M., Kellogg R. M., Feringa B. L., *Angew. Chem. Intl. Ed*., 1999, **38**, 1393.

[4] McCulloch I., Heeney M., Bailey C., Genevicius K., MacDonald I., Shkunov M., Sparrowe D., Tierney S., Wagner R., Zhang W., Chabinyc M. L., Kline R. J., McGehee M. D., Toney M. F., *N. Mat*., 2006, **5**, 328.

[5] Choulis S. A., Kim Y., Nelson J., Bradley D. D. C., Giles M., Shkunov M., McCulloch I., *Adv. Phys. Lett.*, 2004, **85**, 3890.

[6] T. J. Marks, M. Ratner, *Angew. Chem*, 1995, **34**, 155.

[7] C. A. Hunter, J. K. M. Sanders, *J. Amer. Chem. Soc*, 1990, **112**, 5525.

[8] A. J. Stone (Ed.), The theory of Intermolecular forces, *Oxford University Press*, 1996; A. J. Stone, H. Ratajczac and W. J. Orville-Thomas (Eds.), Molecular Interactions, *Wiley*, 1980.

[9] T. Steiner, *Angew. Chem*, 2002, **41**, 48; T. Steiner, G. R. Desiraju, The weak Hydrogen Bond in Structural Chemistry and Biology, *Oxford University Press*, 1999.

[10] D. S. Chemla, J. S. Zyss, Nonlinear Optical Properties of Organic Crystals and Molecules, *Academic Press*, 1987.

[11] (a) A. Dutta, S. K. Pati, *Chem. Soc. Rev.*,2006, **35**, 1305; (b) A. Dutta, S. K. Pati, *J. Mol. Struct. (Theochem)*, 2005, **97**, 756.

[12] K. Morukuma, *Acc. Chem. Res.*, 1977, **10**, 294;

[13] J. A. Platts, *Phys. Chem. Chem. Phys*, 2000, **2**, 3115; A. M. Pendas, M. A. Blancos, E. Francisco, *J. Chem. Phys.*, 2006, **125**, 184112.

[14] S. R. Marder, J. W. Perry, C. P. Yakymyshyn, *Chem. Mater.*, 1994, **6**, 1137.

[15] F. Lortie, S. Boileau, L. Bouteiller, *Chem. Eur. J*., 2003, **9**, 3008.

[16] G. te Velde, F.M. Bickelhaupt, S.J.A. van Gisbergen, C. Fonseca Guerra, E.J. Baerends, J.G. Snijders, T. Ziegler , *J. Comput. Chem*.., 2001,22, 931; C. Fonseca Guerra, J.G. Snijders, G. te Velde, and E.J. Baerends, *Theor. Chem. Acc*., 1998, **99**, 391; ADF2007.01, SCM, Theoretical Chemistry, Vrije Universiteit, Amsterdam, The Netherlands, http://www.scm.com.

[17] Gaussian 03, Revision C.02, Frisch, M. J.; Trucks, G. W.; Schlegel, H. B.; Scuseria, G. E.; Robb, M. A.; Cheeseman, J. R.; Montgomery, Jr., J. A.; Vreven, T.; Kudin, K. N.; Burant, J. C.; Millam, J. M.; Iyengar, S. S.; Tomasi, J.; Barone, V.; Mennucci, B.; Cossi, M.; Scalmani, G.; Rega, N.; Petersson, G. A.; Nakatsuji, H.; Hada, M.; Ehara, M.; Toyota, K.; Fukuda, R.; Hasegawa, J.; Ishida, M.; Nakajima, T.; Honda, Y.; Kitao, O.; Nakai, H.; Klene, M.; Li, X.; Knox, J. E.; Hratchian, H. P.; Cross, J. B.; Bakken, V.; Adamo, C.; Jaramillo, J.; Gomperts, R.; Stratmann, R. E.; Yazyev, O.; Austin, A. J.; Cammi, R.; Pomelli, C.; Ochterski, J. W.; Ayala, P.

Y.; Morokuma, K.; Voth, G. A.; Salvador, P.; Dannenberg, J. J.; Zakrzewski, V. G.; Dapprich, S.; Daniels, A. D.; Strain, M. C.; Farkas, O.; Malick, D. K.; Rabuck, A. D.; Raghavachari, K.; Foresman, J. B.; Ortiz, J. V.; Cui, Q.; Baboul, A. G.; Clifford, S.; Cioslowski, J.; Stefanov, B. B.; Liu, G.; Liashenko, A.; Piskorz, P.; Komaromi, I.; Martin, R. L.; Fox, D. J.; Keith, T.; Al-Laham, M. A.; Peng, C. Y.; Nanayakkara, A.; Challacombe, M.; Gill, P. M. W.; Johnson, B.; Chen, W.; Wong, M. W.; Gonzalez, C.; and Pople, J. A.; Gaussian, Inc., Wallingford CT, 2004.

[18] CCDC codes: NIJHUJ, NIJHUJ01, UREAXX08, UREAXX, TIDBIR, THIOUR* (*=1-13), MTUPX01.

[19] A. Datta, S. Mohakud, S. K. Pati, *J. Chem. Phys.*, 2007, **126**, 144710; A. Datta, S. Mohakud, S. K. Pati, J. Mater. Chem., 2007, **17**, 1933.

[20] J. J. Dannenberg, L. Haskamp, A. Masunov, *J. Phys. A.*, 1999, **103**, 7083.

[21] Y. C. Choi, C. Pak, K. S. Kim, *J. Chem. Phys*., 2006, **124**, 4308.

[22] M. Ramos, I. Alkorta, J. Elguero, N.S. Golubev, G.S. Denisov, H. Benedict and H.H. Limbach, *J. Phys. Chem*., 1997, **101**, 9791

[23] C. J. Eckhardt, *J. Chem. Phys*., 1972, **56**, 3947

[24] Hulliger J., Martin L., Gervais C., Wust T., Budde F., *Chem. Phys. Lett*., 2003, **377**, 340.

[25] J. Ouyang, C. Chu, D.Sieves, Y. Yang, *Appl. Phys. Lett*., 2005, **86**, 123507.

[26] Stahn J., Pietsch U., Blaha P., Schwarz K., *Phys. Rev. B*., 2001, **63**, 165205.

[27] ADF user's Documentation: www.scm.com

[28] Chemistry with ADF, www.scm.com

[29] van Gisbergen S. J. A., Snijders J. G., Baerends E. J., *Comp. Phys. Commun*., 1999, **118**, 119.

[30] J. L. Bredas, J. P. Calbert, D. A. Silva Filho, J. Cornil, *Proc. Natl. Acad. Sci. USA*, 2002, **99**, 5804.

[31] R. A. Markus, *Rev. Mod. Phys*., 1993, **65**, 599.

[32] Y. A. Berlin, G. R. Hutchinson, P. Pampala, M. A. Ratner, J. Michl, *J. Phys. Chem. A*, 2003, **107**, 3970.

[33] 'Ultrapure, High Mobility Organic Photoconductors', *Applied Physics A: Materials Science and Processing*, 1985, 36.

[34] Laquindanum J. G., Katz H. E., Dodabalapur A., Lovinger A. J., *J. Amer. Chem. Soc*., 1996, **118**, 11331.

[35] Chesterfield R. J., McKeen J. C., Newman C. R., Ewbank P. C., da Silva Filho D. A., Bredas J. L., Miller L. L., Mann K. R., Frisbie D. C., *J. Phys. Chem. B*., 2004, **50**, 19281.

Chapter V

V. Semiconductor to Metal Transition in Single Walled Carbon Nanotubes upon Interactions with Noble Metals: The Nature of Interactions

Introduction:

Carbon is probably the most studied element in the periodic table, not just because it is the 4th most abundant element on the earth but because of its versatility in forming a wide range of structures in the elemental form. The variety of these structures, called allotropes, range from the relatively well known structures like amorphous carbon, diamond and graphite, to the more recent fullerenes [1], carbon nanotubes [2], and nanofibres [3]. Recent research has also lead to the discovery of other allotropes like aggregated diamond nanorods [4], lonsdaleite [5], glassy carbon [6], carbon nanofoam [7] and linear acetylenic carbon [8]. It is with the discovery of fullerenes [9] in 1985, and graphene [10] and carbon nanotubes [11-13] that the chemistry and physics of carbon took a new turn. Graphene has been gaining prominence only recently due to the recent progress in experimental techniques [14], however carbon nanotubes have been the subject of extensive studies in the last two decades owing to their relative ease of synthesis and fascinating properties. Although single wall carbon nanotubes may be realized by rolling a sheet of graphene into a tubular structure, they exhibit properties much different from those of graphene.

Single-walled carbon nanotubes (SWNTs) exhibit attractive properties, both from the synthetic and application perspectives. The interesting properties of carbon nanotubes, coupled with the technological advancements in optical instruments has led to the spate of activity in this field resulting in significant breakthroughs in structure-property correlations [15] and chemo-synthetic insights [16]. Apart from the fascinating properties of the pristine carbon nanotubes, recent developments involving composites of SWNTs with systems like CdS [17] and polymers [18-20] being employed as opto-electronic devices are immense. Furthermore, SWNTs doped with various atoms like B

and N offer promising applicabilities as chemical sensors [21], nano-medicines [22], and DNA recognizers [23]. SWNTs also find use as quantum wire FETs, as being assembled into hybrid materials behaving as rectifying diodes as well as charge-transfer induced light harvesting semiconductor-CNT assemblies [24].

Interactions of SWNTs with metals involve modulation of the electronic structure of the SWNTs. Experimental investigations in this regard have a certain drawback considering the fact that understandings cannot be pinpointed to either metallic or semiconducting SWNTs, unless adequate measures are taken to isolate one from the other [25-28]. When such measures are taken, SWNT composites prove to be exciting materials from the viewpoint of modulation of the band structure, which is experimentally realized by monitoring the increment in the Raman G band, accompanied by a decrease in the line width [29], depending on whether the SWNTs are metallic or semiconducting [30]. However, chemical functionalization of SWNTs towards achieving SWNT composites is not preferable, as this severely alters the electronic structure. To this regard, SWNT composites involving physisorbed metals prove to be very interesting. Metals like Pt, Al, Ag and even Au have been deposited onto SWNTs [31-37] to study the metal-CNT interactions in the recent years. These involve both capping the termini as well as curvatures of the SWNTs with different metals. SWNTs have even been used as templates to develop linear chains of certain metals like Ti [38]. Furthermore, the metal attached to the SWNTs can be functionalized for further applications. [39].

In this chapter, we attempt to elucidate the nature of interactions between metallic clusters of the noble metals Au and Pt of varying geometries and SWNTs of various chiralities. We also attempt to rationalize the extent of interactions necessary to sufficiently modulate the band gap of pristine metallic and semiconducting SWNTs, separately, and comment on the metal-semiconductor (and vice-versa) transitions of the composites.

Computational Procedure:

This study is based on first-principles spin-polarized density functional theory. The SIESTA code [40] was employed to perform fully self-consistent calculation of the Kohn-Sham equations. The Kohn-Sham orbitals are expanded using linear combinations

of pseudoatomic orbitals proposed by Sankey-Nikelewski [41]. For the exchange and correlation term, the generalized gradient approximation (GGA) is used as proposed by Perdew-Burke-Ernzerhof [42]. Core electrons are replaced by non-local, norm-conserving Troullier-Martins pseudopotentials [43]. Valence electrons are described within the linear combination of atomic orbitals (LCAO) and a double-zeta basis set with a polarization function. A cut-off of 150 Ry for the grid integration was utilized to represent the charge density. A Monkhorst-Pack [44] grid of 1x1x60 was used for the Brillouin zone integration, where the tube is placed along the z-axis. The relaxed atomic configurations of the tubes were obtained by a minimization of the total energy using the Hellman-Feymann forces including Pulay-like corrections. Structural optimizations were performed in all calculations using conjugate gradient algorithm until the residual forces were always smaller than 0.05 eV/Å.

Results and discussion:

To understand the nature of interaction of carbon SWNTs with physisorbed metals, we consider metal systems with various nuclearities and geometries. We report here our results from calculations on composite systems involving the noble metals Au and Pt together with both metallic and semiconducting carbon nanotubes. SWNTs can be either metallic or semiconducting depending on the geometry of how the graphene sheet is rolled up into a tube (i.e. diameter and chirality). The unique properties of the SWNTs are caused by the quantum confinement of the mobile π electrons normal to the carbon nanotube's long axis. In the radial direction, the electrons are confined by the monolayer thickness of the graphene sheet. Consequently, electrons can propagate only along the carbon nanotube axis. The sharp intensity peaks in the DOS of the SWNTs are due to one-dimensional quantum conduction. Metallic SWNTs have finite DOS at the Fermi energy, while semiconducting SWNTs have small band gaps (< 1 eV) that decrease with increasing diameter of the SWNT. An empirical relation that usually suffices for this is, $E_g = 0.8eV / d$, where d is the diameter of the SWNT. Therefore, in order to elucidate the nature of interactions of physisorbed metals with pristine SWNTs, and to estimate the extent to which such interactions can modulate the electronic structure of the SWNTs, we chose metallic and semiconducting SWNTs with sufficiently small diameters.

We choose SWNTs of chiralities (6, 0), (6, 6), (8, 0), and (10, 0). The first two of the above mentioned four SWNTs are metallic, while the latter two are semiconducting. From our calculations, we find that the band gaps for the (8, 0), and (10, 0) are 0.53 and 0.68 eV, respectively. On comparison with values reported in recent literature [45, 46], we find that our results are in good agreement. To study the composites, we consider zigzag chains and metal clusters of Au and Pt. We also consider composites wherein the whole external curvature of the SWNT is covered by a cylindrical monolayer of Au and Pt atoms. We present our results systematically.

First we consider adsorbed Au and Pt chains on the SWNT surface. For calculating the binding energy per atom of the metal chain onto the SWNTs (defined as the difference between the total energy of the metal-deposited SWNT and the sum of the total energies of the individual SWNT and the free metal chain), we calculate the energies of the pristine SWNT, the free-standing metal chain, and the metal-deposited SWNT composite. The binding energy values, $E_{b,}$ indicated in table 5.1, clearly indicate that Au and Pt chains are most likely physisorbed [38] onto the SWNTs. Upon interaction with the SWNT the metal-metal bond distance decreased in all the cases. Further, we find that the distance of the metal from the external surface of the SWNT, depends not only on the choice of the metal but also on the chirality of the tube, although the variations with changes in chirality are small. The metal-metal as well as Metal-SWNT distances are indicated in table 5.2. The deviation from the circular tube, measured by the aspect ratio (r_{max}/r_{min}) [47] in this case is less than 1%.

Table 5.1: Binding energies (eV) for the metal chains deposited onto the SWNTs of different chiralities (indicated in parenthesis). Positive energies indicate stabilization.

	(6,0)	**(6,6)**	**(8,0)**	**(10,0)**
Au	0.262	0.274	0.422	0.410
Pt	0.331	0.347	0.390	0.402

Table 5.2: Metal-Metal bonding distance (Å) in the metal-SWNT composites after full relaxation. The Au-Au and Pt-Pt distances in the optimized free standing chain were 2.53 and 2.41 Å respectively.

	6,0	**6,6**	**8,0**	**10,0**
Au-Au	2.48	2.48	2.50	2.51
Pt-Pt	2.37	2.37	2.38	2.39
Au-SWNT	2.76	2.78	2.84	2.88
Pt-SWNT	2.68	2.69	2.73	2.77

Upon interaction, the band gap of the semiconducting SWNTs, viz. for the (8,0) and the (10,0) tubes vanish, however, the single metallic chain fails to alter the electronic structure of the tubes considerably. There is a shift in the Fermi energy, however, the density of stated (DOS) at the Fermi level still remains zero, as indicated in figure 5.1. However, we also find that, compared to the pristine SWNTs, the band gap decreases after interaction with the single chain of the metals, Au and Pt. We find similar results from our calculations of Au-(10,0) SWNT and Pt-(10,0) SWNT composites. The band gaps are indicated in table 5.3.

Table 5.3: Comparison of the band gaps (eV) of the pristine (8, 0) and (10, 0) SWNTs with Metal-(8, 0) and Metal-(10, 0) composites, where Metal = Au and Pt.

	(8, 0)	**(10, 0)**
Pristine SWNT	0.53	0.68
Au-SWNT	0.27	0.23
Pt-SWNT	0.16	0.14

To increase the extent of interaction further, we consider two chains of metal, located on diametrically opposite sides of the SWNT. Interestingly, in this case, we find that the overall metal-SWNT composite shows a metallic character. The DOS projected onto the SWNT, still, however, shows that the SWNTs remain semiconducting, as shown in figure 5.2. We find that in the optimized structures of the metal chain-SWNT composites, shown in figure 5.3, each metal atom sits above a hexagon of the SWNT. For the metal-SWNT,

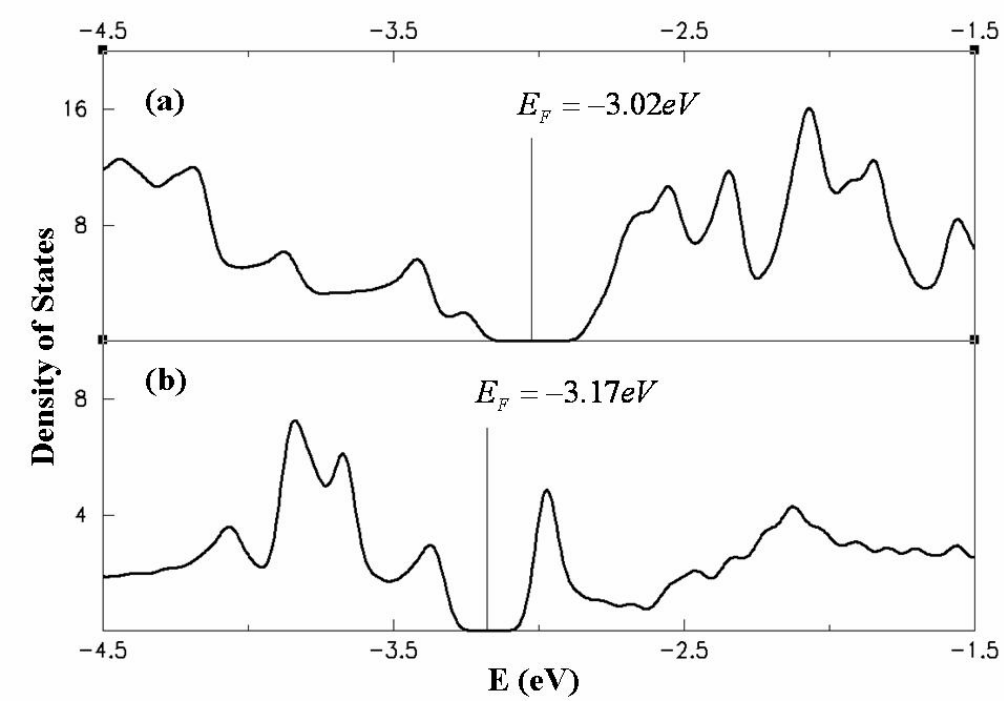

Figure 5.1: Density of States plots for metal-chain-SWNT composites. (a) Au-(8,0) SWNT and (b) Pt-(8,0) SWNT

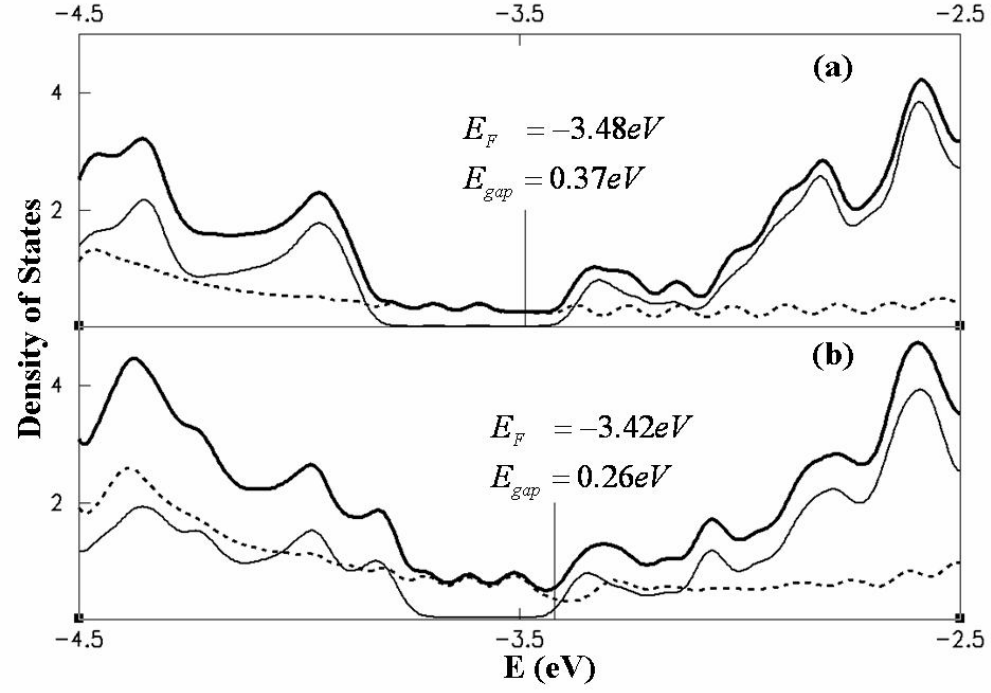

Figure 5.2: Density of States plots for metal-SWNT composites with two chains [on diametrically opposite sides of SWNT] for (a) Au-(8,0) SWNT and (b) Pt-(8,0) SWNT. The thick solid lines, dashed lines, and the thin solid lines indicate, respectively, the DOS for the metal-SWNT composite, the pDOS for the metal and the SWNT.

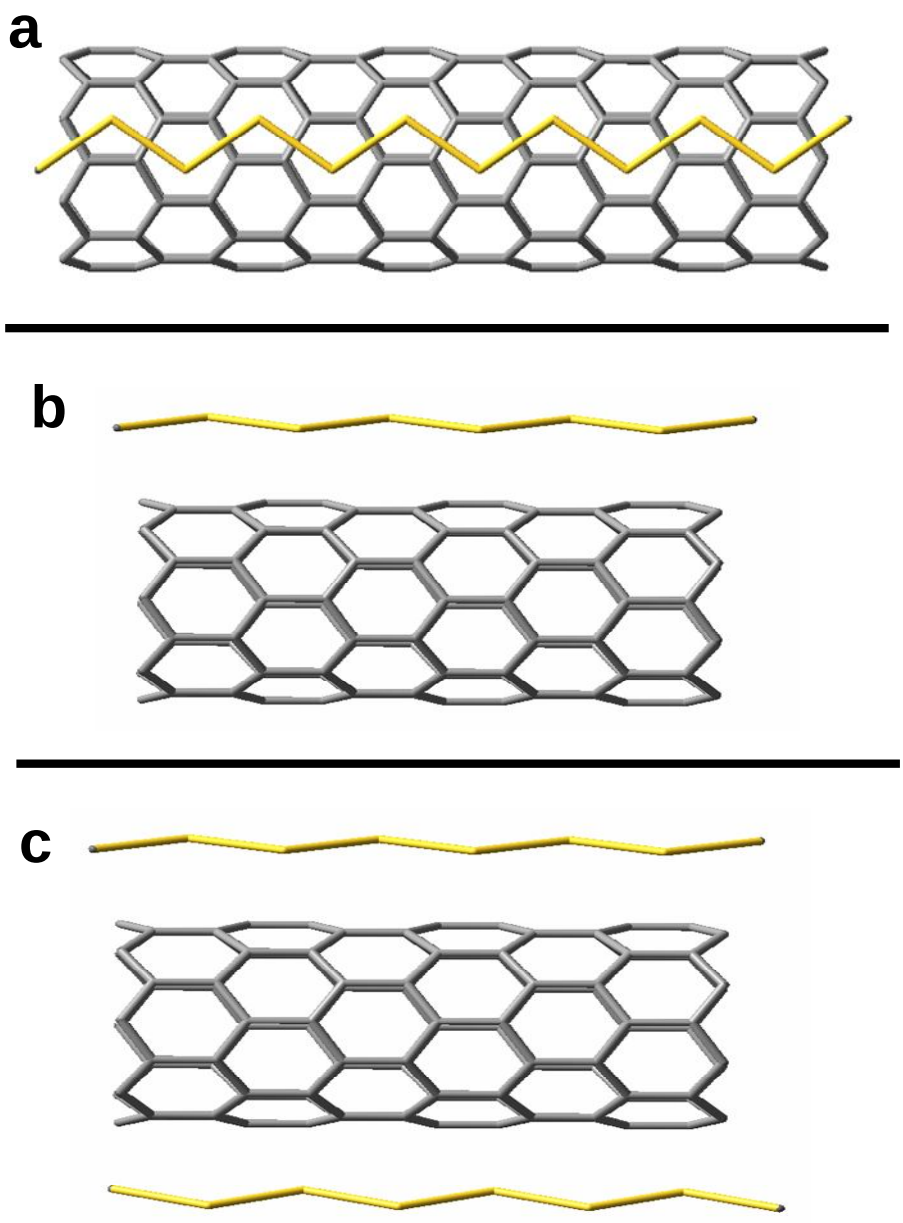

Figure 5.3: (a) Optimized structure of adsorbed Au chain on (8,0) CNT indicating position of Au atoms (5 unit cells are shown). Sidewise view of (b) one Au chain and (c) two Au chains on the (8,0) CNT (3 unit cells are shown).

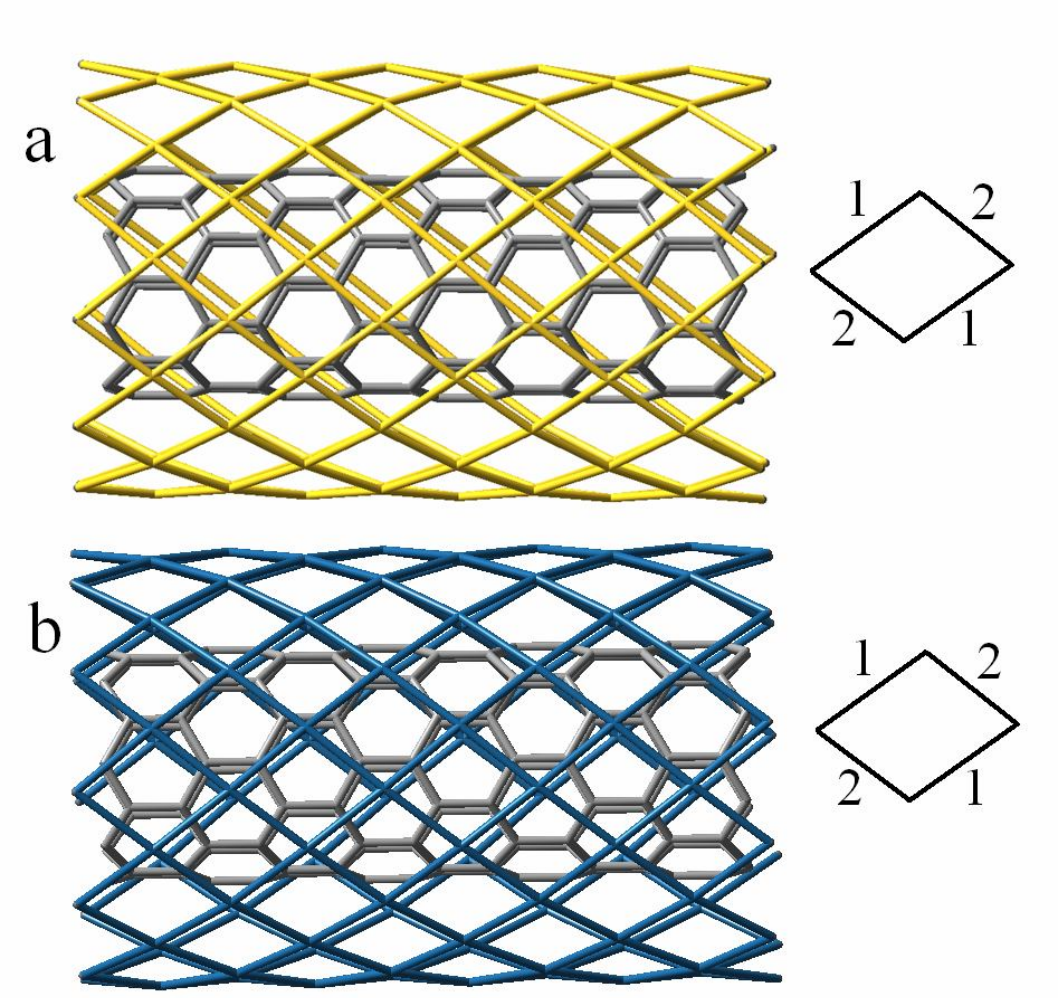

Figure 5.4: Optimized structure of the cylindrical monolayer of (a) Au and (b) Pt covering the whole surface of the CNT. Four unit cells are shown. The metal atoms adopt a rhombic arrangement, with alternating metal –metal bond lengths, as shown in the adjoining figure.

composites consisting of the metallic tubes, viz. (6,0) and (6,6), we find that there is a finite density of states at the Fermi energy, indicating that there is no transition to semiconducting character.

To further increase the extent of interaction between the metal and the SWNT, we consider next, cylindrical monolayers of Au and Pt. In the fully optimized structures, we find that the full external curvature of the SWNT is covered by the monolayer of the metal, as shown in Figure 5.4. The average distance, at which the metal atoms are located from the surface, i.e. the difference between the radius of the cylindrical monolayer of metal and the radius of the SWNT is 2.84 Å and 2.82 Å for the Au-SWNT and the Pt-SWNT systems, respectively. It is noteworthy to mention here that the metal atoms in the cylindrical monolayer form a distorted rhombic geometry, the distortion being necessary to accommodate the curvature of the SWNT. The metal-metal bond length alternates between two values, as shown schematically in figure 5.4. For Au, the bond distances are 2.76 and 2.73 Å, while for Pt, the distances are 2.69 and 2.72 Å. Interestingly, due to strong interactions between the metal monolayer and the SWNT, we observe transition of the semiconducting SWNTs to metallic character. The DOS plots for the composites of the cylindrical metal monolayer and SWNTs are shown in Figure 5.5. It is very interesting to note that, with such strong interaction between the pristine semiconducting SWNT and the cylindrical monolayer of the metal, not only do the metal-SWNT composites become metallic, but, as seen from the projected density of states (pDOS) plots (figure 5.5), the SWNTs also become metallic. However, as in the earlier cases, the metallic tubes, viz. those with chiralities (6,0) and (6,6), upon interaction with either cylindrical monolayer of Au and Pt metals, fail to show any change in the DOS at the Fermi level.

Structural evidences obtained from high-resolution microscopy [48] reveal that the smallest metal nano-clusters deposited on the SWNTs are of sizes of the order of 2-3 nm. Metal clusters of even such small dimensions have, on a rough estimate, more than 500 atoms. *Ab initio* computational studies involving so many atoms are very expensive. Theoretically speaking, one can have a rough estimate of the nature of interactions between metal clusters and SWNTs by considering clusters of smaller sizes by extrapolating a similar trend of results from calculations on small clusters of various

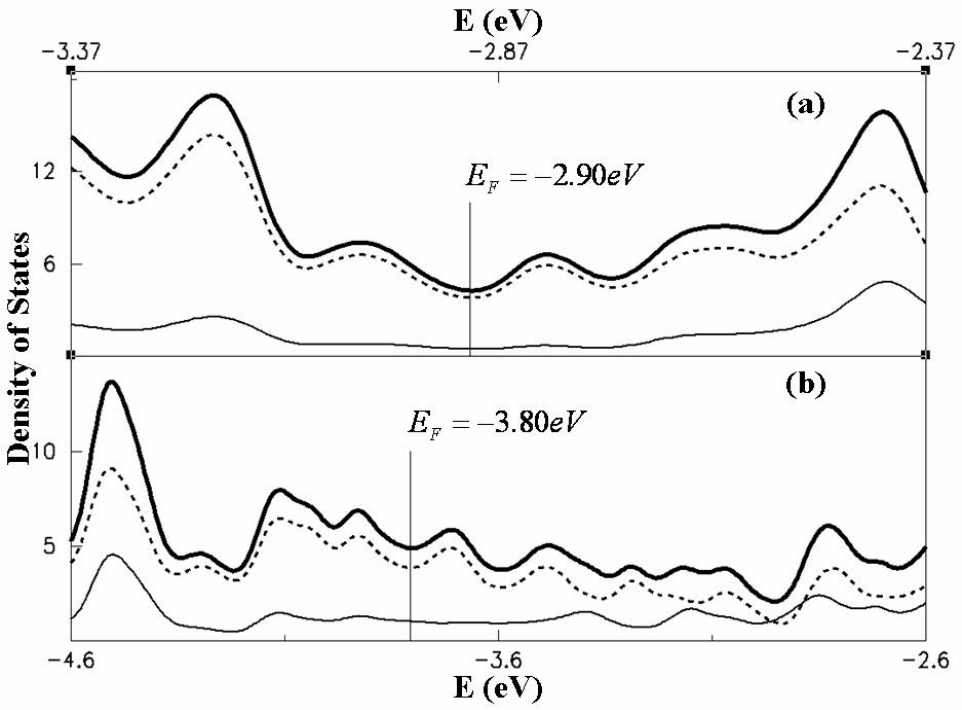

Figure 5.5: DOS plots for the cylindrical monolayers adsorbed on the (8,0) SWNT. pDOS for the metal-SWNT composite (thick solid line), metal (dashed line), and SWNT (thin solid line) for (a) Pt and (b) Au.

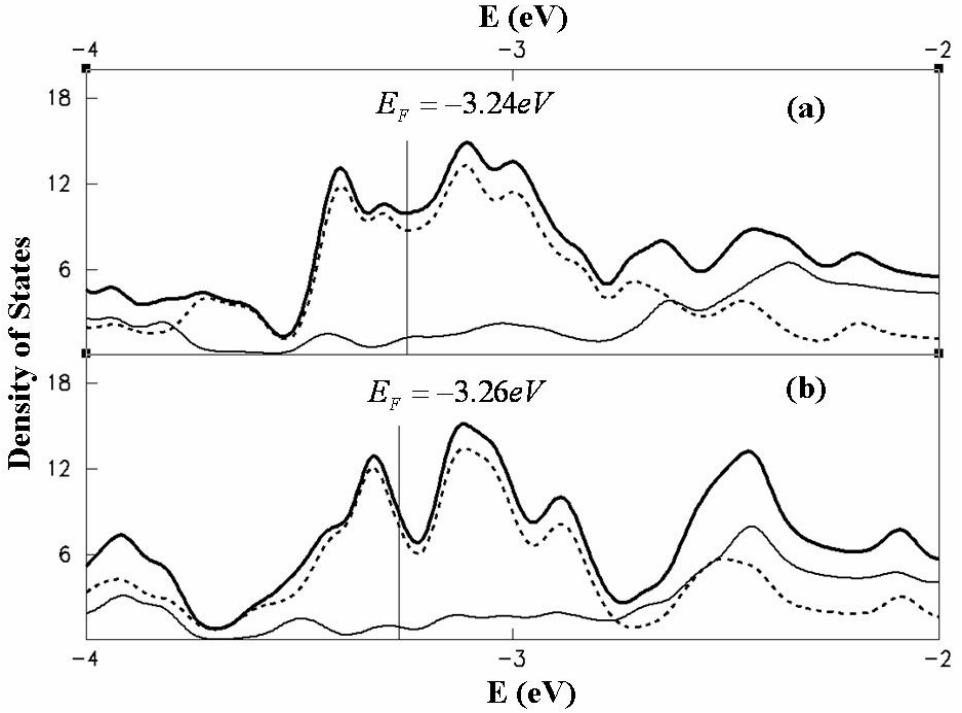

Figure 5.6: DOS plots for the (a) Au_{40}-(8,0) SWNT and (b) Au_{12}-(8,0) SWNT composites. pDOS for the metal-SWNT composite (thick solid line), metal (dashed line), and SWNT (thin solid line).

nuclearities. In order to understand the effect of metal clusters (adsorbed onto the external curvature of the SWNTs) on their electronic structure, we consider Au and Pt clusters of various nuclearities. We present here typical results from our calculations involving clusters of nuclearities 12 and 40. To ensure that consecutive clusters do not interact with each other, we replicate individual clusters along the direction of periodicity of the SWNT. We follow the variation of the energy of the metal clusters with integral multiples of the translation vector of the pristine SWNT. When the energy of the clusters becomes constant, we assume that there are no interactions between individual clusters in the direction of periodicity. We find that the distances along the direction of periodicities at which the clusters do not interact are larger than 13 Å. For the Au-cluster-SWNT composites, it is sufficient to take 4 times and 5 times the translation vectors of the (8,0) SWNT for the Au_{12} and Au_{40} clusters respectively, i.e. 17.08 and 21.35 Å, respectively. As an initial guess, the clusters were placed 'on' the (8,0) SWNT external curvature so that one vertex was at a distance of 3.0 Å from the nearest C atom. Interestingly, after full geometry relaxation, the clusters retain their symmetrical structure, with the nearest proximity of the cluster to the external curvature of the SWNT being 2.6 Å and 2.4 Å for the Au_{12} and Au_{40} clusters, respectively. The electronic structure of the optimized Au_{12}-SWNT and Au_{40}-SWNT composites show that the system is metallic. The DOS projected onto the SWNT shows that the (8,0) SWNT has become metallic, with finite density of states at the Fermi level. The DOS and pDOS plots for the Au_{12}-SWNT and Au_{40}-SWNT composites are shown in figure 5.6. The optimized geometries of Au_{12}-SWNT and Au_{40}-SWNT composites are shown in figure 5.7. Again, as in all the earlier cases, the metallic SWNTs fail to show any transformation into semiconducting character.

In order to understand the mechanism of semiconductor-metal transition, we have calculated the energy and charge densities of the composites by varying the distance between the Au fragments and the SWNT. Since, the semiconductor-metal transition was observed for Au_{12}-SWNT composites as well, we calculated the interaction energy as a function of the distance between the Au_{12} cluster and the SWNT. The initial structure chosen was the fully relaxed geometry of the Au_{12}-SWNT composite. As mentioned earlier, in the fully relaxed geometry, the nearest proximity of the cluster to the external

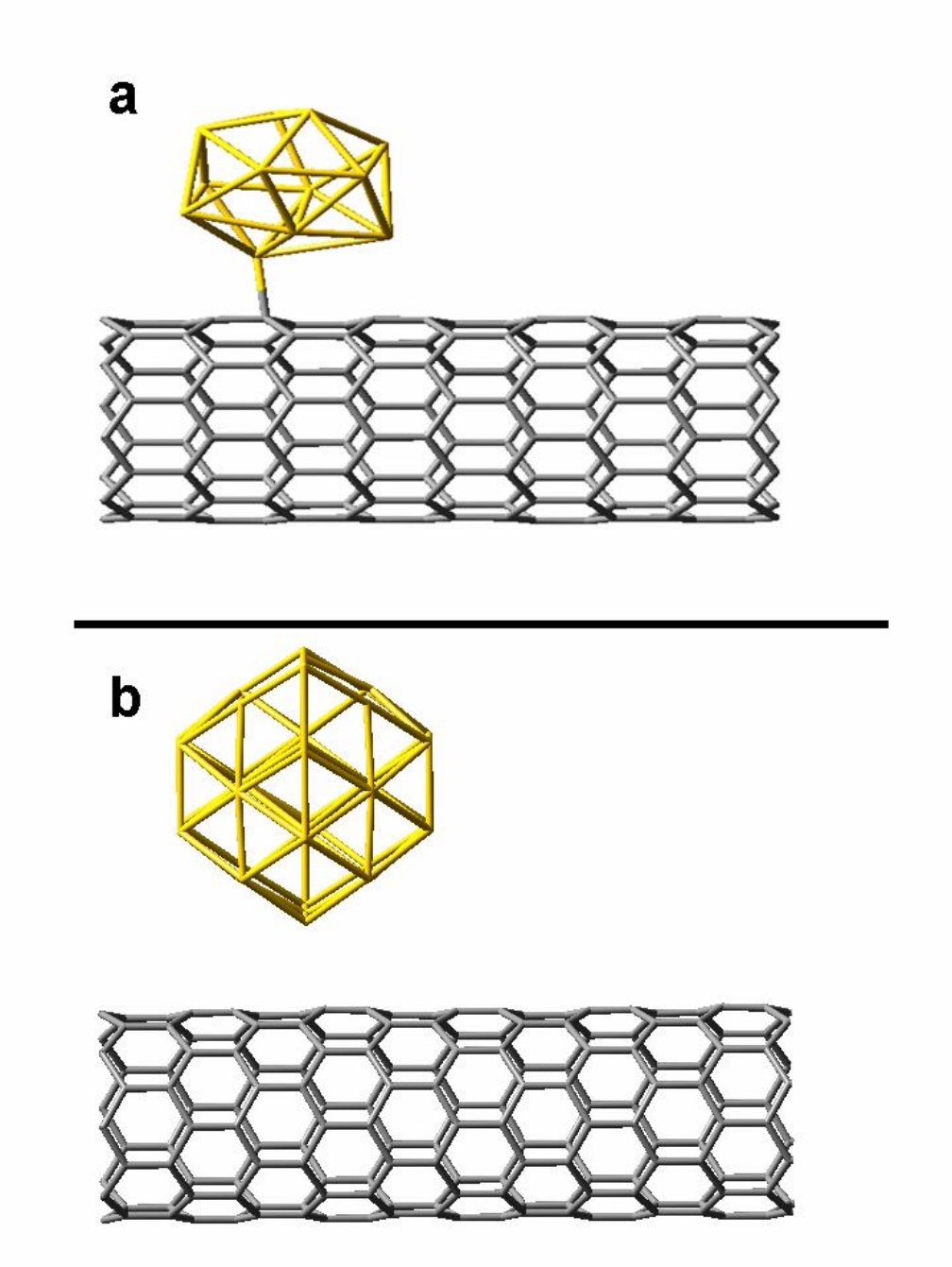

Figure 5.7: Optimized structure of the (a) Au_{12}-SWNT and (b) Au_{40}-SWNT composite.

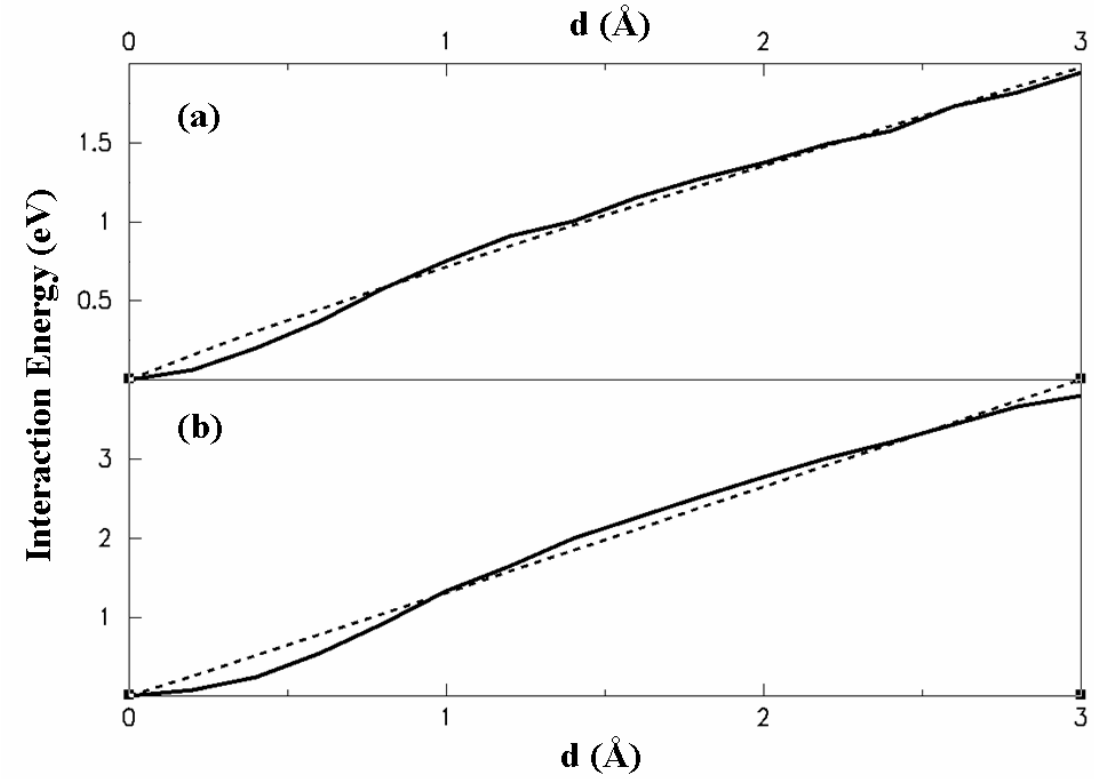

Figure 5.8: Interaction energy (solid line) between the Au fragment and the (8, 0)-SWNT in the Au-(8, 0) SWNT composite, scaled w.r.t the energy minima for the composites where the Au fragments are (a) a single chain of Au, (b) an Au_{12} cluster. The minima correspond to (a) -6754.8225 and (b) -8563.2065 eV. The dashed line indicates the 1/r dependence of energy fitted to the equation, $\Delta E = A_1 / d$, where d is the shortest distance between the Au fragment and the SWNT surface.

curvature of the SWNT is 2.6 Å.

We varied the distance between these two atoms to see the variation of energy of interaction, defined as, $\Delta E_{\text{int}} = \Delta E_{Au-SWNT} - (\Delta E_{Au} + \Delta E_{SWNT})$. We find that the interaction energy varies inversely with the distance considered, *d* (Å), as shown in figure 5.8, clearly indicating that the semiconductor-metal transition is due to Coulombic charge-transfer. Interestingly, such interactions are due to resonance between the Au-plasmon band and the excitation continuum of the SWNTs. From a charge density analysis, we also find that electron density at the outermost valence orbitals increases, while that at the carbon atoms at the closes proximity to the Au cluster decreases. Thus our results indicate that such a phase transfer is primarily due to Coulombic charge transfer between Au and SWNT systems.

References:

[1] Kratschmer W., Lamb L. D., Fostiropoulos F., Huffman D., *Nature*, 1990, **347**, 354.

[2] Carbon Nanotubes: Synthesis, structures, properties and applications, *Topics in Applied Physics*, 2001, **80**.

[3] Vieira R., Ledoux M. J., Pham-Huu C., *Applied Catalysis A*, 2004, **274**, 1.

[4] Dubrovinskaia N., Dubrovinsky L., Crichton W., Langerhost F., Richter A., *App. Phys. Lett.*, 2005, **87**, 083106.

[5] Frondel C., Marvi U. B., *Nature*, 1967, **214**, 587.

[6] Harris P. J. F., *Philosophical Magazine*, 2004, **84**, 3159.

[7] Rode A. V., Hyde S. T., Ganaly E. G., *Applied Physics A-Materials Science & Processing*, 1999, **69**, S755.

[8] *Carbyne and Carbynoid Structures Series: Physics and Chemistry of Materials with Low-Dimensional Structures*, Heimann, R.B., Evsyukov, S.E., Kavan, L. (Eds.), 1999, **21**, 452.

[9] Kroto H. W., Heath J. R., O'Brien S. C., Curl R. F., Smalley R. E., *Nature*, 1985, **318**, 162

[10] Katsnelson M. I., *Materials Today*, 2007, **10**, 20.

[11] Radushkevich L.V., Lukyanovich V.M., *Zurn Fisic Chim.*, 1952, **111**, 24.

[12] Oberlin A., Endo M., Koyama T., *J. Cryst Growth*, 1976, **32**, 335.

[13] Ijima S., *Nature*, 1991, **354**, 56; Ijima S., Ichihashi T., *Nature*, 1993, **363**, 603.

[14] Geim A. K., Novoselov K. S., *Nat. Mater.*, 2007, **6**, 183.

[15] Saito R., Dresselhaus G., Dresselhaus M. S., 1998, *Physical Properties of Carbon Nanoutbes* (London: Imperial College Press).

[16] Rao C. N. R., Govindaraj A., 2005, *Nanotubes and Nanowires* (Cambridge: Royal Society of Chemistry).

[17] Robel I., Bunker B. A., Kamat P. V., *Adv. Mater*., **17**, 2458.

[18] Fournet, P., Coleman J. N., O'Brien D. F., Lahr B., Drury A., Hörhold H. H., Blau W. J., *J. App. Phys.*, 2001, **90** , 969.

[19] O' Flaherty S. M., Hold S. V., Brennan M. E., Cadek M., Drury A., Coleman J. N., Blau W. J., *JOSA B*, 2003, **20**, 49.

[20] Borghetti J., Derycke V., Lenfant S., Chenevier P., Filoramo A., Goffman M., Vuillaume D., Bourgoin J. P., *Adv. Mater*., 2006, **18**, 2535.

[21] Peng S., Cho K., *Nano Lett*., 2003, **3**, 513.

[22] Doped Carbon Nanotubes: Synthesis, Characterization and Applications, *Topics in Applied Physics*, Spinger Berlin / Heidelberg, 2007, **ISBN: 978-3-540-72864-1**.

[23] Williams K. A., Veenhuizen P. T. M., Torre B. G., Eritja R., Dekker C., *Nature*, 2002, **420**, 761.

[24] Rotkin S. V., Subramoney S. (Eds), *Applied Physics of Carbon Nanotubes: Fundamentals of Theory, Optics, and Transport Devices*, 2005, Nanoscience and Technology.

[25] Krupke R., Hennrich F., van Lohneysen H. and Kappes M. M., *Science*, 2003, **301**, 344.

[26] Maeda Y., Kimura S., Kanda M., Hirashima Y., Hasegawa T., Wakahara T., Lian Y., Nakahodo T., Tsuchiya T., Akasaka T., Lu J., Zhang X., Gao Z., Yu Y., Nagase S., Kazaoui S., Minami N., Shimizu T., Tokumoto H. and Saito R., *J. Am. Chem. Soc*., 2005, **127**, 10287.

[27] Arnold M. S., Sharping J. E., Stupp S. I., Kumar P., Hesam M. C., *Nano Lett.*, 2003, **3**, 1549.

[28] Campidelli S., Meneghetti M. and Prato M., *Small*, 2007, **3**, 1672.

[29] Das A., Sood A. K., Govindaraj A., Saitta M., Lazzeri M., Mauri F. and Rao C. N. R., *Phys. Rev. Lett*., 2007, **99**, 136803.

[30] Scolari M., Mews A., Fu N., Myalitsin A., Assmus T., Balasubramanian K., Burghard M. and Kern K., *J. Phys. Chem. C*., 2008, **112**, 391.

[31] Kim B., Sigmund W. M., *Langmuir*, 2004, **20**, 8239.

[32] Han L., Wu W., Kirk F. L., Luo J., Maye M. M., Kariuki N. N., Li Y. H., Wang C., Zhong C. J., *Langmuir*, 2004, **20**, 6019.

[33] Carrillo A., Swartz J. A., Gamba J. M., Kane R. S., Chakrapani N., Wei B., Ajayan P. M, *Nano Lett*., 2003, **3**, 1437.

[34] Zhang J., Wang G., Shon Y. S., Zhou O., Superfine R., Murray R. W., *J. Phys. Chem. B*., 2003, **107**, 3726.

[35] Li Y. H., Xu C., Wei B., Zhang X., Zheng M., Wu D., Ajayan P. M., *Chem. Mater*., 2002, **14**, 483.

[36] Planeix J. M., Coustel N. , Coq B., Brotons V., Kumbhar P. S., Dutartre R., Geneste P., Bernier P., Ajayan P. M., *J. Am. Chem. Soc*., 1994, **116**, 7935.

[37] Satishkumar B. C., Vogl E. M., Govindaraj A., Rao C. N. R., *J. Phys. D: Appl. Phys*., 1996, **29**, 3173.

[38] Yang C. K., Zhao J., Lu J. P., *Phys. Rev. B*., 2002, **66**, 041403.

[39] Rahman G. M. A., Guldi D. M., Zambon E., Pasquato L., Tagmatarchis N., Prato M., *Small*, 2005, **1**, 527.

[40] Ordejón P., Artacho E., and Soler J. M., *Phys. Rev. B*.,1996, **53**, 10441.

[41] Sankey O. F. and Nikelewski D. J., *Phys. Rev. B*., 1989, **40**, 3979.

[42] Perdew J. P., Burke K., and Ernzerhof M., *Phys. Rev. Lett*., 1996, **77**, 3865.

[43] Troullier N. and Martins J. L., *Phys. Rev. B*.,1991, **43**, 1993.

[44] Monkhorst H. J. and Pack J. D., *Phys. Rev. B*., 1996, **13**, 5188.

[45] Lemos V., Veloso M. V. D., Fagan S. B., Mendes-Filho J., *Phys. Stat. Sol. (c)*, 2004, **1**, S219.

[46] Cho E., Kim H., Kim C., Han S., *Chem. Phys. Lett*., 2006, **419**, 134.

[47] Zhao J. J., Buldum A., Lu J. P., *Phys. Rev. Lett*., 2000, **85**, 1706.

[48] Subramaniam C., Sreeprasad T. S., Pradeep T., Pavan Kumar G. V., Narayana C., Yajima T., Sugawara Y., Tanaka H., Ogawa T. and Chakrabarti J., Physical Review Letters, 2007, 99, 167404.

List of Publications

I. Publications pertaining to this thesis:

1. “Role of Dipolar Interactions in Fine-Tuning the Linear and Nonlinear Optical Responses in Porphyrins”, Shrinwantu Pal, Ayan Datta and Swapan K. Pati, *Computing Letters*, **3**, 367 (2008).
2. “Understanding the role of Intermolecular Interactions and Co-operative Phenomena in Magnesium Complexes of Bacteriochlorin, Chlorin and Porphyrin”, Shrinwantu Pal, Swapan K. Pati, (Submitted) (2008).
3. “The role of H-bonding and Dipole-Dipole Interactions on the Electrical Polarizations and Charge Mobilities in Linear Arrays of Urea, Thiourea and their Derivatives”, Shrinwantu Pal, Swapan K. Pati, (Submitted) (2008).
4. "Semiconductor to Metal Transition in SWNTs Caused by Interaction with Gold and Platinum Nanoparticles", Rakesh Voggu, Shrinwantu Pal, Swapan K. Pati and C. N. R. Rao, *J. Phys.: Cond. Matt.*, **20**, 215211 (2008).

II. Other Publications:

1. “Functionalization and solubilization of BN nanotubes by interaction with Lewis bases", Shrinwantu Pal, S. R. C. Vivekchand, A. Govindaraj and C. N. R. Rao, *J. Mater. Chem*., **17**, 403 (2007).
2. "Charge density analysis of two proton transfer complexes: Understanding Hydrogen Bonding and determination of in-crystal Dipole Moments", Reji Thomas, Shrinwantu Pal, Ayan Datta, Mariusz K. Marchewka, Henryk Ratajczak, Swapan K. Pati and G. U. Kulkarni (submitted) (2008).